

Important Notice

This copy may be used only for the purposes of research and private study, and any use of the copy for a purpose other than research or private study may require the authorization of the copyright owner of the work in question. Responsibility regarding questions of copyright that may arise in the use of this copy is assumed by the recipient.

UNIVERSITY OF CALGARY

Time-lapse seismic surveys:

Rock physics basis

by

John Jianlin Zhang

A THESIS

**SUBMITTED TO THE FACULTY OF GRADUATE STUDIES
IN PARTIAL FULFILLMENT OF THE REQUIREMENTS FOR
THE DEGREE OF MASTER OF SCIENCE**

**DEPARTMENT OF GEOLOGY AND GEOPHYSICS
CALGARY, ALBERTA**

AUGUST, 2001

© John J. Zhang 2001

**THE UNIVERSITY OF CALGARY
FACULTY OF GRADUATE STUDIES**

The undersigned certify that they have read, and recommended to the Faculty of Graduate Studies for acceptance the thesis entitled "Time-lapse seismic surveys: Rock physics basis" submitted by John Jianlin Zhang in partial fulfilment of the requirements for the degree of Master of Science.

Supervisor, L. R. Bentley, Geology and Geophysics

L. R. Lines, Geology and Geophysics

Ron C. K. Wong, Civil Engineering

Date:

ABSTRACT

The major factor that determines the elastic moduli of a rock is the pore geometry. Based on the inverse Kuster-Toksoz modelling of sandstone samples, it is found that the concentration of round pores is in direct proportion to porosity while that of cracks is small and has no correlation with porosity or clay content. The variability in the elastic moduli at a given porosity can be attributed chiefly to the variability in the crack concentration. Moreover, the effect of cracks on the elastic moduli decreases with increasing porosity. Consequently variation of the elastic moduli with changing effective pressure will generally become smaller at high porosity.

The effect of fluids on the elastic moduli is most important in the rock of low dry elastic moduli. Effective pressure has a greater impact on the dry elastic moduli at low effective pressure and the rate of change of the dry elastic moduli with respect to effective pressure can be modelled as the quasi-exponential function. Temperature has a small effect on the dry elastic moduli unless it changes drastically.

ACKNOWLEDGEMENTS

My deep appreciation goes to Larry Bentley, my supervisor and mentor, who has offered unlimited guidance, support, encouragement and friendship. His seriousness and spirit of seeking truth from facts in scientific research have profoundly affected my attitude toward academic life. The success of my graduate study is largely a result of continuous interactions with him. He, more than any other individuals, has made my career in the University of Calgary, intellectually stimulating and enjoyable.

I would also like to take this opportunity to thank the industrial sponsors and NSERC for their financial support, which made it possible to carry out the CREWES research. Their continued funding through the years freed me from the family financial burden so that I could concentrate on the research work whether in winter or summer. I acknowledge their generosity.

It has been my good fortunate to come into close contact with a number of people who have facilitated the production of this thesis. Xinxing Li helped me overcome the difficulty in computer drawing and document edition. My familiarity with Matlab programming was due to his kindness and patience in my learning. Hugh Geiger was always enthusiastic to answer my questions. His advice in optimisation was invaluable. Without the suggestions, it would have taken longer to attack the problem in numerical modelling. My understanding of seismology also benefited immeasurably from the discussion with him. The mathematical assistance from Zhengsheng Yao was very helpful. He put me in the right direction of doing statistical analysis. Mark Kirtland and Henry Bland

were the first people to be called whenever I encountered any computer problems. I sincerely thank these people.

Lastly I wish to express my great gratitude to my wife, Joyce Zhang and my son, Ben Zhang, who have been instrumental in my success. My wife took the major part of the housework and assumed the role of tutoring the kid. My academic gains were chiefly from her commitment to the family. My son was cheerful and always willing to play with me when I was relaxed. His existence basked me in the family happiness. I extend my heart-felt appreciation to them.

TABLE OF CONTENTS

TITLE PAGE.....	i
APPROVAL PAGE.....	ii
ABSTRACT.....	iii
ACKNOWLEDGEMENTS.....	iv
TABLE OF CONTENTS.....	vi
LIST OF TABLES.....	ix
LIST OF FIGURES.....	x
CHAPTER 1: INTRODUCTION.....	1
CHAPTER 2: ELASTIC MODULI OF ROCKS.....	6
2.1 Effective medium theories.....	7
2.2 Elastic moduli and densities of rock solid.....	15
2.3 Elastic moduli and densities of fluids.....	17
2.4 Frequency dependence of the elastic modulus of fluid-saturated rocks.....	23
2.5 Conclusions.....	32
CHAPTER 3: A PORE GEOMETRICAL MODEL FOR SANDTONES.....	33
3.1 Introduction.....	33
3.2 Forward numerical modelling of elastic moduli and velocities.....	34
3.3 Inversion of pore aspect ratio spectra from velocity measurements.....	37
3.4 Parameter acquisition.....	40
3.5 Inversion results.....	43
3.6 Pore aspect ratio spectra and elastic moduli at atmospheric pressure.....	48
3.7 Effect of round pores on the variability in the elastic moduli.....	54

3.8 A pore geometrical model for sandstones	55
3.9 Pore geometry and change of the elastic moduli with effective pressure	59
3.10 Effect of clay content on pore geometry	61
3.11 Discussion.....	62
3.12 Conclusions	64

CHAPTER 4: A QUANTITATIVE MODEL FOR THE RATE OF CHANGE OF THE ELASTIC MODULI OF DRY SANDSTONES WITH EFFECTIVE PRESSURE	65
4.1 Calculation of the rate of change of the dry elastic moduli with effective pressure	65
4.2 A quantitative model for the rate of change of the dry elastic moduli with effective pressure	68
4.3 Conclusions	71

CHAPTER 5: EFFECT OF TEMPERATURE ON ELASTIC MODULI OF DRY SANDSTONES	72
---	----

CHAPTER 6: FEASIBILITY OF SEISMIC MONITORING OF SANDSTONE RESERVOIRS.....	75
6.1 Introduction	75
6.2 Quantitative rock physics models.....	75
6.3 Quantitative evaluation of production or injection process in terms of velocities and acoustic impedance	80
6.4 Depth effect on seismic monitoring of sandstone reservoirs.....	101
6.5 Discussion.....	104
6.6 Conclusions	106

CHAPTER 7: FEASIBILITY OF SEISMIC MONITORING OF THE BLACKFOOT RESERVOIRS	107
7.1 Introduction	107
7.2 Exploration and production history	108
7.3 Data acquisition	111
7.4 Scenarios for computation of seismic responses.....	114
7.5 Synthetic seismograms	116
7.6 Difference between 1995 and 1997.....	119
7.7 Conclusions	120
 CHAPTER 8: CONCLUSIONS.....	 122
 REFERENCES	 124
 APPENDIX A Compressibility of the rock with spherical pores and cracks	 133
APPENDIX B Isothermal compressibility of gas.....	137
APPENDIX C Deviation of the Gassmann's equation.....	138
APPENDIX D The effect of effective pressure on the volume change of rock solid.....	141
APPENDIX E Effective bulk modulus of the fluid mixture due to patchy Saturation.....	144
APPENDIX F The parameters for the KT equations.....	147

LIST OF TABLES

2.1 Elastic moduli and densities of major rock-forming minerals	16
2.2 Coefficients for water properties computation.....	18
3.1 Pore aspect ratio spectra and elastic moduli of rock solid for the first set of water saturated sandstones.....	44
3.2 Pore aspect ratio spectra and elastic moduli of rock solid for the second set of twenty-two dry sandstones	46
5.1 Dry velocities and elastic moduli for Massilion sandstones.....	74
7.1 Fluid properties	112
7.2 PVT values.....	112

LIST OF FIGURES

2.1 Model of isostrain (Voigt)	8
2.2 Model of isostress (Reuss).....	9
3.1 Elastic moduli of rock solid versus clay content for the samples from Han et al. and from Khaksar et al.....	42
3.2 Velocity percentage errors for the first set (left) and the second set (right) ...	47
3.3 Results of inversion for samples 6, 14, 25 and 42.....	47
3.4 Results of inversion for samples D1 and S4	48
3.5 Plot of porosity versus the bulk and shear modulus for the first set of seventy-five dry sandstones.....	49
3.6 Plot of weighted concentrations versus dry elastic moduli computed based on the constant elastic moduli of rock solid	50
3.7 Plot of weighted concentrations versus dry elastic moduli computed based on the elastic moduli of rock solid from Table 3.1.....	51
3.8 Plot of weighted concentrations versus clay content.....	51
3.9 Plot of total porosity versus weighted concentrations	51
3.10 Plot of total porosity versus clay content.....	51
3.11 Plot of total porosity versus concentrations of spherical pores and cracks of varying aspect ratios for seventy-five dry sandstones	53
3.12 Plot of total porosity versus weighted concentration of round pores (right) and weighted crack concentration (left).....	53
3.13 Plot of weighted crack concentration versus crack concentration.....	53
3.13 Plot of total porosity versus elastic moduli for four cases: spherical pores only, lower crack concentration added, medium crack concentration added and high crack concentration added	54
3.15 Conceptual model of pore geometry for sandstones	55

3.16 Plot of total porosity versus the volume concentrations of cracks of varying aspect ratios and the weighted crack concentrations for the second set of sandstones	57
3.17 Plot of porosity versus the dry bulk modulus and shear modulus	57
3.18 Plot of total porosity versus weighted concentration of spherical pores (right) and weighted crack concentration (left) at 40 Mpa	58
3.19 Plot of porosity versus dry bulk modulus and shear modulus at 40 Mpa	58
3.20 Plot of porosity versus water-saturated bulk modulus	59
3.21 Plot of total porosity versus the rate of change of elastic moduli with respect to effective pressure at 10 and 30 MPa for the first set of sandstones.....	60
3.22 Plot of total porosity versus the rate of change of elastic moduli for the dry sandstones, which are lower than 3 GPa in bulk modulus at atmospheric pressure	60
3.23 Plot of clay content versus concentration of spherical pores and low-aspect-ratio cracks, respectively, for the first set.....	61
3.24 Plot of clay content versus concentration of spherical pores and low-aspect-ratio cracks, respectively, for the second set	62
4.1 Plot of elastic moduli versus effective pressure for the first set of dry sandstones	67
4.2 Plot of elastic moduli versus effective pressure for the second set of dry sandstones	67
4.3 Rate of change of dry elastic moduli with effective pressure	70
5.1 Bulk moduli versus temperature for sandstones.....	73
5.2 Shear moduli versus temperature for sandstones.....	73
6.1 Contours of the absolute change and the percentage change in fluid-saturated bulk modulus	82

6.2	Contours of the fluid-saturated bulk modulus before and after water drive.....	83
6.3	Contours of Vp and AI percentage changes.....	83
6.4	Contours of increase in Vp and AI percentage changes due to an increase in water bulk modulus to 3.1 Gpa.....	84
6.5	Contours of decrease in Vp and AI percentage changes due to a decrease in water bulk modulus to 1.4 Gpa.....	84
6.6	Contours of decrease in Vp percentage change and increase in AI percentage change due to an increase in the density contrast.....	85
6.7	Contours of increase in Vp and AI percentage changes due to increasing saturation contrast.....	87
6.8	Change of water density with pressure.....	87
6.9	Change of oil density with pressure.....	88
6.10	Change of water bulk modulus with pressure.....	89
6.11	Change of oil bulk modulus with pressure.....	89
6.12	Contours of increase in Vp and AI percentage changes due to a decrease of 5 MPa in fluid pressure.....	90
6.13	Contours of decrease in Vp and AI percentage changes due to a decrease of fluid bulk modulus.....	90
6.14	Contours of Vs percentage change.....	91
6.15	Contours of Vp and AI percentage changes.....	92
6.16	Contours of Vp and AI percentage changes.....	94
6.17	Contours of Vp and AI percentage changes.....	95
6.18	Contours of Vs percentage changes.....	95
6.19	Contours of Vp and AI percentage changes.....	96
6.20	Contours of Vp and AI percentage changes.....	97
6.21	Contours of Vs percentage changes.....	98
6.22	Contours of Vp and AI percentage changes.....	99

6.23	Contours of Vs percentage change	99
6.24	Contours of Vp and AI percentage changes.....	100
6.25	Compaction curve of sandstones	102
6.26	Change of the depth with the fluid pressure gradient at a given effective pressure	104
7.1	Blackfoot reservoir isopach.....	109
7.2	North-south cross section of Blackfoot reservoir showing lower channel (30), lithic channel (35) and upper channel (40)	110
7.3	Reservoir condition scenarios used in computation of seismic response.....	116
7.4	Comparison of a NMO corrected synthetic shot gather seismogram of the original reservoir conditions with that of post-production inside of the water flood area	117
7.5	Comparison of synthetic seismogram of the original reservoir conditions with post-production conditions outside of the water flood zones	118
7.6	Comparison of synthetic seismogram of outside the water flood with inside the water flood zone	120
7.7	Difference section	121

CHAPTER 1

INTRODUCTION

Global oil production is growing at an approximately 2% per annum on a smoothed basis, while annual discovery volumes are dwindling (Jack, 1998). This trend pushes the oil industry to maintain reserves by making improvements in the recovery rate of oil and gas. In fact, recovery on average is low, as indicated by BP's statistics of 13 major fields. Nur (1989) pointed out that a 10% increase in recovery efficiency in the United States would amount to a doubling of present estimates of recoverable reserves. Analyses by the Bureau of Economic Geology indicate that, excluding Alaska, up to 80 billion bbl oil and 180 trillion cubic feet gas can be added to current US onshore reserves by infill drilling and other enhanced oil recovery methods (Johnston, 1989).

The most obvious way to significantly enhance recovery efficiency of existing fields is to identify bypassed oil zones and conduct infill drilling. Reservoirs are much more heterogeneous than anybody likes to believe, leading to considerable uncertainty in reservoir description. Reservoir simulation based on this reservoir description could not give accurate predictions of reservoir performance even though it may be well matched to production data. We still do not know what is going on between the wells and how fluids migrate in reservoirs. In the past, reservoir engineers only resorted to dense drilling and extracting cores for information needed to determine the details of a reservoir's structure and its flow behaviour, an expensive and less efficient way. Today repeat or time-lapse seismic surveys in mature fields open a new avenue to track fluid flow and target these unswept zones. Recent successful examples in seismic monitoring of steam injection, water floods, CO₂ flood etc. (Jack, 1998) demonstrate a great potential for inferring reservoir conditions from seismic data.

Time-lapse seismic surveys are designed to investigate changes in reservoir conditions (saturation, pressure and temperature and sometimes porosity) due to production or/and injection by using seismic data. There are two closely connected steps involved in the application of this method. Rock physics is the basics, which relates reservoir conditions and other reservoir properties to the elasticity-anelasticity properties of reservoir rocks and consequently velocities and attenuation. The elasticity of a rock, if the rock is isotropic and homogeneous, includes only two independent elastic constants (e.g., bulk and shear moduli), which can be expressed as a function of the elastic constants of rock solid and pore fluids and the pore geometry, which vary with reservoir conditions. Anelasticity is determined by cracks and pore fluids, which also vary with reservoir conditions. Anelasticity is believed to vary much more than elasticity as a result of changes in reservoir conditions (Pros et al., 1962). The second step involves selecting the seismic attributes, which are most sensitive to changes in velocities and attenuation in response to changes in reservoir conditions. For example, when water displaces oil zones, P-velocity increases and S-velocity decreases if the rock is not too stiff. Accordingly, a reduced travel time to the reservoir bottom interface reflection can cause a pull-up on P-P seismic section. On P-S section, a pull-down is small due to a slight decrease in velocity. Moreover, an amplitude decrease on both the top and bottom of the reservoir can be observed, which may be greater at far offset. In addition, a change in effective pressure and fluid viscosity may result in enough change in attenuation for the change in the amplitude spectrum on the bottom reflection event to be seen.

Numerous theories and models exist in literature on elasticity-anelasticity properties of rocks. Wang and Nur (1991) and Toksoz and Johnston (1981) reviewed the important theories and models up to the publication dates. Despite

diversity of learning, it is widely accepted that the pore geometry is a major factor in determining the elastic moduli and attenuation. The spherical pores are most stable and have little effect on attenuation, while the cracks, despite being small in volume, may decrease the effective elastic moduli and attenuate seismic waves substantially. The existence of varying-shape pores and their role in determining the elastic moduli have been dealt with by many authors (Brace et al., 1972; Eshelby, 1957; Kuster and Toksoz, 1974; MacKenzie, 1949; Mavko and Nur, 1978; Sprunt and Brace, 1974; Timur et al., 1971; Walsh, 1965; and so on). Among these theories, Kuster-Toksoz model (KT model), which was derived based on scattering theory, is recognized as the most realistic and simplest one and thus used very often in the geophysical community. The assumption that pore geometry is simplified as a series of spheroids with varying pore aspect ratios (i.e., the pore aspect ratio spectrum) is a reasonable approximation to the reality in spite of the noninteracting limitation. The spheres represent relatively round pores, and the spheroids of very low aspect ratios are similar to cracks and grain contacts. The computation of the effective elastic moduli for a given pore aspect ratio spectrum is relatively easy. The inversion of the pore aspect ratio spectrum from the effective elastic moduli (derived from velocity measurements) is also fairly amenable to mathematical manipulation. Walsh (1966) formulated the problem of attenuation by frictional sliding (frictional dissipation). For random orientation of cracks, the Q values for compressional and shear waves were computed using the friction coefficient κ , effective Poisson's ratio σ , and rock solid and bulk rock moduli as parameters.

Fluid is another factor to determine the elastic moduli. According to the Gassmann equation, both the dry elastic moduli and porosity seem to be the most important parameters in the second term. In other words, the effect of fluids becomes more obvious at low dry elastic moduli and low porosity. These two factors, however, vary inversely with each other. The case of low dry elastic

moduli and low porosity cannot be expected in a general sense. Which factor dominates needs to be addressed. In addition, the fluid effect on the elastic moduli is frequency dependent. At high frequencies (a relative concept depending on pore geometry and permeability and fluid viscosity), the fluid seems stiffer and the Gassmann's equation is invalid. The proposition of the concept of the frequency-dependent effective fluid may solve the problem. The arithmetic averaging of the bulk moduli of fluids is an example of the application.

Fluid also has an impact on attenuation, which peaks at frequencies at which fluid relaxation (or pressure equilibrium) due to squirt flow (local and global flows) is reached. Relaxation time depends on pore geometry, permeability and fluid viscosity.

The third factor is the elastic moduli of rock solid, which lack the due attention among rock physicists. As a matter of fact, they are not easily obtained. Generally speaking, the theoretical models such as the Gassmann equation and KT model need the rock solid to be homogeneous and isotropic, which most rocks such as sandstones do not satisfy. Sandstones consist of various minerals. Quartz, a major sandstone-forming mineral, differs by as much as 40% in elastic moduli along the different crystallographic axes (Clark, 1966; Zimmerman, 1991). Other minerals such as feldspar, clay, calcite etc. are also anisotropic. The anisotropy and homogeneity pose a question of how accurately we can use these theoretical models.

Obviously, it is impossible to cover such a wide range of topics. This thesis deals with the factors to determine the elastic moduli with an emphasis on the pore geometry of sandstones. A pore geometrical model is proposed to interpret the elastic moduli of dry sandstones and their changes with effective

pressure. The effect of temperature on the dry elastic moduli is also discussed. The major factor that controls the impact of fluids on the fluid-saturated elastic moduli is investigated. Finally these rock physics principles are applied to evaluate the changes in velocities and acoustic impedance due to recovery processes and assess the feasibility of the Blackfoot oilfield.

CHAPTER 2

ELASTIC MODULI OF ROCKS

A medium is said to be elastic if it regains its original dimensions after the forces acting on it are removed, that is, the strains must be uniquely determined by the stresses and conversely. Furthermore, it is of linear elasticity if the strains are so small that the strains are in direct proportion to the stresses, which is modelled by Hooke's law. Rocks are generally considered to be elastic within the

range of moderate pressure changes. Pressure changes are considered moderate if they do not cause the opening of new cracks and the propagation of old cracks. The assumption of elasticity is not completely true because crack closing is never completely reversible (Gueguen and Palciauskas, 1994), as evidenced by hysteresis in the closure of a crack due to permanent damage to the crack surface (Scholz and Hickman, 1983). In the case of elastic wave propagation, rocks show linear elasticity as a result of small strain (less than 10^{-9} , Sheriff and Geldart, 1995) and Hooke's law is an adequate model. Accordingly, the elastic moduli, which model the linear stress-strain relation can be found. In the real world of seismology, however, seismic waves in the earth propagate in stressed rocks, and small strains due to wave motion are superimposed on the large strains due to gravitational and tectonic forces. This complex stress-strain relation was first addressed in the literature by Murnaghan (1937) and Birch (1938). Birch (1938) proposed that the elastic moduli at any initial state are determined by the relation of infinitesimal stresses and strains, which are superimposed on the large stresses and strains of that state, and he calculated the dependence of the elastic moduli of solids on the hydrostatic pressure. In other words, the elastic moduli at any initial state can be defined by the tangent moduli at that state in the stress-strain curves. This definition of the elastic moduli will be used throughout the thesis.

2.1 Effective medium theories

Rocks are often viewed as effective media since seismic wavelength is much longer than grain size. In other words, despite microscopic heterogeneity, rocks behave physically like a homogeneous continuous medium on the macroscopic scale. The elastic properties of the effective medium can be defined and calculated as the average elastic properties of a representative volume element. Intuitively, the elastic moduli of an effective medium depend on the elastic moduli of the constituents, their volume fractions and geometric

distributions over that representative volume element. The first approach to determining effective elastic moduli is direct calculation (Gueguen and Palciauskas, 1994). It calculates the elastic moduli by dividing volume-averaged stress by volume-averaged strain as follows:

$$M = S / \varepsilon \quad 2.1$$

where M is the effective elastic moduli. S and ε are averages of stresses and strains, respectively, over the representative volume element. Let $C_1, C_2, C_3, \dots, C_n$ represent the volume fractions of n constituents, $M_1, M_2, M_3, \dots, M_n$ their respective elastic moduli, $S_1, S_2, S_3, \dots, S_n$ their respective stresses and $\varepsilon_1, \varepsilon_2, \varepsilon_3, \dots, \varepsilon_n$ their respective strains. Equation 2.1 can be rewritten as:

$$\begin{aligned} M &= S / \varepsilon \\ &= (C_1 S_1 + C_2 S_2 + C_3 S_3 + \dots + C_n S_n) / \varepsilon \\ &= C_1 S_1 / \varepsilon + C_2 S_2 / \varepsilon + C_3 S_3 / \varepsilon + \dots + C_n S_n / \varepsilon \\ &= (C_1 M_1)(\varepsilon_1 / \varepsilon) + (C_2 M_2)(\varepsilon_2 / \varepsilon) + (C_3 M_3)(\varepsilon_3 / \varepsilon) \\ &\quad + \dots + C_n M_n)(\varepsilon_n / \varepsilon) \end{aligned} \quad 2.2$$

The terms $\varepsilon_1 / \varepsilon, \varepsilon_2 / \varepsilon, \varepsilon_3 / \varepsilon, \dots, \varepsilon_n / \varepsilon$ require a precise geometric model for the distribution of constituents. If it is unavailable, the best way we can do is to find the upper and lower bounds by assuming some ideal cases.

If the strain is constant over all constituents as indicated by Fig 2.1, then $\varepsilon_1 / \varepsilon = 1, \varepsilon_2 / \varepsilon = 1, \varepsilon_3 / \varepsilon = 1, \dots, \varepsilon_n / \varepsilon = 1$ and the effective elastic moduli become arithmetic average. This model of isostrain was first proposed first by Voigt (1928); it is called Voigt's model.

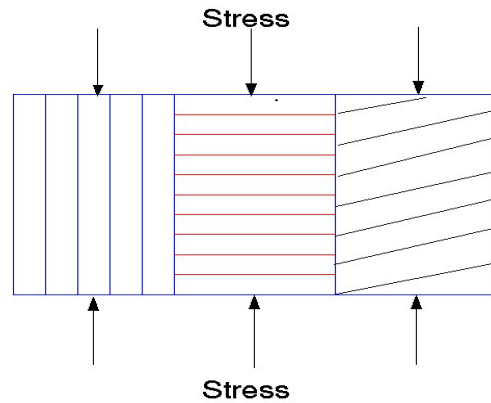


Figure 2.1 Model of isostrain (Voigt)

The equation with the arithmetic average is as follows:

$$M = C_1M_1 + C_2M_2 + C_3M_3 + \dots + C_nM_n \quad 2.3$$

Rewrite equation 2.2 as follows:

$$\begin{aligned} 1 / M &= \varepsilon / S \\ &= (C_1\varepsilon_1 + C_2\varepsilon_2 + C_3\varepsilon_3 + \dots + C_n\varepsilon_n) / S \\ &= C_1\varepsilon_1 / S + C_2\varepsilon_2 / S + C_3\varepsilon_3 / S + \dots + C_n\varepsilon_n / S \\ &= (C_1/M_1)(S_1/S) + (C_2/M_2)(S_2/S) + (C_3/M_3)(S_3/S) \\ &\quad + \dots + (C_n/M_n)(S_n/S) \end{aligned} \quad 2.4$$

According to equation 2.4, if the stress is constant over all constituents as demonstrated by Fig. 2.2, then $S_1 / S = 1$, $S_2 / S = 1$, $S_3 / S = 1$, ..., $S_n / S = 1$ and the effective elastic moduli are the harmonic average for all constituents.

Reuss (1929) proposed this model of isostress, which was then called Reuss's model afterwards.

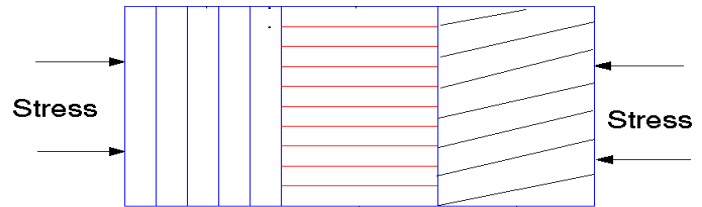


Figure 2.2 Model of isostress (Reuss)

The equation with the harmonic average is as follows:

$$1 / M = C_1/M_1 + C_2/M_2 + C_3/M_3 + \dots + C_n/M_n \quad 2.5$$

Wood (1941) derived the same result when he studied wave propagation in a physical mixture of liquids or liquids plus solid particles. The model can be

applied to uncompacted sediments (no physical contact, or in suspension state). Once sediments are contacted, they have non-zero shear rigidity and non-equal pressure distribution, and it is no longer valid.

It can be shown that M_V calculated from Voigt's model is the upper bound for the average value and M_R calculated from Reuss's model is the lower bound for the average value ($M_V > M_R$). Thus, Hill (1952) averaged them in an attempt to derive a better approximation:

$$M = (M_V + M_R) / 2 \quad 2.6$$

$$(M_V > M > M_R)$$

Equation 2.6 is named VRH model after Voigt, Reuss and Hill. The major usefulness of these models is their simplicity. However, if the magnitude of the elastic moduli of constituents differs significantly, the bounds provided by the models may be too large to be useful.

As mentioned above, the accurate calculation needs the precise geometric details. However, the geometry is never known and there are also mathematical difficulties in computation. So equation 2.2 must be restricted to simple models. In a general, two phases are only considered with one phase in the form of particles embedded in the second matrix phase. The simplest case is dilute concentration of spherical and ellipsoidal particles of constituent 2 in matrix 1 (Hashin, 1983). The definition of "dilute" is that the state of strain in any one particle in the effective medium under homogeneous boundary conditions is not affected by the other particles. Thus the strain is that of a single particle in an infinite body.

Rewrite equation 2.2 as:

$$M = S / \varepsilon$$

$$\begin{aligned}
&= (C_1 M_1)(\varepsilon_1 / \varepsilon) + (C_2 M_2)(\varepsilon_2 / \varepsilon) \\
&= (C_1 \varepsilon_1) M_1 / \varepsilon + (C_2 \varepsilon_2) M_2 / \varepsilon \\
&= M_1(\varepsilon - C_2 \varepsilon_2) / \varepsilon + (C_2 M_2)(\varepsilon_2 / \varepsilon) \\
&= M_1 + (M_2 - M_1) C_2 (\varepsilon_2 / \varepsilon) \quad 2.7
\end{aligned}$$

For spherical particles, $\varepsilon_2 / \varepsilon$ are (Hashin, 1983; Landau and Lifshitz, 1967):

$$\left(\frac{\varepsilon_2}{\varepsilon}\right)_v = \frac{3K_1 + 4\mu_1}{3K_2 + 4\mu_1} \quad 2.8$$

$$\left(\frac{\varepsilon_2}{\varepsilon}\right)_s = \frac{5(3K_1 + 4\mu_1)}{9K_1 + 8\mu_1 + 6(K_1 + 2\mu_1)\mu_2/\mu_1} \quad 2.9$$

where $(\varepsilon_2 / \varepsilon)_v$ and $(\varepsilon_2 / \varepsilon)_s$ are volume strain and shear strain respectively, K_1, K_2, μ_1, μ_2 are bulk moduli and shear moduli for matrix 1 and constituent 2 respectively. Substituting 2.8 and 2.9 into 2.7 results in:

$$K = K_1 + (K_2 - K_1) C_2 \frac{3K_1 + 4\mu_1}{3K_2 + 4\mu_1} \quad 2.10$$

$$\mu = \mu_1 + (\mu_2 - \mu_1) C_2 \frac{5(3K_1 + 4\mu_1)}{9K_1 + 8\mu_1 + 6(K_1 + 2\mu_1)\mu_2/\mu_1} \quad 2.11$$

In the case of rocks, equations 2.10 and 2.11 can be simplified as:

$$K = K_s + (K_f - K_s) \phi \frac{3K_s + 4\mu_s}{3K_f + 4\mu_s} \quad 2.12$$

$$\mu = \mu_s - \mu_s \phi \frac{5(3K_s + 4\mu_s)}{9K_s + 8\mu_s} \quad 2.13$$

where K_s and μ_s are the bulk and shear moduli of rock solid, K_f is the fluid bulk modulus and ϕ is porosity. If pore space in rocks is empty, equation 2-12 is further simplified into:

$$K = K_s - K_s \phi \frac{3K_s + 4\mu_s}{4\mu_s} \quad 2.14$$

For randomly oriented ellipsoidal particles, much more complicated expressions were given by Eshelby (1957).

Strictly speaking, equations 2.12 and 2.13 are not always valid since rocks do not always satisfy the assumption of dilute concentration. In other words, porosity is not small and the interactions between pores (particles) are not negligible. We introduce self-consistent methods to take into account these complexities. Assume that a small amount of constituent 2 is embedded into a medium that has the properties of the effective medium (K and μ) instead of matrix 1 (K_1 and μ_1). So equations 2.8 and 2.9 are modified as:

$$\left(\frac{\varepsilon_2}{\varepsilon}\right)_v = \frac{3K + 4\mu}{3K_2 + 4\mu} \quad 2.15$$

$$\left(\frac{\varepsilon_2}{\varepsilon}\right)_s = \frac{5(3K + 4\mu)}{9K + 8\mu + 6(K + 2\mu)\mu_2/\mu} \quad 2.16$$

By considering that constituent 2 is imbedded into the effective medium rather than matrix 1, one takes into account the interaction between pores (particles). Thus, equations 2.15 and 2.16 should be a better approximation than equations 2.8 and 2.9. Substituting equations 2.15 and 2.16 into equation 2.7 leads to two coupled equations with two unknowns (K and μ), which can be solved consistently. Another way to satisfy the assumption of dilute concentration is to

add a few pores at a time and calculate the effective elastic moduli. The effective elastic moduli computed from the previous step are used as the elastic moduli of rock solid or matrix to calculate the new effective elastic moduli for the next set of pores. The process is repeated until all pores are introduced.

Another approach is to derive the compressibility (or bulk modulus) of the effective medium based on the rate of change of pore volume. Suppose that pore space is empty and let V , V_p represent the volumes of the representative volume element and its pore space, respectively, P be applied external pressure, C , C_s be the compressibilities of the effective medium and rock solid respectively, and ϕ be the porosity. The compressibility of rock solid can be expressed as (see APPENDIX D for detailed derivation):

$$d(V - V_p) = -C_s V dP \quad 2.17$$

Dividing two sides by $-V dP$ and reorganizing it give:

$$-(1/V) (dV/dP) = C_s - (dV_p/V)/dP \quad 2.18$$

The left side of equation 2.18 is the definition of effective medium compressibility, and dV_p / V on the right is $d\phi$ if dV_p is small. Rewriting equation 2.18 leads to:

$$C = C_s - d\phi/dP \quad 2.19$$

Equation 2.19 is the general expression of effective medium calculation regardless of pore shape and the magnitude of porosity. However, in order to find $d\phi/dP$, dilute concentration of pores still needs to be assumed. For spherical pores, we have the following expression (equation A7 in Appendix A):

$$C = C_s \left(1 + \frac{3}{2} \frac{1 - \nu_s}{1 - 2\nu_s} \frac{\phi}{1 - \phi} \right) \quad 2.20$$

where C is the effective compressibility and ν_s is Poisson's ratio of rock solid. In terms of the bulk modulus, we have (equations A.8 and A.9 in Appendix A):

$$K = 2K_s \frac{(1 - 2\nu_s)/(1 + \nu_s)}{2(1 - 2\nu_s)/(1 + \nu_s) + \phi} (1 - \phi) \quad 2.21$$

or

$$K = K_s - K_s \phi \frac{4/3\mu_s + K_s}{4/3\mu_s + K_s \phi} \quad 2.22$$

For a dilute set of pores, ϕ is small and $4/3\mu_s \gg K_s \phi$. We can drop the term $K_s \phi$ so that equation 2.22 is almost identical to equation 2.14, indicating the two approaches are equivalent.

For penny-shaped cracks of average half length c_{ave} in the average region volume v_{ave} , another expression can be derived from equation 2.18 (equation A.15 in APPENDIX A):

$$C = C_s \left(1 + \frac{16}{9} \frac{1 - \nu_s^2}{1 - 2\nu_s} \frac{c_{ave}^3}{v_{ave}} \right) \quad 2.23$$

The effect of pore shape on compressibility can be illustrated by comparison of spherical pores and cracks. If we assume that all spherical pores have the average radius r_{ave} in the average region volume v_{ave} , equation 2.20 can be rewritten:

$$\begin{aligned}
C &= C_s \left(1 + \frac{3}{2} \frac{1 - \nu_s}{1 - 2\nu_s} \frac{V_p/V}{1 - V_p/V} \right) \\
&\cong C_s \left(1 + \frac{3}{2} \frac{1 - \nu_s}{1 - 2\nu_s} \frac{V_p}{V} \right) \\
&= C_s \left(1 + \frac{3}{2} \frac{1 - \nu_s}{1 - 2\nu_s} \frac{V_{p,ave}}{V_{ave}} \right) \\
&= C_s \left(1 + 2\pi \frac{1 - \nu_s}{1 - 2\nu_s} \frac{r_{ave}^3}{V_{ave}} \right)
\end{aligned} \tag{2.24}$$

Equation 2.24 is similar to equation 2.23. By evaluating various values of the Poisson's ratio, we found that the coefficient of the last term in 2.24 is two to three times that of equation 2.23. In other words, the effect of a crack on compressibility equals the effect of a sphere with a diameter roughly two-thirds the length of the crack. However, the porosity of two cases differs enormously. The result demonstrates that the compressibility of cracks is enormously larger than that of spherical pores. So cracks can decrease the bulk moduli considerably in spite of being small in volume.

KT model is the effective medium theory based on scattering theory (Kuster and Toksoz, 1974). It also needs the assumption of dilute concentration of spherical and spheroidal pores, but this limitation may be relaxed to some degree in the practical application. The formulae and calculation will be detailed in the following chapter.

Other approaches include applying the extremum principles of minimum potential and minimum complementary energy to set lower and upper bounds (Hashin and Shtrikman, 1963) and contact theories (Love, 1944; Mindlin, 1949) etc.

2.2 Elastic moduli and densities of rock solid

As discussed above, an effective medium is generally assumed to be composed of a pore phase and a solid phase. The pore phase is a population of pores of specified shapes dispersed in rock solid. The elastic moduli of the effective medium are determined by the elastic moduli of rock solid and the pore fluid and the pore geometry (pore shapes and their respective concentration). The section focuses on the elastic moduli of rock solid.

The rock solid is an aggregate of minerals, whose elastic moduli and densities are listed in Table 2.1. Given mineral compositions, the elastic moduli of rock solid may be calculated using VRH model or HS model. But the location of low-elastic-moduli minerals has a considerable impact on calculation. Other two new methods for calculation of the elastic moduli of rock solid will be proposed in Chapters 3 and 6.

Table 2.1 Elastic moduli and densities of major rock-forming minerals

Minerals	K (bulk modulus, GPa)	μ (shear modulus, GPa)	Density (g/cm ³)	References
Quartz	37.88	44.31	2.65	Carmichael, 1989
Feldspar	61.98	29.62	2.65	Carmichael, 1989
Shale*	24.46	18.82	2.68	Touloukian et al., 1981
Gulf clay	23	8	2.55	After Mavko et al., 1998
Clay quartz	39	33	2.65	Mavko et al., 1998

Muscovite	51.9	30.9	2.79	Carmichael, 1989
Calcite	70.2	29.0	2.71	Mavko et al., 1998
Dolomite	69.4	51.6	2.88	Mavko et al., 1998
Siderite	123.7	51.0	3.96	Mavko et al., 1998
Anhydrite	56.1	29.1	2.98	Mavko et al., 1998
Aragonite	44.8	38.8	2.92	Mavko et al., 1998
Halite	24.8	14.9	2.16	Mavko et al., 1998
Kerogen	2.9	2.7	1.3	Mavko et al., 1998

*The elastic moduli are obtained from the shale of 1% porosity

The pressure dependence of the elastic moduli of rock solid is small. For quartz, dK/dP is 0.00957 GPa/MPa and $d\mu/dP$ is 0.00043 GPa/MPa (Carmichael, 1989). In the following chapters, we will find that the pressure dependence of the dry elastic moduli is much higher than that of rock solid. No experimental results are available for the temperature dependence of these moduli, but it may be on the order of $(1-9) \cdot 10^{-3}$ GPa/ $^{\circ}\text{C}$ (after Carmichael, 1989). Thus, the change of the elastic moduli of rock solid with pressure and temperature is generally neglected in calculation.

As shown in Table 2.1, the densities of the minerals that constitute most sedimentary rocks fall in a relatively narrow range of about 7% (except halite, kerogen, siderite) (Sheriff and Geldart, 1995). Variation in porosity is the major reason that rocks vary in density.

2.3 Elastic moduli and densities of fluids

There are three reservoir fluids: water, oil and gas. The bulk moduli and densities of these fluids depend on the compositions, temperature and pressure.

2.3.1 Water Most sandstone reservoirs are preferentially water-wet, with irreducible water (or connate water) saturation in the range of 10-50% (25% on average) (Smith et al., 1992). It is a most common reservoir fluid. Wave propagation in water has been studied extensively, and a vast amount of acoustic data is available (e.g., Carmichael, 1989; Spiesberger and Metzger, 1991). Batzle and Wang (1992) present formulae to calculate seismic velocities of pure water (to 100 °C and about 100 MPa) and brine as follows:

$$V_w = \sum_{i=0}^4 \sum_{j=0}^3 W_{ij} T^i P^j \quad 2.25$$

where V_w is pure water velocity (m/s), T and P are temperature (°C) and pressure (MPa) respectively, W_{ij} are constants given in Table 2.2

$$V_B = V_W + S(1170 - 9.6T + 0.055T^2 - 8.5 \cdot 10^{-5} T^3 + 2.6P - 0.0029TP - 0.0476P^2) + S^{1.5} (780 - 10P + 0.16 P^2) - 820 S^2 \quad 2.26$$

where V_B is brine velocity (m/s), S is salinity (ppm). Given density (ρ), the bulk modulus of water can be calculated:

$$K_w = \rho V_B^2 \quad 2.27$$

Table 2.2 Coefficients for water properties computation

$W_{00} = 1402.85$	$W_{01} = 1.524$	$W_{02} = 3.437 \cdot 10^{-3}$	$W_{03} = -1.197 \cdot 10^{-5}$
--------------------	------------------	--------------------------------	---------------------------------

$W_{10} = 4.871$	$W_{11} = -0.0111$	$W_{12} = 1.739 * 10^{-4}$	$W_{13} = -1.628 * 10^{-6}$
$W_{20} = -0.04783$	$W_{21} = 2.747 * 10^{-4}$	$W_{22} = -2.135 * 10^{-6}$	$W_{23} = 1.237 * 10^{-8}$
$W_{30} = 1.487 * 10^{-4}$	$W_{31} = -6.503 * 10^{-7}$	$W_{32} = -1.455 * 10^{-8}$	$W_{33} = 1.327 * 10^{-10}$
$W_{40} = -2.197 * 10^{-7}$	$W_{41} = 7.987 * 10^{-10}$	$W_{42} = 5.230 * 10^{-11}$	$W_{43} = -4.614 * 10^{-13}$

Similarly, the expressions for the densities of brine and pure water are:

$$\rho_b = \rho_w + S\{0.668 + 0.44S + 1 * 10^{-6}[300P - 2400PS + T(80 + 3T - 3300S - 13P + 47PS)]\} \quad 2.28$$

$$\rho_w = 1 + 1 * 10^{-6}(-80T - 3.3 * T^2 + 0.00175 T^3 + 489P - 2TP + 0.016T^2 P - 1.3 * 10^{-5}T^3P - 0.333P^2 - 0.002TP^2) \quad 2.29$$

where ρ_b and ρ_w are the densities of water and brine in g/cm³, S is the weight fraction (ppm) of sodium chloride, P and T are in MPa and °C (Batzle and Wang, 1992). Equation 2.28 is limited to sodium chloride solutions and can vary when other mineral salts are present.

2.3.2 Oil Oil consists chiefly of hydrocarbons, which vary in carbon number. Light oil, a mixture of hydrocarbons of low carbon number, can dissolve large quantities of hydrocarbon gases, which significantly decrease the modulus. Heavy oil contains heavy hydrocarbons and viscous bitumen. Bitumen can be stiffer and denser than water. Oil is characterized by the parameters, API, R_{so} , B_o and γ_g . API is the American Petroleum Institute oil gravity number, defined as

$$API = 141.5 / \gamma_o - 131.5 \quad 2.30$$

where γ_o is the ratio of the oil density to water density at standard conditions. R_{so} is the ratio of the volume of solution gas to that of oil at standard conditions; B_o is the ratio of the volume of oil at reservoir conditions to that of the oil at standard conditions. γ_g is specific gravity of gas. Vazquez and Beggs (1980) proposed a relationship to compute the bulk modulus of oil above bubble point pressure:

$$K_o = 10^2 P / (-1433.0 + 5.0R_{so} + 17.2T - 1180.0\gamma_g + 12.61API) \quad 2.31$$

where K is in GPa, P is reservoir pressure in MPa, R_{so} is solution gas ratio, scf/STB, at bubble point pressure, T is reservoir temperature in °F, γ_g is specific gravity of separator gas at separator pressure of 100 psig, and API is gravity number of stock-tank oil in °API.

The density of oil is more dependent on temperature than pressure. The relation can be described as (Batzle and Wang, 1992):

$$\rho_p = \rho_0 + (0.00277P - 1.71 \cdot 10^{-7} P^3)(\rho_0 - 1.15)^2 + 3.49 \cdot 10^4 P \quad 2.32$$

$$\rho_o = \rho_p / [0.972 + 3.81 \cdot 10^{-4} (T + 17.78)^{1.175}] \quad 2.33$$

where ρ_o and ρ_0 are the densities of oil at formation (P and T) and standard conditions, P and T are in MPa and °C. Equations 2.32 and 2.33 assume that the composition of the oil is unchanged, exception for gas dissolving in oil at elevated pressure and temperature.

With gas dissolving in oil, the density can be calculated according to mass balance as follows:

$$\rho_o = \frac{\rho_o^{std} + R_{so}^{std} \rho_G^{std}}{B_o} \quad 2.34$$

where ρ_G^{std} and ρ_o^{std} are the densities of gas and oil at standard conditions, B_o and R_{so} are the oil formation volume factor and solution gas oil ratio at reservoir pressure and temperature.

2.3.3 Gas The isothermal compressibility of gas is (see APPENDIX B for derivation):

$$C_g = \frac{1}{P} - \frac{1}{Z} \frac{\partial Z}{\partial P} \quad 2.35$$

where P is pressure and Z is the compressibility factors or gas deviation factors.

The process of wave propagation in a gas is adiabatic not isothermal. In most solid materials, the difference between the isothermal and adiabatic compressibilities is negligible. However, due to the larger coefficient of thermal expansion in gas, the temperature changes associated with the compression and dilatation of an acoustic wave have a substantial effect. Adiabatic compressibility is related to isothermal compressibility through γ , the ratio of heat capacity at constant pressure to heat capacity at constant volume (Batzle and Wang, 1992). Thus the adiabatic compressibility of gas can be expressed as:

$$C_g = \left(\frac{1}{P} - \frac{1}{Z} \frac{\partial Z}{\partial P} \right) / \gamma \quad 2.36$$

The inverse of equation 2.36 is the bulk modulus:

$$K_g = \frac{\gamma P}{\left(1 - \frac{1}{Z} \frac{\partial Z}{\partial P} \right)} \quad 2.37$$

Equation 2.37 has three parameters (γ , Z and $\partial Z/\partial P$), which depend on pressure and temperature. The shapes of the isotherms of compressibility factors Z for nearly all real gases are similar, which leads to the development of the Law of Corresponding States. It states that all pure gases have the same z -factor at the same values of reduced pressure and reduced temperature (McCain, 1990). Reduced pressure and reduced temperature are defined as:

$$P_r = P / P_c \text{ and } T_r = T / T_c \quad 2.38$$

where P_c and T_c refer to the critical pressure and critical temperature respectively. The law has been extended to cover mixtures of closely related pure gases, in which case P_{pc} and T_{pc} , called pseudocritical pressure and temperature, are used instead of P_c and T_c . Therefore P_r and T_r are replaced by P_{pr} ($=P / P_{pc}$) and T_{pr} ($=T / T_{pc}$), pseudoreduced pressure and pseudoreduced temperature, respectively (McCain, 1990). Z is related to P_{pr} and T_{pr} by (Batzle and Wang, 1992)

$$Z = [0.03 + 0.00527(3.5 - T_{pr})^3]P_{pr} + (0.642T_{pr} - 0.007T_{pr}^4 - 0.52) + E \quad 2.39$$

where

$$E = 0.109(3.85 - T_{pr})^2 \exp\{- [0.45 + 8(0.56 - 1/T_{pr})^2]P_{pr}^{1.2} / T_{pr}\} \quad 2.40$$

Thomas et al. (1970) found a simple relationship between γ_g (the ratio of the gas density to air density at standard conditions) and P_{pr} , T_{pr} :

$$P_{pr} = P/P_{pc} = P/(4.892 - 0.4048 \gamma_g) \quad 2.41$$

$$T_{pr} = P/T_{pc} = T/(94.72 + 170.75 \gamma_g) \quad 2.42$$

where P is in MPa and T is in absolute temperature [$T=T(^{\circ}\text{C})+273.15$]. The parameter γ can be estimated as (Batzle and Wang, 1992):

$$\gamma = 0.85 + 5.6/(P_{pr} + 2) + 27.1/(P_{pr} + 3.5)^2 - 8.7 \exp[-0.65(P_{pr} + 1)] \quad 2.43$$

Therefore the bulk modulus of gas can be expressed as:

$$K_g = \frac{\gamma P}{\left(1 - \frac{P_{pr}}{Z} \frac{\partial Z}{\partial P_{pr}}\right)} \quad 2.44$$

where $\partial Z/\partial P_{pr}$ can be obtained from equations 2.39 and 2.40. In addition, Batzle and Wang (1992) also derived the expression of gas densities based on Thomas' work (1970):

$$\rho_g \cong \frac{28.8 \gamma_g P}{ZRT} \quad 2.45$$

In summary, if gas specific gravity and reservoir pressure and temperature are given, we can calculate P_{pr} and T_{pr} , which are used to calculate γ , Z and $\partial Z/\partial P_{pr}$, then K_g .

2.4 Frequency dependence of the elastic moduli of fluid-saturated rocks

Fluid is a factor to affect the effective elastic moduli but its impact is limited to the rocks of low dry elastic moduli, which will be detailed in Chapter 6. This section will discuss the frequency dependence of the fluid effect.

If pores of varying shapes in rocks, as assumed in the simple case for theoretical calculations, are small and noninteracting, fluids are trapped inside these pores without relative motion and frequency does not affect the elastic behaviour of fluids. In reality, pores in reservoir rocks are connected, enabling fluid movement to take place in response to the movement of the solid framework and stress change caused by the passing of a seismic wave. Three kinds of relative movements in connected pores exist: 1) relative movement at high frequencies along the direction of wave propagation because inertia causes the fluid motion to lag behind that of the solid framework; 2) local flow perpendicular to the direction of wave propagation, with fluids moving out of or into cracks induced due to pore-scale pressure gradients; 3) global flow in the same direction as the local flow, resulting from saturation heterogeneity or patchy saturation on a coarse scale. At low frequencies, there is no relative motion along the direction of wave propagation because the motion of the solid framework and fluids is coupled by viscous friction, and the local and global flows have enough time to equilibrate the pressure distribution. At high frequencies, however, the movement of the solid framework and fluids are decoupled, and the local and global flows do not have enough time to reach a fluid pressure equilibrium at half period. The movement of fluids out of phase with the solid framework and the unrelaxed state of fluids always lead to a stiffer rock and higher velocity. Velocity dependence on frequency is called velocity dispersion. In the following, we will discuss the effect of frequencies on the elastic behaviour of fluids.

2.4.1 Gassmann's equation

If the fluid keeps in equilibrium during the process of deformation, we can derive the bulk modulus of a fluid-saturated rock from the bulk modulus of its corresponding dry rock as follows (see APPENDIX C for detailed derivation):

$$K = K_d + \frac{(1 - \frac{K_d}{K_s})^2}{\frac{\phi}{K_f} + \frac{1 - \phi}{K_s} - \frac{K_d}{K_s^2}} \quad 2.46$$

where K , K_d , K_f and K_s are the bulk modulus of the fluid-saturated rock, dry rock, fluid and rock solid, respectively, and ϕ is porosity. Equation 2.46 is the well-known Gassmann's equation. The model assumes fluid pressure equilibrium, which is satisfied when the seismic frequency is low enough that local and global flows can equilibrate the pressure distribution over all fluid phases. It is called the low or zero-frequency model. Note that in the derivation we use K_f , the effective bulk modulus of the pore fluid mixture. Under the condition of fluid pressure equilibrium, K_f can be calculated using the harmonic average (Wood's or Reuss's model).

2.4.2 Global-flow dispersion

If the pressure equilibrium between the different fluid phases cannot be reached due to coarse-scale saturation heterogeneity (patchy saturation), the harmonic average is no longer a valid method for calculating the effective bulk

modulus of the fluid mixture. It can be shown that for well-consolidated rocks the volume weighted arithmetic average of the fluid phases is the appropriate fluid bulk modulus for the Gassmann's equation (Mavko and Mukerji, 1998, see APPENDIX E for proof).

Mavko and Mukerji (1998) has shown that, for Massilon sandstone (soft rock), the fluid bulk modulus approximated with the arithmetic average always overestimates the bulk modulus of the fluid-saturated rock while, for Estailades limestone (stiff rock), the arithmetic average does a good job of estimating the fluid modulus.

2.4.3 Local-flow dispersion

At high frequencies the pressure equilibrium cannot be reached on grain scale between soft cracks and stiff pores. It is not appropriate to calculate the bulk modulus of the fluid-saturated rock just by bringing the bulk modulus of the fluid (one fluid assumed in the pore space) into the Gassmann's equation. So far, there has been no theoretical model to compute the bulk modulus of the effective fluid, which depends on seismic frequency, pore geometry, permeability and fluid viscosity. Here we only give a qualitative discussion.

When a wave propagates, it deforms rock, resulting in pressure changes in fluid. Spherical pores are less compressible, tending to shelter the contained fluid and therefore having relatively less pressure changes, while compliant cracks are more compressible, tending to transfer more of the stress change to the pore fluid and therefore having relatively more pressure change (after Mavko and Jizba,

1991; Wang and Nur, 1991). This phenomenon can be illustrated with the following formula:

$$\Delta S = \Delta \sigma + \Delta P \quad 2.47$$

where ΔS is the total stress increment, $\Delta \sigma$ is the effective stress increment, and ΔP is the fluid pressure increment.

When stress is applied, pores are deformed. If ΔS is the same, spherical pores have more change in σ and less change in P than flat cracks due to the lower compressibility, and more change in fluid pressure occurs in flat cracks. This case is independent of ΔS being compressive or extensive. If ΔS is compressive, fluid pressure in flat cracks will increase more than that in spherical pores; if ΔS is extensive, fluid pressure in flat cracks will decrease more than that in spherical pores.

It is the pressure difference between spherical pores and flat cracks that leads to grain-scale fluid movement called local flow. If frequencies are high, the fluid cannot reach pressure equilibrium within a half period. The fluid within cracks maintains a higher or lower pressure, depending on whether ΔS is compressive or extensive. The higher or lower fluid pressure resists further crack deformation by ΔS and cracks become stiffer. If frequencies are low, the fluid has enough time to reach pressure equilibrium and ΔS continues to deform cracks, resulting in softer cracks. It is noted that spherical pores go the opposite, i.e., softer at high frequencies and stiffer at low frequencies. Cracks, however, contribute much more strain to the whole rock's due to the high compressibility. The end results are chiefly affected by the behaviour of cracks. To summarize:

$$\begin{aligned} \text{Compressive: } \Delta \sigma &= \Delta S - \Delta P, \quad \Delta P (\text{high frequency}) > \Delta P (\text{low frequency}) \rightarrow \\ &\Delta \sigma (\text{high frequency}) < \Delta \sigma (\text{low frequency}) \rightarrow \end{aligned}$$

$$\Delta V(\text{high frequency}) < \Delta V(\text{low frequency}) \rightarrow$$

$$M(\text{high frequency}) > M(\text{low frequency}) \rightarrow$$

$$\text{Vel}(\text{high frequency}) > \text{Vel}(\text{low frequency})$$

$$\text{Extensive: } -\Delta\sigma = -\Delta S + \Delta P, \quad \Delta P(\text{high frequency}) > \Delta P(\text{low frequency}) \rightarrow$$

$$|-\Delta\sigma|(\text{high frequency}) < |-\Delta\sigma|(\text{low frequency}) \rightarrow$$

$$|-\Delta V|(\text{high frequency}) < |-\Delta V|(\text{low frequency}) \rightarrow$$

$$M(\text{high frequency}) > M(\text{low frequency}) \rightarrow$$

$$\text{Vel}(\text{high frequency}) > \text{Vel}(\text{low frequency})$$

where ΔV is volume change, M is the elastic modulus of rock, and Vel is the velocity of rock. Thus velocity depends on frequency. The higher frequency, the larger elastic modulus and the higher velocities.

The local flow mechanism was introduced by Biot (1962), O'Connell and Budiansky (1974) and Mavko and Nur (1979), and regarded as a major contribution to velocity dispersion by Dvorkin et al. (1994), Murphy (1982, 1984 a,b), Murphy III et al. (1986), Tittmann et al. (1984), Wang and Nur (1990) and Winkler and Nur (1979). Akbar et al. (1994) defined the unit of local flow and its length (i.e., characteristic length), which Dvorkin et al. (1994) considered a fundamental property that doesn't depend on frequency, fluid viscosity or compressibility and can be determined experimentally. At a given frequency, the length, in which local flow can equilibrate, is based on a diffusivity constant:

$$L = [\kappa / (\phi \eta C_t f)]^{0.5} \quad 2.48$$

where κ and ϕ are the permeability and porosity of flat cracks respectively, η is fluid viscosity, C_t is compressibility [$C_t = C(\text{fluid compressibility}) + C_f(\text{pore volume}$

compressibility)] and f is wave frequency (after Craft and Hawkins, 1991). If the characteristic length is small, and shorter than L , fluid pressure will reach equilibrium and therefore no dispersion occurs. This case happens to well-rounded and well-sorted sandstones or rocks at high effective pressure. The theory has been verified with no local-flow dispersion showed for glass beads (Winkler, 1985). Winkler (1986) also found velocity dispersion decreasing with elevated effective pressure. If the characteristic length is big, and longer than L , fluid pressure will be in non-equilibrium, leading to stiffer rock and higher velocity, i.e., dispersion. This case is often observed at ultrasonic frequency in velocity measurements (Winkler 1985, 1986; Wang and Nur, 1990).

Local flow is further complicated by saturation heterogeneity on grain scale. If the characteristic length is small or wave frequency is low, fluid pressure tends to be equilibrated regardless of uneven fluid distribution in pores of different shapes. In this case, the bulk modulus of the effective fluid can be modeled with Wood's equation (1941) and the bulk modulus of the fluid-saturated rock can be calculated using Gassmann equation (1951) as discussed in section 2.4.1. If the characteristic length is big or wave frequency is high, however, the bulk modulus of the rock depends entirely on detailed fluid distribution in pores of different shapes. In laboratory, Knight and Nolen-Hoeksema(1990) observed during imbibition velocity changes with water saturation, which is very similar to Domenico effect (1974). Before the critical water saturation (a saturation beyond which velocity begins to increase quickly), water absorbs along the pore wall and grows layer by layer with increasing water saturation, and gas forms a continuous network going through all pores of different shapes. The effective bulk modulus of fluids increases with increasing water saturation. But the density of fluids increases with a rate higher than the increase in the effective bulk modulus of fluids. The end result is velocity decrease with water saturation increasing. This scenario has been modelled by

Endres and Knight (1989). The local flow is less active due to the fluid pressure difference between spherical pores and cracks being minimal for high-compressibility gas. Beyond the critical saturation, water fills fully thin pores. The absence of gas in cracks can cause significant change in the bulk modulus. At low frequencies or for rocks of low characteristic length, fluid pressure equilibrium is reached, i.e., the compressibility is still controlled by gas according to the Wood's equation. However, at high frequency, local flow can't equilibrate fluid pressure, and water in cracks is unrelaxed, resulting in an increase of the bulk modulus and velocity.

In water-wet rocks, very thin cracks are occupied by water, and oil and gas stay in large pores. We can calculate the diffusivity constant assuming the following parameters.

$$K=1(\text{MD})=10^{-15}(\text{m}^2), \phi=0.001(\text{only consider cracks}), \eta=1(\text{cp})=10^{-3}(\text{Pa}\cdot\text{S})$$

$$C_t=C + C_f = 10^{-9}/2.3 + 10^{-10}/10/0.001 = 1.04*10^{-8}(1/\text{Pa}), f = 100 \text{ Hz}$$

Using equation 2.48, L can be calculated as:

$$L = [10^{-15}/(0.001*10^{-3} * 1.04*10^{-8} * 100)]^{0.5} = 0.031 \text{ (m)} = 3.1 \text{ (cm)}$$

Obviously the number exceeds the characteristic length (on the order of millimeter, Dvorkin and Nur, 1993), implying the fluid pressure always in equilibrium. This result indicates that no dispersion due to local flow will occur within seismic frequencies. At ultrasonic frequencies (e.g. 1mHz) in laboratory, however, L is only 0.031 cm, smaller than the characteristic length. Accordingly, local flow cannot equilibrate the fluid pressure distribution.

2.4.4 Biot's flow dispersion

At very high frequencies, the motion of the solid framework and fluids are decoupled and velocity dispersion happens. Biot (a and b, 1956) developed a model covering a full range of frequencies. The characteristic frequency f_c , which divides the high and low frequency, is defined as:

$$f_c = \frac{\eta\phi}{2\pi k\rho_f} \quad 2.49$$

where η is the fluid viscosity, ϕ is the porosity of rock, ρ_f is the density of rock, k is the permeability of rock. If $f \leq f_c$, f is considered as low frequencies. His model of very high frequencies is shown as follows:

$$V_s^2 = \frac{\mu_d}{\rho_d + (1 - 1/\alpha)\phi\rho_f} \quad V_p^2 = \frac{A + (A^2 - 4B(PR - Q)^2)^{1/2}}{2B} \quad 2.50$$

where:

$$A = P\rho_{22} + R\rho_{11} - 2Q\rho_{12}$$

$$B = \rho_{11}\rho_{22} - \rho_{12}^2$$

$$P = \frac{(1 - \phi)(1 - \phi - \frac{K_d}{K_s})K_s + \phi K_d \frac{K_s}{K_f}}{D} + \frac{4}{3}\mu_d$$

$$R = \frac{2}{D} \phi \frac{K_s}{K_f}$$

$$Q = \frac{(1 - \phi - \frac{K_d}{K_s})\phi K_f}{D}$$

$$D = 1 - \phi - K_d/K_s + \phi K_s/K_d$$

$$\rho_{11} = \rho_d - (1-a)\phi \rho_f$$

$$\rho_{22} = a\phi \rho_f$$

$$\rho_{12} = (1-a)\phi \rho_f$$

a : tortuosity, ($a=1$ for parallel tube and $a=2-3$ for sandstone)

ρ_d, ρ_f : density of dry rock and fluid

K_d, K_s, K_f : bulk moduli of dry rock, rock solid and fluid

The dispersion due to Biot's flow is small compared with that due to local flow at ultrasonic frequencies ($0.1 \cdot 10^6$ Hz) (Wang and Nur, 1990). Therefore, at seismic frequencies, Biot's flow dispersion is negligible.

2.5 Conclusions

The theoretical derivation shows that the pore geometry affects the elastic moduli substantially. A crack decreases the elastic moduli much more than a sphere does unless the latter is enormously larger than the former in volume.

The elastic moduli of minerals are another factor. The existence of minerals of low elastic moduli may have a more effect. In a general, the elastic moduli of minerals are not sensitive to the changes in pressure and temperature.

The pore fluids can increase the elastic moduli of fluid-saturated rocks appreciably especially at high frequencies. But the effect is conditional on low dry elastic moduli, which will be dealt with in Chapter 6. In seismic frequencies, local-flow dispersion may never occur, Biot's flow dispersion is negligible, and global-flow dispersion may be roughly approximated with the arithmetic

average of the bulk modulus of fluids. In addition, the bulk modulus of fluids especially oil and gas depend on the compositions, pressure and temperature.

CHAPTER 3

A PORE GEOMETRICAL MODEL FOR SANDSTONES

3.1 Introduction

The elastic moduli of dry sandstones are determined by the elastic moduli of rock solid and pore geometry. The former may depend chiefly on clay content since the elastic moduli of the other major sandstone-forming minerals do not differ by so large amounts (after Zimmerman, 1991). The latter refers to a series of varying-shape varying-volume pores. Due to difficulty obtaining pore geometrical details, efforts have been made by many authors to simply connect porosity and clay content to the elastic moduli, evidenced by the linear velocity-porosity-clay models (Castagna et al., 1985; Kowallis et al., 1984; Han et al., 1986; Tosaya and Nur, 1982). These models are key to link reservoir properties to seismic observables. Without pore shape information, however, such a quantitative relationship does not exist in a general sense. At a given porosity, the elastic moduli vary because of the variability in clay content and in the distribution of pore volume to different pore shapes. For theoretical interpretation, it is therefore necessary to distinguish the role these two factors play in affecting the elastic moduli and further to find a quantitative pore geometrical model to give a reasonable explanation of nonexistence of the relationship between the elastic moduli and porosity in general and the possibility of linearity in some specific situations.

The increase of the elastic moduli with increasing effective pressure is caused by the closure of cracks. The magnitude depends not only on the amount of cracks closed but also on the distribution of other pores. In other words, it is controlled by pore geometry. It is again important to use this pore geometrical

model to assess the change of the elastic moduli with effective pressure at varying porosity.

In this chapter, the KT model (Kuster and Toksoz, 1974), which is recognized as the most realistic and simplest one among effective medium theories, was selected to obtain the pore geometry (simplified as the pore aspect ratio spectrum) of two sets of sandstone samples from Han et al. (1986) and Khaksar et al. (1999). First, the numerical modelling and the inverse problem (Cheng and Toksoz, 1979; Toksoz et al., 1976) were formulated to obtain the pore aspect ratio spectra of these sandstone samples based on velocity measurements. The results were then analysed to establish a pore geometrical model, which interprets the dry elastic moduli and their change with effective pressure and linearity in specific situations. In addition, the effect of clay is also discussed.

3.2 Forward numerical modelling of elastic moduli and velocities based on pore aspect ratio spectra

The KT equations were derived based on scattering theory. It is assumed that pore spaces in rocks can be represented by spheres and oblate spheroids, which are randomly distributed in rock solid (Toksoz et al., 1976). The effective moduli K and μ can be expressed as a function of the elastic moduli of rock solid (K_s and μ_s) and pore fluid (K_f and μ_f) and the pore aspect ratio spectrum. The pore aspect ratio spectrum is the volume concentration distributions $[c_{(\alpha_m)}]$ of pore aspect ratios (α_m). The pore aspect ratio (α_m) is defined as the ratio of the length of the short axis to that of the long axis on pore cross section. The volume concentration $[c_{(\alpha_m)}]$ is the volume of pores of aspect ratio α_m divided by the total bulk volume of the rock. The KT equations relates the pore aspect ratio spectrum to the elastic moduli as follows (Kuster and Toksoz, 1974):

$$\frac{K - K_s}{3K_f + 4\mu_s} = \frac{K_f - K_s}{3K_f + 4\mu_s} c_{(\alpha_1)} + \frac{K_f - K_s}{3K_s + 4\mu_s} \sum_{m=2}^M c_{(\alpha_m)} \frac{1}{3} T_{ijj(\alpha_m)} \quad 3.1$$

$$\begin{aligned} \frac{\mu - \mu_s}{6\mu(K_s + 2\mu_s) + \mu_s(9K_s + 8\mu_s)} &= \frac{\mu_f - \mu_s}{6\mu_f(K_s + 2\mu_s) + \mu_s(9K_s + 8\mu_s)} c_{(\alpha_1)} \\ &+ \frac{\mu_f - \mu_s}{25\mu_s(3K_s + 4\mu_s)} \sum_{m=2}^M c_{(\alpha_m)} [T_{ijj(\alpha_m)} - \frac{1}{3} T_{ijj(\alpha_m)}] \end{aligned} \quad 3.2$$

where T_{ijj} and T_{ijj} (see APPENDIX F for the formula) are scalars, dependent on K_s , μ_s , K_f , μ_f , and pore aspect ratio α_m . The density of rock (ρ) is derived from the pore concentrations and the densities of rock solid (ρ_s) and pore fluid (ρ_f):

$$\rho = \sum_{m=1}^M c_{(\alpha_m)} \rho_f + (1 - \sum_{m=1}^M c_{(\alpha_m)}) \rho_s \quad 3.3$$

where M is the total number of pore aspect ratios.

The velocities (V_p and V_s) are related to the effective moduli as:

$$V_p = \sqrt{\frac{K + 4/3 \mu}{\rho}} \quad V_s = \sqrt{\frac{\mu}{\rho}} \quad 3.4$$

In order to model the change of effective moduli and velocities of a rock with effective pressure (defined as differential pressure between confining pressure and fluid pressure, i.e., $P = P_c - P_f$), we have to model the change of the pore aspect ratio spectrum with effective pressure. The expression to compute the fractional change ($\Delta c/c$) in the volume of a sphere or oblate spheroid (α_m) due to an increment in effective pressure (ΔP) (after Toksoz et al., 1976) is:

$$\frac{\Delta c_{(\alpha_m)}}{c_{(\alpha_m)}} = \int_{c_{(\alpha_m)}}^{c_{(\alpha_m)} + \Delta c_{(\alpha_m)}} \frac{dc_{(\alpha_m)}}{c_{(\alpha_m)}} = - \int_P^{P+\Delta P} \frac{dP}{K} / [E_1^m - E_2^m E_3^m / (E_3^m + E_4^m)] \quad 3.5$$

where $c_{(\alpha_m)}$ is the concentration corresponding to the pore aspect ratio α_m at pressure P (generally taken to be atmospheric pressure P_0), K (pressure dependent) is the static bulk modulus of the dry rock, E_i^m (pressure dependent, see APPENDIX F for the formula) are functions of the aspect ratio α_m and effective matrix moduli K_A^m and μ_A^m calculated as the static elastic moduli of the dry rock with all pores except those with aspect ratio α_m . The volume concentration of an oblate spheroid is expressed as $c_{(\alpha_m)} = (4\pi r^3 \alpha_m / 3) / v$ (r is the radius of the spheroid and v is the total bulk volume of the rock). $dc_{(\alpha_m)} / c_{(\alpha_m)}$ is then equivalent to $d\alpha_m / \alpha_m$ if we assume changes in r are minimal. Under these conditions, the rate of change in volume is the same as the rate of change in aspect ratio. However, spherical pores do not deform in shape while decreasing in volume. The pore aspect ratio spectrum at any effective pressure P_n ($\Delta P = P_n - P_0$) can be calculated as:

$$c_{n(\alpha_{mn})} = c_{(\alpha_m)} \left[1 + \frac{\Delta c}{c}(\alpha_m, P_n) \right] \quad 3.6$$

$$\alpha_{mn} = \alpha_m \left[1 + \frac{\Delta \alpha}{\alpha}(P_n) \right] = \alpha_m \left[1 + \frac{\Delta c}{c}(\alpha_m, P_n) \right] \quad 3.7$$

Using equations 3.1 to 3.7, the elastic moduli (K and μ) and velocities (V_p and V_s) at any effective pressures can be calculated if the pore aspect ratio spectrum at P_0 and other parameters in these formulae are specified.

3.3 Inversion of pore aspect ratio spectra from velocity measurements

To determine the pore aspect ratio spectrum of a rock from velocity measurements at different effective pressures is an inverse problem. We choose a set of pore aspect ratios (from 1 to very small numbers), assign the corresponding concentrations and calculate theoretical velocities as a function of effective pressure according to equations 3.1-3.7. Then the pore aspect ratio spectrum is adjusted and the calculation is repeated until a good fit to the experimental data is obtained. This process is time consuming since we simultaneously resolve both the pore aspect ratios and their respective concentrations. To simplify problem, the pioneering work of Cheng and Toksoz (1979) and Toksoz et al. (1976) was used as a guide. For a number of sandstones, they (Cheng and Toksoz, 1979; Toksoz et al., 1976) found the distributions of pore aspect ratios, which are very similar even though they differ in pressure dependence. The major difference is variation in the volume concentrations. Hence, it is possible to choose one of them to represent the distributions of pore aspect ratios in our samples. In this study, the set of pore aspect ratios of the Navajo sandstone (Cheng and Toksoz, 1979; see table 1) was selected to represent the set of pore aspect ratios of all samples due to its wide range of distribution. Accordingly, the inverse problem reduces to resolving the volume concentrations of the pore aspect ratios for these samples.

At any pressure P_n , equations 3.1 and 3.2, by substitution of equations 3.6 and 3.7, are converted to:

$$\frac{K_n - K_s}{3K_n + 4\mu_s} \frac{3K_s + 4\mu_s}{K_f - K_s} = \left\{ \frac{3K_s + 4\mu_s}{3K_f + 4\mu_s} \alpha_1 \left[1 + \frac{dc}{c}(\alpha_1, P_n) \right] \right\} \frac{c^{(\alpha_1)}}{\alpha_1} \quad 3.8$$

$$+ \sum_{m=2}^M \left\{ \alpha_m \left[1 + \frac{dc}{c}(\alpha_m, P_n) \right] \frac{1}{3} T_{ijj}(\alpha_m) \right\} \frac{c^{(\alpha_m)}}{\alpha_m}$$

$$\frac{(\mu_n - \mu_s)25\mu_s(3K_s + 4\mu_s)}{[6\mu_n(K_s + 2\mu_s) + \mu_s(9K_s + 8\mu_s)](\mu_r - \mu_s)} = \frac{25\mu_s(3K_s + 4\mu_s)}{6\mu_r(K_s + 2\mu_s) + \mu_s(9K_s + 8\mu_s)} \left\{ \alpha_1 \left[1 + \frac{dc}{c}(\alpha_1, P_n) \right] \right\} \frac{c_{(\alpha_1)}}{\alpha_1}$$

$$+ \sum_{m=2}^M \left\{ \alpha_m \left[1 + \frac{dc}{c}(\alpha_m, P_n) \right] \left[T_{ijj(\alpha_m)} - \frac{1}{3} T_{ijj(\alpha_m)} \right] \right\} \frac{c_{(\alpha_m)}}{\alpha_m} \quad 3.9$$

whose left-hand sides are known from velocity measurement. The terms inside the braces on the right-hand sides can be calculated using equation 3.5 and APPENDIX F if the values of K and E_i^m in equation 3.5 are given. By denoting $x_m = c_{(\alpha_m)} / \alpha_m$, equations 3.8 and 3.9 are simplified to $b = Ax$. b is 2×1 matrix and A is $2 \times M$ matrix. At another effective pressure, another set of two equations can also be formulated similarly and incorporated. Thus the size of A depends on the number of effective pressures, at which velocities (V_p and V_s) were measured, and the number of pore aspect ratios. If we have N effective pressure points and M pore aspect ratios, A will be $(2N) \times M$ and b is $(2N) \times 1$. According to equations 3.5, 3.8 and 3.9, A is a function of x if the differences between static and dynamic moduli are ignored. b depends on velocity measurements. In addition, we must satisfy the following constraint of total porosity:

$$\sum_{m=1}^M x_m \alpha_m = \phi \quad 3.10$$

where ϕ is porosity. Thus, there are only $(M-1)$ independent variables. The new A and b (termed as A_1 and b_1) can be obtained by solving any x_i from equation 3.10 and substituting it into $b = Ax$.

To solve $b_1 = A_1 x$, it is necessary to compute A_1 and b_1 , which are functions of x . Moreover, x also must impose other two constraints:

$$x_m \geq 0 \quad (m = 1, 2, \dots, 11) \quad \text{and} \quad \sum_{m=1}^M x_m < 1 \quad 3.11$$

The second is the noninteraction assumption (Kuster and Toksoz, 1974) and may be relaxed to $x_m < 1$ (Toksoz et al., 1976). Consequently, the problem mathematically reduces to solving the non-linear equations $b_1 = A_1 x$ subject to the constraints in equation 3.11.

$b_1 = A_1 x$ can be solved by constructing an objective function and minimizing it in the feasible areas delineated by the constraints in equation 3.11. The objective function is defined as:

$$S = \sum_{i=1}^{10} [(A_1 x)_i - b_{1i}]^2 \quad 3.12$$

At any x , the gradient (g) of S is calculated as:

$$g = A_1^T A_1 x - A_1^T b_1 \quad 3.13$$

where A_1^T is the transpose of A_1 . Given an initial guess, the minimum can be found by decent gradient method subject to the constraints.

3.4 Parameter acquisition

In order to achieve the above computation, we need to know the parameters in these equations. Unfortunately, these parameters are not easily obtained. The KT equations require that the matrix solid materials be homogeneous and isotropic, which most sandstones do not satisfy. Sandstones consist of various minerals. Quartz, a major sandstone-forming mineral, differs by as much as 40% in elastic moduli along the different crystallographic axes (Clark, 1966; Zimmerman, 1991). Other minerals such as feldspar, clay, calcite etc. are also anisotropic. The anisotropy and inhomogeneity pose a question of how accurately we can use the model. Generally, these minerals in sandstones are more or less randomly orientated due to the process of deposition and statistical isotropy may be reasonably assumed. Brown and Korringa (1975) investigated the effect of mineral anisotropy on the Gassmann's equation and found that it is still applicable even though anisotropic minerals are uniformly orientated as if the porous medium were carved out of a single crystal. Consequently, the restriction of mineral anisotropies may be lifted. The second assumption of homogeneity can be satisfied if constituent minerals are statistically randomly distributed. 'Statistically randomly distributed' refers to the constant probability of any minerals in any position (stress bearing or stress free) with the magnitude determined by their respective volume fractions. Then given the mineralogical compositions (and their respective elastic moduli), the VRH model may be employed to compute the elastic moduli of the solid material. However, minerals are not statistically randomly distributed especially for clay. The contribution of a mineral to the elastic moduli of the solid material stems from its participation in the stress bearing area and the probability at this position depends on not only the volume fraction but also the process of deposition and diagenesis. In other words, it is impossible to calculate the elastic moduli of the rock solid solely based on the volume fractions. Clays may chiefly fill the large pores with less amounts at grain contacts or as rock fragments. Some fine-grained quartz and feldspar may not support stress in clay-rich siltstone. In

addition, the elastic moduli of clay minerals are difficult to measure because of the difficulty of obtaining samples of 'pure clay' that are large enough to perform tests on (Zimmerman, 1991). Some data are available in literature (Woeber et al., 1963; Wang et al., 1980), but they are measured on an aggregate of clay minerals, which contains microporosity (Kowallis et al., 1984). Toksoz et al. (1976) proposed that at very high pressures, pores close and the velocities can be interpreted in terms of matrix moduli. Yet the method is impractical to apply since sandstones will fail with grain crushing and cleavage fracturing before all pores close (Zhang et al., 1990). Second, even if closing of all pores is assumed in the range of elasticity, the minerals staying at stress free areas are included in the calculation of the elastic moduli of the rock solid, which is not right as stated above. In this paper, we present a new theoretical approach to attack this difficulty. At high effective pressure (assumed still in the range of elasticity), cracks or low-aspect-ratio pores close and the remaining ones staying open can be interpreted as spherical shape, in which case the second terms on the right in equations (1) and (2) vanish and K_s and μ_s can be solved from velocities. The velocities at high effective pressure can be acquired through extrapolation if velocity measurements are unavailable. However, the definition of 'high effective pressure' differs among authors who studied different sandstones. Khaksar et al. (1999) obtained the microcrack-closure pressure of approximately 81 MPa for twenty-two sandstone samples. Freund et al. (1992) set 120 MPa as the boundary value to distinguish the large non-linear rate of velocity increase at low pressures from the small linear rate at high pressures. Jones (1995) considered 60 MPa to be high effective pressure. St. Peter sandstone is flattened around 30 MPa in the velocity-pressure curves, lower than Berea and Bandera sandstones (Tosaya and Nur, 1982). West Delta Block sandstones' rate of velocity increase declines at 20 MPa (Kowallis et al., 1984). Despite the variability of 'high effective pressure' among individual samples, we can choose a high value to represent all samples. The high value does not affect the calculation substantially if approximately

linear elasticity is assumed in the range of 'high effective pressure'. The effective pressure of 100-120 MPa, which is high enough to close all cracks and low-aspect ratio pores for most sandstones, is considered to be the 'high effective pressure' in this study. According to this principle, we calculated the velocities at these pressures by extrapolation, and then obtained the elastic moduli of rock solid for all samples through equations 3.1 and 3.2. The results are shown in Tables 3.1 and 3.2. Figure 3.1 shows that increasing clay content decreases the elastic moduli of rock solid. The values of the calculated solid elastic moduli and their decrease with increasing clay content are within expected ranges.

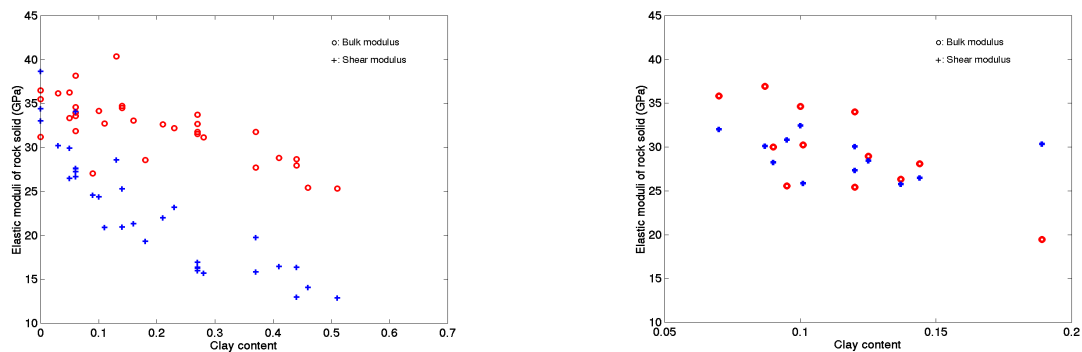


Figure 3.1 Elastic moduli of rock solid versus clay content for the samples from Han et al. (1986) on the left and from Khaksar et al. (1999) on the right. Porosity ranges from 10% to 20%.

The left (Han et al.'s data, water-saturated) of Figure 3.1 exhibits a larger gradient of the decrease of the shear modulus with increasing clay content than that of the bulk modulus, but the right (Khaksar et al.'s data, dry rock) does not. This behaviour may come from the more effect of clay on the shear modulus than on the bulk modulus in the presence of water.

The integral on the right hand side of equation 3.5 must be evaluated. K and E_i^m are static properties, which vary with effective pressure. If the static modulus is approximated by the dynamic modulus, the integral can be

calculated numerically. Given an initial guess of the pore aspect ratio spectrum, K and E_i^m at atmospheric pressure are computed through equations 3.1 and 3.2 and APPENDIX F. Suppose that the values of K and E_i^m keep constant over a small subinterval of ΔP , $\Delta\alpha/\alpha$ and $\Delta c/c$ and the new pore aspect ratio spectrum over that small subinterval can be calculated. The new pore aspect ratio spectrum is the starting point for the next subinterval. The process is repeated until ΔP is reached.

3.5 Inversion results

The inversion scheme was applied to seventy-five water-saturated sandstones (Han et al., 1986) and twenty-two dry sandstones (Khaksar et al., 1999) measured as a function of effective pressures. The first set contains a wide range of porosity and clay content and were sampled from a variety of geological settings. The second set was taken from sandstone reservoirs within the gas-producing fields in the southern Cooper Basin, South Australia. A detailed description of these samples and experimental conditions can be found in Han et al. (1986) and Khaksar et al. (1999). In inverse KT modelling, the elastic moduli of fluid were set to be 2.3 GPa for the first set and 0 GPa for the second set. The results are shown in Tables 3.1 and 3.2, where the first rows are the pore aspect ratios and the following rows are the corresponding volume concentrations for the samples. These pore aspect ratio spectra are under atmospheric pressure. The elastic moduli of rock solid and the percentage mismatch errors of V_p and V_s are in the right four columns. As seen in Figure 3.2, the errors are no more than a few percent. So the inversion results are reliable. Figure 3.3 depicts the fit of theoretical calculations (black lines) based on Table 3.1 and equations 3.1 to 3.7 to velocity measurements (red solid circles) for four samples in the first set. The corresponding dry velocities represented by green lines were also computed. It

can be seen that with increasing effective pressure dry P-wave velocities approach water-saturated ones but there is no such trend for S-wave velocities. Figure 3.4 plots the fits of theoretical calculations based on Table 3.2 and equations 3.1 to 3.7 (green lines) to velocity measurements (red solid circles).

Table 3.1 Pore aspect ratio spectra and elastic moduli of rock solid for the first set of seventy-five water saturated sandstones at atmospheric pressure

No.	1	0.1	0.01	0.0035	0.0028	0.0021	0.0016	0.0012	0.0009	0.0006	0.0003	Err_Vp	Err_Vs	Ks	Us
1	0.15868	0.02678	0.00054	0.00023	0.00027	0.00020	0.00022	0.00016	0.00008	0.00012	0.00011	1.22%	1.24%	37	34
2	0.17990	0.02225	0.00030	0.00016	0.00022	0.00016	0.00019	0.00014	0.00007	0.00011	0.00011	0.61%	1.36%	33	30
3	0.01817	0.04813	0.00106	0.00011	0.00010	0.00005	0.00005	0.00003	0.00000	0.00011	0.00017	1.31%	1.40%	41	44
4	0.12941	0.02603	0.00054	0.00022	0.00026	0.00019	0.00021	0.00016	0.00007	0.00011	0.00011	0.72%	1.29%	36	39
5	0.17774	0.02255	0.00032	0.00016	0.00022	0.00016	0.00019	0.00015	0.00007	0.00011	0.00011	0.65%	0.99%	31	33
6	0.20443	0.03474	0.00092	0.00035	0.00036	0.00025	0.00024	0.00017	0.00009	0.00012	0.00011	0.61%	0.73%	24	21
7	0.22701	0.03764	0.00107	0.00040	0.00037	0.00025	0.00023	0.00018	0.00008	0.00012	0.00011	1.52%	1.56%	20	17
8	0.20961	0.03468	0.00090	0.00034	0.00036	0.00024	0.00023	0.00017	0.00009	0.00012	0.00011	1.32%	0.90%	26	19
9	0.12856	0.03543	0.00087	0.00032	0.00034	0.00023	0.00023	0.00016	0.00008	0.00012	0.00011	1.44%	0.57%	31	16
10	0.08020	0.02818	0.00089	0.00031	0.00030	0.00022	0.00021	0.00016	0.00008	0.00009	0.00008	0.81%	0.89%	35	34
11	0.20267	0.03187	0.00079	0.00031	0.00033	0.00023	0.00023	0.00017	0.00008	0.00012	0.00011	1.44%	1.93%	28	23
12	0.13107	0.02734	0.00057	0.00023	0.00027	0.00020	0.00022	0.00016	0.00008	0.00011	0.00011	0.45%	1.73%	36	30
13	0.07898	0.02922	0.00093	0.00032	0.00031	0.00023	0.00022	0.00017	0.00009	0.00009	0.00008	1.16%	1.56%	36	30
14	0.23352	0.02610	0.00047	0.00020	0.00025	0.00018	0.00020	0.00015	0.00007	0.00011	0.00011	0.44%	1.11%	32	18
15	0.00757	0.03682	0.00061	0.00002	0.00002	0.00000	0.00001	0.00000	0.00006	0.00015	0.00010	1.09%	0.92%	40	31
16	0.09625	0.03217	0.00090	0.00032	0.00032	0.00024	0.00022	0.00016	0.00008	0.00010	0.00009	2.29%	2.39%	32	17
17	0.15017	0.03301	0.00084	0.00032	0.00034	0.00025	0.00024	0.00017	0.00008	0.00012	0.00011	0.89%	1.18%	34	27
18	0.23431	0.02675	0.00051	0.00022	0.00026	0.00018	0.00020	0.00015	0.00007	0.00011	0.00011	1.34%	1.04%	25	17
19	0.00647	0.05128	0.00097	0.00008	0.00007	0.00003	0.00004	0.00002	0.00003	0.00004	0.00005	0.61%	0.68%	36	32
20	0.09881	0.03448	0.00099	0.00035	0.00035	0.00026	0.00023	0.00016	0.00008	0.00011	0.00010	1.72%	1.43%	35	21
21	0.14614	0.03260	0.00082	0.00031	0.00033	0.00025	0.00024	0.00017	0.00009	0.00012	0.00011	0.90%	1.31%	34	28
22	0.16806	0.04183	0.00125	0.00044	0.00043	0.00032	0.00029	0.00020	0.00010	0.00012	0.00011	1.89%	1.36%	31	23
23	0.14922	0.04121	0.00124	0.00043	0.00043	0.00032	0.00028	0.00020	0.00010	0.00013	0.00011	1.22%	1.21%	33	26
24	0.06495	0.02760	0.00093	0.00031	0.00030	0.00022	0.00020	0.00015	0.00008	0.00009	0.00007	0.88%	0.77%	35	32
25	0.06301	0.02979	0.00105	0.00035	0.00033	0.00024	0.00022	0.00017	0.00009	0.00009	0.00007	0.45%	0.77%	39	36
26	0.20986	0.03115	0.00074	0.00029	0.00032	0.00024	0.00022	0.00017	0.00008	0.00012	0.00011	0.97%	1.21%	28	24
27	0.13703	0.05410	0.00192	0.00064	0.00059	0.00044	0.00036	0.00024	0.00012	0.00015	0.00011	1.43%	1.42%	32	28
28	0.18978	0.03066	0.00072	0.00029	0.00031	0.00023	0.00022	0.00017	0.00008	0.00012	0.00011	0.89%	0.91%	28	24
29	0.19770	0.02826	0.00060	0.00025	0.00028	0.00021	0.00021	0.00016	0.00008	0.00011	0.00011	1.28%	1.44%	30	23
30	0.16345	0.02994	0.00069	0.00027	0.00031	0.00023	0.00023	0.00017	0.00008	0.00012	0.00011	1.35%	1.58%	27	25
31	0.01525	0.07382	0.00034	0.00041	0.00029	0.00027	0.00055	0.00004	0.00033	0.00025	0.00000	1.51%	1.65%	38	29
32	0.02081	0.04480	0.00127	0.00030	0.00027	0.00019	0.00058	0.00055	0.00021	0.00005	0.00018	1.83%	1.21%	39	27
33	0.07195	0.00000	0.00110	0.00079	0.00071	0.00056	0.00047	0.00037	0.00014	0.00027	0.00028	1.47%	3.87%	25	40

34	0.03346	0.03340	0.00134	0.00043	0.00037	0.00027	0.00023	0.00018	0.00010	0.00009	0.00005	1.26%	2.22%	43	24
35	0.01671	0.01773	0.00097	0.00034	0.00029	0.00022	0.00018	0.00028	0.00024	0.00040	0.00019	0.44%	2.28%	36	30
36	0.00888	0.02094	0.00093	0.00029	0.00024	0.00018	0.00015	0.00011	0.00007	0.00006	0.00003	1.10%	1.38%	40	34
37	0.01895	0.01486	0.00104	0.00040	0.00035	0.00026	0.00022	0.00022	0.00020	0.00030	0.00026	1.31%	2.88%	39	30
38	0.02466	0.01941	0.00059	0.00017	0.00015	0.00011	0.00010	0.00007	0.00004	0.00023	0.00014	1.34%	1.62%	37	30
39	0.00823	0.01747	0.00034	0.00005	0.00004	0.00003	0.00003	0.00002	0.00002	0.00006	0.00012	1.13%	0.84%	38	28
40	0.03087	0.03424	0.00137	0.00043	0.00037	0.00027	0.00023	0.00018	0.00010	0.00008	0.00006	0.50%	1.26%	40	27
41	0.03616	0.03040	0.00119	0.00038	0.00034	0.00025	0.00022	0.00016	0.00009	0.00007	0.00005	0.45%	0.66%	31	24
42	0.04313	0.03151	0.00116	0.00038	0.00034	0.00025	0.00022	0.00015	0.00008	0.00007	0.00006	0.43%	0.93%	32	22
43	0.08182	0.03427	0.00106	0.00036	0.00035	0.00026	0.00022	0.00015	0.00008	0.00010	0.00008	0.87%	0.93%	32	20
44	0.05149	0.03971	0.00147	0.00047	0.00042	0.00031	0.00027	0.00018	0.00010	0.00009	0.00007	0.81%	2.03%	32	23
45	0.05997	0.03671	0.00130	0.00043	0.00039	0.00029	0.00026	0.00018	0.00009	0.00009	0.00007	1.02%	1.61%	32	21
46	0.04212	0.03011	0.00114	0.00037	0.00034	0.00025	0.00022	0.00015	0.00008	0.00007	0.00006	1.00%	1.16%	31	23
47	0.04401	0.09776	0.00000	0.00262	0.00000	0.00059	0.00079	0.00000	0.00000	0.00009	0.00000	1.84%	2.66%	40	29
48	0.13373	0.03311	0.00083	0.00031	0.00034	0.00025	0.00024	0.00017	0.00008	0.00012	0.00011	1.52%	1.67%	35	25
49	0.10189	0.05525	0.00192	0.00063	0.00058	0.00043	0.00036	0.00024	0.00012	0.00015	0.00011	1.88%	2.08%	34	24
50	0.15047	0.02745	0.00055	0.00023	0.00027	0.00020	0.00021	0.00016	0.00008	0.00011	0.00011	2.28%	3.07%	33	21
51	0.11562	0.05635	0.00192	0.00063	0.00058	0.00043	0.00036	0.00025	0.00012	0.00013	0.00011	1.75%	1.71%	33	21
52	0.10484	0.03101	0.00078	0.00029	0.00030	0.00021	0.00020	0.00014	0.00007	0.00010	0.00009	1.47%	1.30%	29	13
53	0.09996	0.03731	0.00111	0.00039	0.00038	0.00026	0.00023	0.00016	0.00008	0.00010	0.00009	1.18%	0.21%	25	14
54	0.09013	0.03386	0.00097	0.00034	0.00034	0.00023	0.00021	0.00015	0.00008	0.00010	0.00008	2.03%	1.96%	25	13
55	0.26982	0.03826	0.00103	0.00034	0.00032	0.00024	0.00023	0.00016	0.00008	0.00011	0.00011	1.99%	1.41%	23	13
56	0.26729	0.03522	0.00089	0.00030	0.00030	0.00022	0.00022	0.00017	0.00008	0.00011	0.00011	1.24%	1.41%	22	13
57	0.10202	0.05378	0.00173	0.00057	0.00054	0.00036	0.00031	0.00021	0.00012	0.00013	0.00011	3.09%	2.57%	34	16
58	0.11462	0.03836	0.00106	0.00038	0.00038	0.00026	0.00024	0.00017	0.00009	0.00012	0.00010	2.43%	2.73%	33	16
59	0.20376	0.04569	0.00145	0.00051	0.00045	0.00030	0.00026	0.00020	0.00009	0.00013	0.00011	2.43%	4.11%	23	15
60	0.21145	0.04799	0.00146	0.00050	0.00043	0.00029	0.00025	0.00019	0.00009	0.00012	0.00011	3.14%	3.44%	29	15
61	0.08887	0.05907	0.00209	0.00069	0.00062	0.00041	0.00033	0.00022	0.00013	0.00013	0.00010	2.45%	2.07%	28	16
62	0.07895	0.03461	0.00111	0.00038	0.00036	0.00027	0.00023	0.00016	0.00008	0.00010	0.00008	1.26%	1.28%	28	16
63	0.06997	0.03244	0.00107	0.00037	0.00035	0.00026	0.00022	0.00015	0.00007	0.00009	0.00008	1.77%	1.81%	29	16
64	0.12254	0.02833	0.00062	0.00025	0.00028	0.00020	0.00020	0.00016	0.00007	0.00011	0.00010	2.03%	2.22%	32	16
65	0.23575	0.03328	0.00085	0.00033	0.00035	0.00024	0.00023	0.00017	0.00009	0.00012	0.00011	2.02%	2.06%	24	20
66	0.23005	0.04315	0.00129	0.00045	0.00045	0.00030	0.00027	0.00019	0.00010	0.00012	0.00011	2.93%	2.89%	27	18
67	0.24040	0.04403	0.00137	0.00048	0.00042	0.00028	0.00025	0.00019	0.00010	0.00012	0.00011	2.62%	2.81%	25	18
68	0.22363	0.04736	0.00150	0.00052	0.00045	0.00030	0.00026	0.00020	0.00011	0.00013	0.00011	3.24%	4.29%	26	17
69	0.23530	0.04435	0.00138	0.00049	0.00047	0.00028	0.00028	0.00019	0.00010	0.00012	0.00011	3.11%	3.98%	26	19
70	0.16043	0.04562	0.00143	0.00049	0.00048	0.00032	0.00028	0.00020	0.00011	0.00012	0.00011	3.35%	3.76%	30	19
71	0.07346	0.04241	0.00149	0.00049	0.00045	0.00033	0.00030	0.00021	0.00011	0.00011	0.00009	2.76%	2.51%	33	22
72	0.11624	0.03963	0.00119	0.00042	0.00041	0.00031	0.00029	0.00021	0.00011	0.00013	0.00011	3.55%	4.06%	38	27
73	0.08502	0.02466	0.00069	0.00025	0.00026	0.00019	0.00019	0.00014	0.00007	0.00009	0.00008	2.43%	3.58%	32	23
74	0.02274	0.04050	0.00129	0.00034	0.00030	0.00021	0.00018	0.00014	0.00014	0.00015	0.00010	1.65%	1.88%	35	27
75	0.12456	0.02715	0.00059	0.00024	0.00027	0.00020	0.00021	0.00016	0.00007	0.00011	0.00010	1.96%	2.32%	29	19

Table 3.2 Pore aspect ratio spectra and elastic moduli of rock solid for the second set of twenty-two dry sandstones at atmospheric pressure

No	1	0.1	0.01	0.0035	0.0028	0.0021	0.0016	0.0012	0.0009	0.0006	0.0003	Err_Vp	Err_Vs	Ks	Us
D1	0.05043	0.02009	0.00090	0.00033	0.00030	0.00023	0.00020	0.00015	0.00016	0.00013	0.00007	1.55%	2.39%	32	34
D2	0.05680	0.02494	0.00121	0.00044	0.00040	0.00030	0.00026	0.00020	0.00020	0.00016	0.00009	2.01%	2.75%	32	33
D3	0.10065	0.02224	0.00062	0.00026	0.00027	0.00020	0.00020	0.00021	0.00012	0.00012	0.00009	1.72%	4.25%	25	27
D4	0.09537	0.03109	0.00116	0.00044	0.00042	0.00031	0.00029	0.00037	0.00023	0.00019	0.00011	3.35%	8.04%	37	30
D6	0.07463	0.03305	0.00156	0.00057	0.00052	0.00039	0.00034	0.00040	0.00026	0.00019	0.00010	1.99%	4.15%	26	31
D7	0.08817	0.02769	0.00109	0.00041	0.00039	0.00029	0.00027	0.00021	0.00021	0.00016	0.00010	2.80%	2.45%	35	32
D8	0.07854	0.02985	0.00130	0.00048	0.00045	0.00033	0.00030	0.00023	0.00024	0.00018	0.00010	2.23%	3.97%	36	32
D10	0.11516	0.03052	0.00101	0.00040	0.00040	0.00030	0.00043	0.00031	0.00020	0.00016	0.00012	2.27%	4.19%	26	26
M1	0.02919	0.01831	0.00097	0.00035	0.00031	0.00023	0.00019	0.00015	0.00010	0.00013	0.00007	1.26%	3.18%	41	41
M2	0.04391	0.01867	0.00091	0.00034	0.00030	0.00023	0.00020	0.00015	0.00010	0.00012	0.00007	1.34%	1.44%	37	40
M7	0.00467	0.02104	0.00003	0.00000	0.00000	0.00000	0.00000	0.00000	0.00000	0.00019	0.00007	1.37%	5.22%	36	32
M8	0.02025	0.01725	0.00100	0.00036	0.00031	0.00023	0.00019	0.00014	0.00010	0.00012	0.00007	1.68%	1.68%	41	40
M10	0.02143	0.01723	0.00092	0.00033	0.00028	0.00021	0.00018	0.00013	0.00009	0.00012	0.00007	1.60%	4.55%	44	42
M11	0.02602	0.00723	0.00025	0.00010	0.00010	0.00007	0.00007	0.00005	0.00003	0.00005	0.00003	1.56%	2.00%	34	35
M13	0.03712	0.01253	0.00048	0.00018	0.00017	0.00013	0.00012	0.00009	0.00006	0.00008	0.00005	2.85%	4.25%	31	33
S1	0.08290	0.02003	0.00065	0.00026	0.00026	0.00020	0.00019	0.00020	0.00012	0.00011	0.00008	2.29%	2.29%	29	28
S2	0.06640	0.02026	0.00081	0.00031	0.00030	0.00022	0.00020	0.00016	0.00014	0.00013	0.00007	2.84%	2.58%	31	31
S3	0.12465	0.02850	0.00082	0.00034	0.00035	0.00026	0.00037	0.00027	0.00017	0.00015	0.00012	2.06%	3.00%	30	26
S4	0.13357	0.02948	0.00086	0.00035	0.00037	0.00028	0.00038	0.00028	0.00016	0.00015	0.00012	1.34%	1.46%	28	26
S5	0.10746	0.02849	0.00099	0.00039	0.00038	0.00029	0.00027	0.00030	0.00019	0.00015	0.00011	1.16%	2.17%	30	28
S6	0.10369	0.02907	0.00106	0.00041	0.00040	0.00030	0.00028	0.00031	0.00019	0.00017	0.00011	2.66%	2.45%	34	30
S7	0.09183	0.03038	0.00134	0.00051	0.00047	0.00035	0.00032	0.00031	0.00021	0.00018	0.00010	1.87%	3.37%	19	30

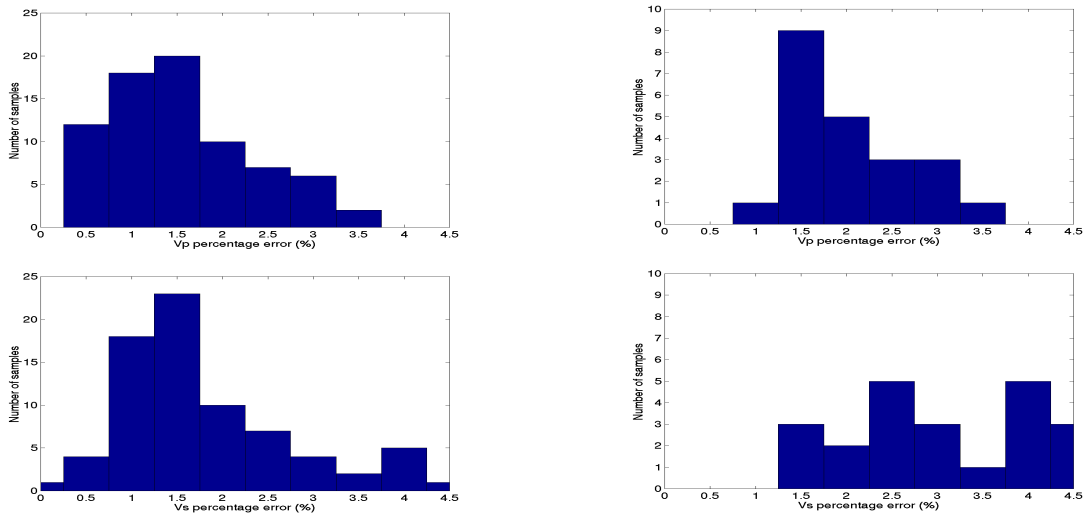


Figure 3.2 Velocity percentage errors for the first set (left) and the second set (right).

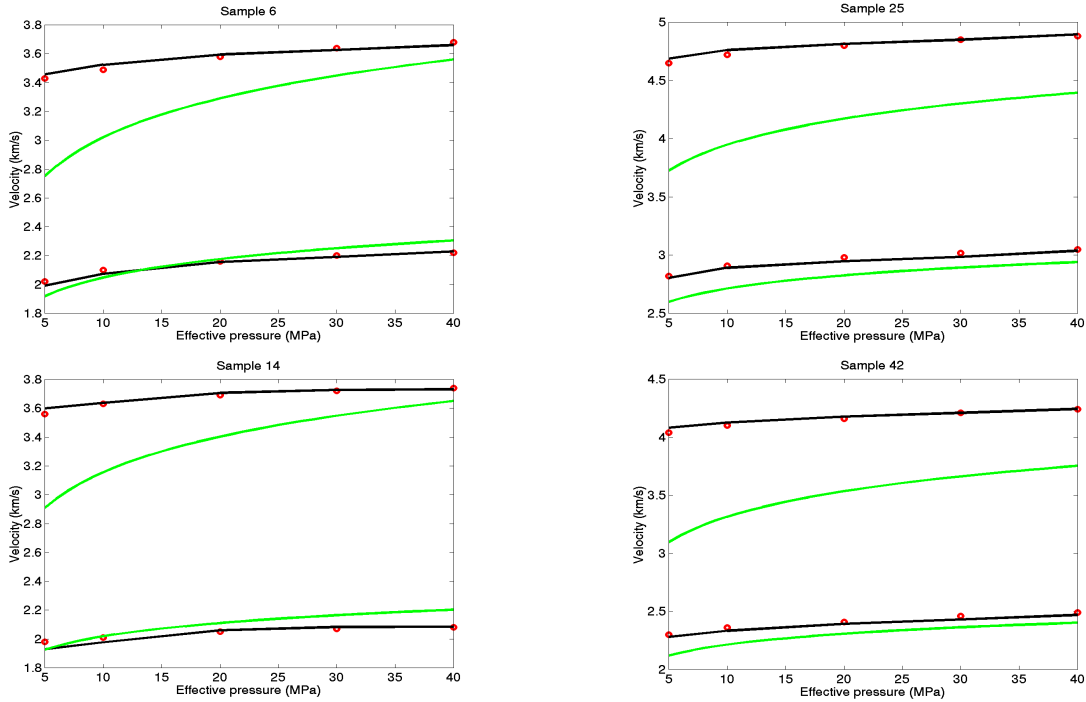


Figure 3.3 Results of inversion for samples 6, 14, 25 and 42. The red solid circles are velocity measurements from Han et al. (1986) for water-saturated sandstones. The black and green solid curves are theoretical velocities calculated based on Table 3.1 for water-saturated and dry sandstones respectively. Upper curves are compressional wave velocities and lower curves are shear wave velocities.

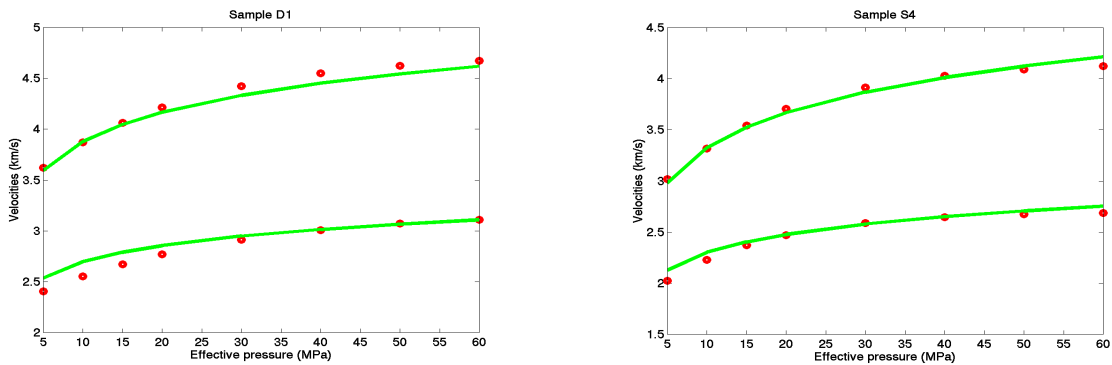


Figure 3.4 Results of inversion for samples D1 and S4. The red solid circles are velocity measurements from Khaksar et al. (1999) for dry sandstones. The green curves are theoretical velocities calculated based on Table 3.2 for dry sandstones. Upper part is compressional wave velocities and lower part is shear wave velocities.

3.6 Pore aspect ratio spectra and the elastic moduli of dry sandstones at atmospheric pressure

Porosity, one of the most important physical properties of rocks, is defined as the ratio of the volume of all pores to the total bulk volume of the rock. It contains some information about pore geometry. Failing to consider pore shapes, however, it cannot uniquely determine the elastic moduli. In this section, the factors responsible for the variability of the elastic moduli at any given porosity will be discussed with emphasis on the effect of pore geometry.

The bulk modulus and shear modulus for seventy-five dry sandstones (Han et al., 1986) were calculated from Table 3.1 using equations 3.1-3.7 and were then plotted against porosity in Figure 3.5. As shown, the points are scattering below an approximate linear trend, indicating the poor correlation of the elastic

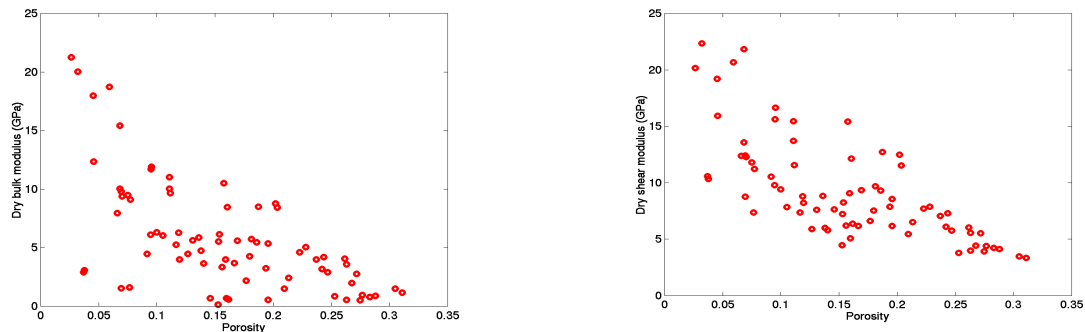


Figure 3.5 Plot of porosity versus bulk modulus and shear modulus for the first set of seventy-five dry sandstones.

moduli with porosity. There are two factors, i.e., clay content and pore geometry, which contribute to the variability in the elastic moduli at any given porosity. The first step is therefore to separate their effects and then examine their importance in elastic moduli determination. In terms of pore geometry, it is natural to resort to weighting the volumes of all pore shapes (or pore aspect

ratios). More weight is given to thin cracks (low aspect ratio pores) than to round pores (high aspect ratio pores). The sum of the weighted volume concentrations of pores of all pore aspect ratios instead of porosity is expected to represent the total effect of pore geometry on the elastic moduli. It should uniquely determine the elastic moduli if clay content is disregarded. After trial-and-error experiments with the KT modelling, the weight coefficients are the inverse of the pore aspect ratios for pores lower than 0.1 in pore aspect ratios and are 3.3 for spherical pores. To test the validity of this principle, we plotted in Figure 3.6 the sum of the weighted volume concentrations against the dry elastic moduli for seventy-five sandstones assuming the elastic moduli of rock solid are $K_s=37$ GPa and $\mu_s=44$ GPa. As predicted, the sum of the weighted volume concentrations are almost perfectly correlated with the dry bulk moduli and strongly correlated to the dry shear moduli. Therefore the sum of the weighted volume concentrations is a parameter to quantify the total effect of pore geometry. In order to view the effect of clay content on the elastic moduli, Figure 3.6 were redrawn but with the elastic moduli of rock solid from Table 3.1. As shown in Figure 3.7, clay content does perturb the elastic moduli, especially shear modulus, but the amount of perturbation does not change the linear trend substantially considering the drastic variation of clay content in Figure 3.8.

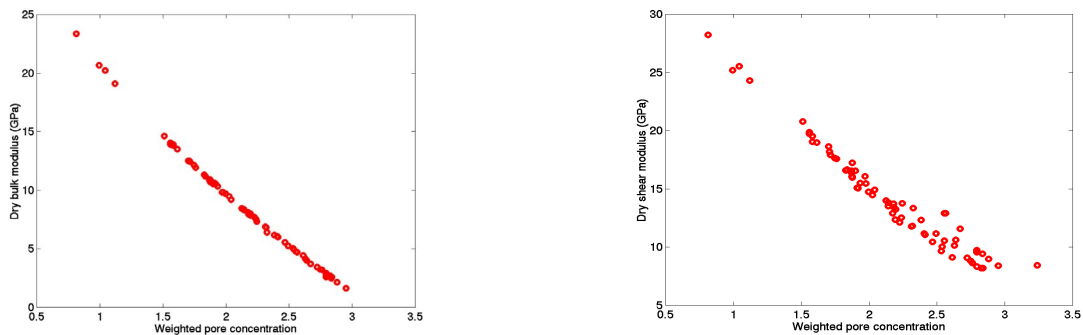


Figure 3.6 Plot of weighted concentrations versus dry elastic moduli computed based on the constant elastic moduli of rock solid ($K_s=37$ GPa and $\mu_s=44$ GPa).

Now we return to Figure 3.5 to distinguish two factors of clay content and pore geometry for their effects on the variability in the elastic moduli at any given porosity. Figures 3.9 and 3.10 are the crossplots of total porosity versus the sum of the weighted volume concentrations and total porosity versus clay content. The reverse of y-axis order is for convenience of comparison due to the inverse variation of the elastic moduli with the sum of weighted volume concentrations and with clay content. Figure 3.9 is very similar to Figure 3.5 especially for the bulk modulus. Figure 3.10, however, has no resemblance to Figure 3.5.

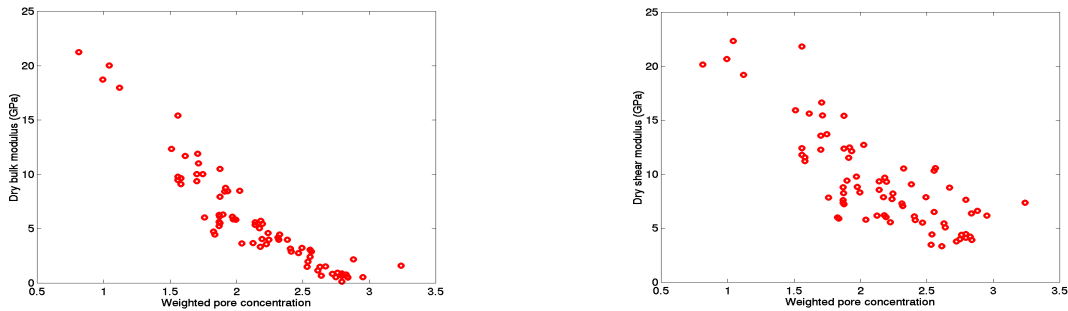


Figure 3.7 Plot of weighted concentrations versus dry elastic moduli computed based on the elastic moduli of rock solid from Table 3.1.

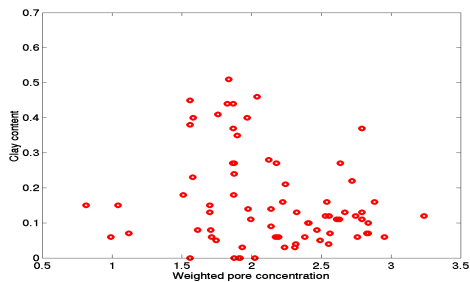


Figure 3.8 Plot of weighted concentrations versus clay content.

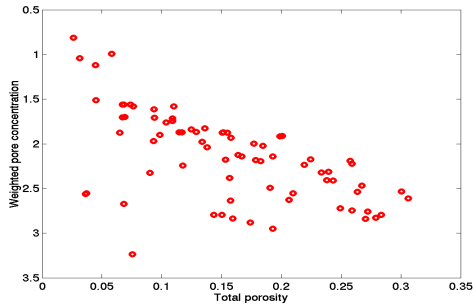


Figure 3.9 Plot of total porosity versus weighted pore concentration.

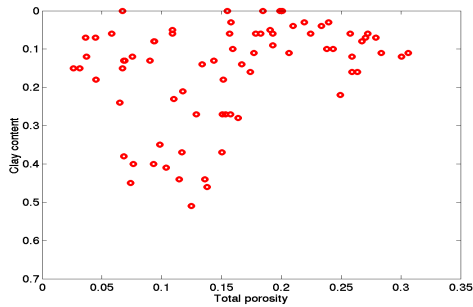


Figure 3.10 Plot of total porosity versus clay content.

The above results strongly suggest that pore geometry is the major factor to influence the elastic moduli, especially the bulk modulus. Clay content plays secondary role. This conclusion agrees with the observations by many other authors such as Zimmerman (1991).

Figure 3.11 plots the relationship between total porosity and porosities of pores of varying pore aspect ratios. For convenience, we call aspect-ratio-equal-to-one pores round or spherical pores, any other pores cracks because their aspect ratios are small, less than 0.1. Strictly speaking, cracks refer to pores of very small aspect ratios. As shown in Figure 3.11, the porosity of spherical pores is less changeable, proportional to total porosity with a good linear trend, but the crack porosities of different pore aspect ratios vary, especially at low porosity, with no systematic connection to total porosity. Consequently, at any given porosity the variability in the sum of the weighted volume concentrations indicated in Figure 3.9 is not caused by round pores but by cracks that take up only a small fraction of pore volume concentrations. This is further supported by

Figure 3.12, in which the weighted volume concentration for round pores is linearly related to total porosity, but the weighted volume concentration for cracks varies especially at low total porosity.

Figure 3.13 shows that the variability in the weighted crack concentration at any given porosity is chiefly due to the change of the crack volume concentration, which stems from a relatively minor change in the volume concentration of round pores (see the right plot of Figure 3.5). The few abnormal points on the right of Figure 3.13 results from a shift of pore volume to thin cracks, in which case the weighted crack concentration is large despite the small crack concentration because a considerable portion of crack volume is distributed among low-aspect-ratio cracks.

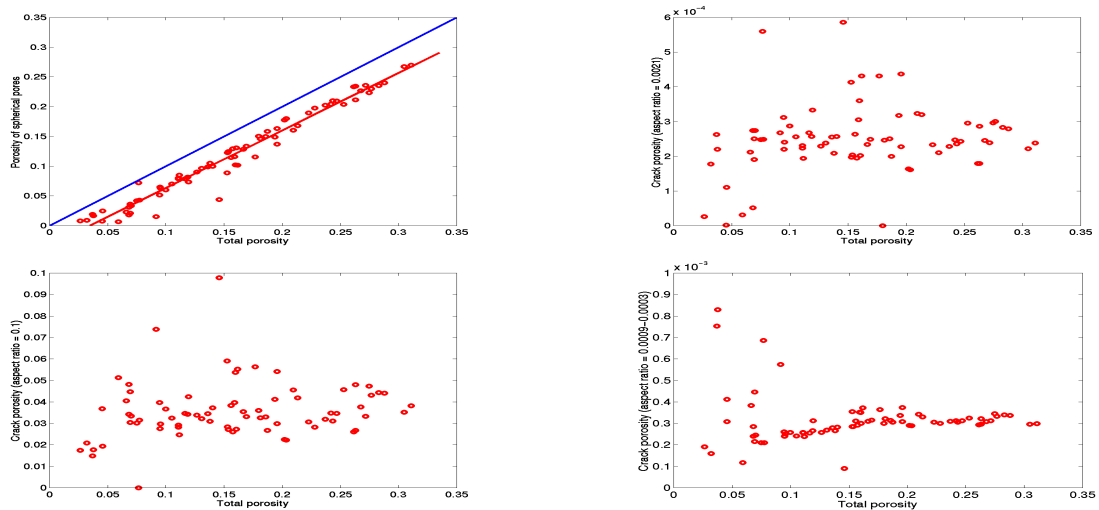


Figure 3.11 Plot of total porosity versus concentrations of spherical pores and cracks of varying aspect ratios for seventy-five dry sandstones.

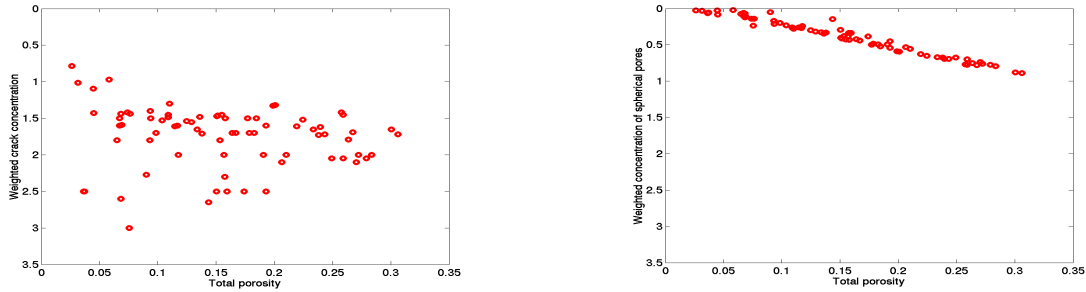


Figure 3.12 Plot of total porosity versus weighted concentration of spherical pores (right) and weighted crack concentration (left).

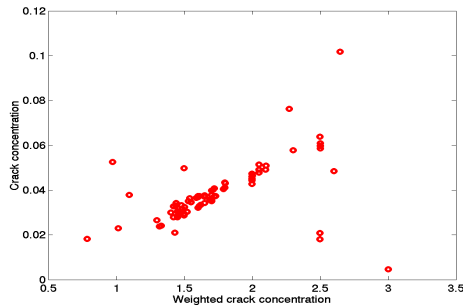


Figure 3.13 Plot of weighted crack concentration versus crack concentration.

3.7 Effect of round pores on the variability in the elastic moduli

It is found by KT modelling that the decrease in the elastic moduli due to addition of the same amount of pores of the same pore aspect ratio will be larger for rocks of high elastic moduli than for those of low elastic moduli. In other words, rocks of high elastic moduli are more sensitive to addition of pores than those of low elastic moduli. As indicated in Figure 3.11 (upper left) and Figure 3.12 (right), the elastic moduli solely due to round pores would increase linearly with decreasing porosity. Consequently, adding a certain amount of cracks would decrease the elastic moduli more for low-porosity sandstones than for high-porosity sandstones. Figure 3.14 demonstrates the role of round pores in determining variability in the elastic moduli. Small cyan points represent the elastic moduli computed assuming only the existence of round pores. The green, red and blue points were obtained by adding low, medium and high weighted

crack concentrations respectively. Being more sensitive to cracks at low porosity is evidenced by the increasing departure of red points from small cyan points with decreasing porosity.

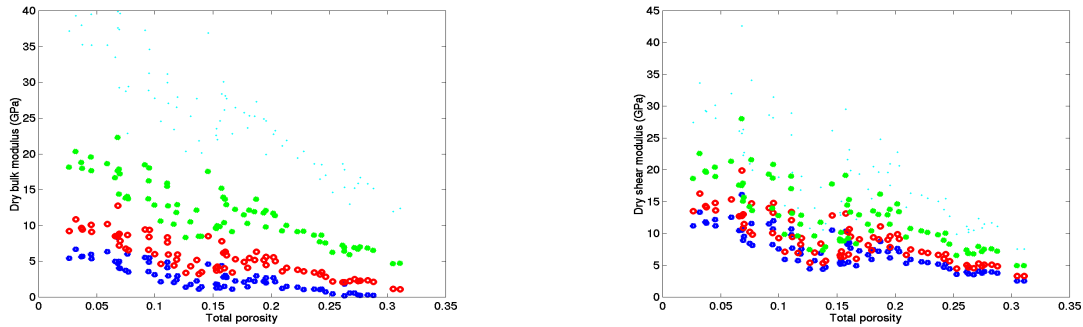


Figure 3.14 Plot of total porosity versus elastic moduli for four cases: spherical pores only (cyan), low crack concentration added (green), medium crack concentration added (red) and high crack concentration added (blue).

According to this principle, the variability in the elastic moduli at any given porosity as shown in Figure 3.5 not only depends on the variability in the weighted crack concentration as shown in Figure 3.12 (left), but also is affected by porosity. The lower porosity, the more variable the elastic moduli. This conclusion is also meaningful in the interpretation of the change of the elastic moduli with effective pressure because the closing of the same amount of cracks may lead to more increase in the elastic moduli at low porosity than at high porosity. The issue will be discussed further.

3.8 A pore geometrical model for sandstones

The concentration of round pores is in direct proportion to porosity, but the crack concentration varies with no systematic connection to porosity in a

general sense. The linearity between the elastic moduli and porosity caused by round pores can be severely altered in the presence of cracks. The conceptual model of pore geometry is summarized in Figure 3.15.

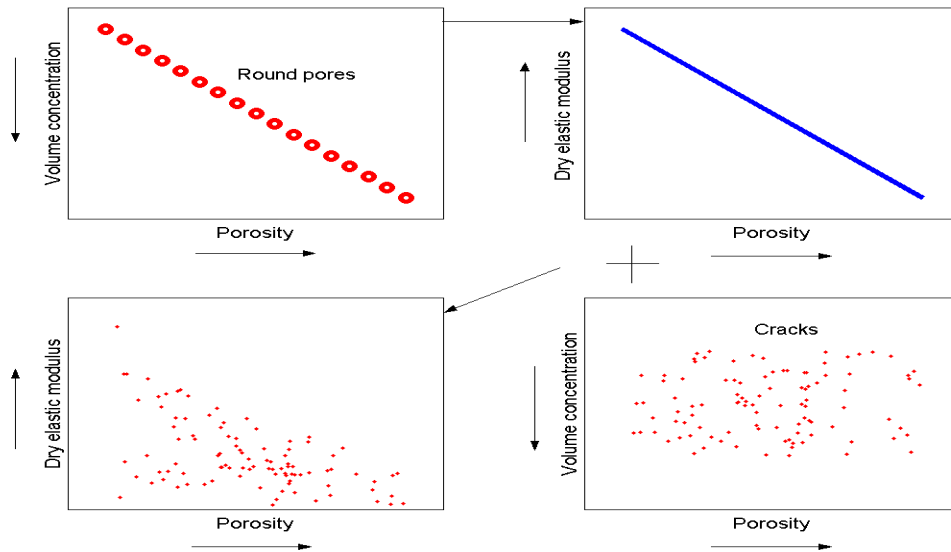


Figure 3.15 Conceptual model of pore geometry for sandstones

According to this pore geometrical model, the linearity between the elastic moduli and porosity depends on cracks. If the crack concentration is less variable and changes regularly with porosity, a linear relationship results. Reservoir rocks formed under a specific geological setting may have this pattern of crack distribution. The cemented sand model (Mavko, 2000) predicts two cases of grain contact cementation. The first type cements both round pores and grain contacts, which leads to the decrease in the crack concentration (grain contact is viewed as cracks) with decreasing porosity. According to Figure 3.15, a steeper linear relationship between the elastic moduli and porosity is expected. The second type cements only round pores and grain contacts stay the same at all porosity. Consequently a linear relationship more gentle relative to the first type can be observed. These results are consistent with theoretical calculations (Mavko, 2000).

The second set of dry sandstones were sampled from the gas-producing fields in the southern Cooper basin, south Australian. The crack concentration may vary regularly with porosity because of similar geological environments. Figure 3.16 does show a linear increase of the crack volume concentration and the weighted crack concentration with increasing porosity. According to the pore geometrical model, it is predicted that the linearity exists between the elastic moduli (and velocities) and porosity. This prediction is proven by calculations using KT modelling in Figure 3.17.

However, crack occurrence is not clearly understood. It is questionable that sandstones in similar geological settings would have crack distribution similar to the above two cases. Caution must be taken when trying to set up a linear relationship based on a small number of samples in a specific area because such linearity may not be developed. This is a fertile field for future study.

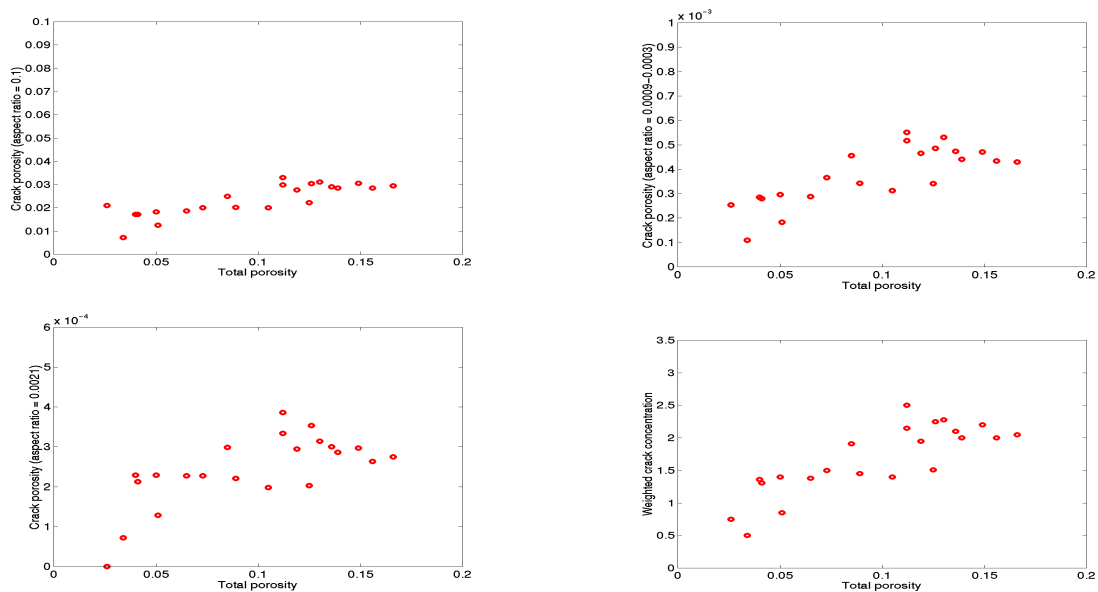


Figure 3.16 Plot of total porosity versus the volume concentrations of cracks of varying aspect ratios (upper part and lower left) and the weighted crack concentration (lower right) for the second set of sandstones.

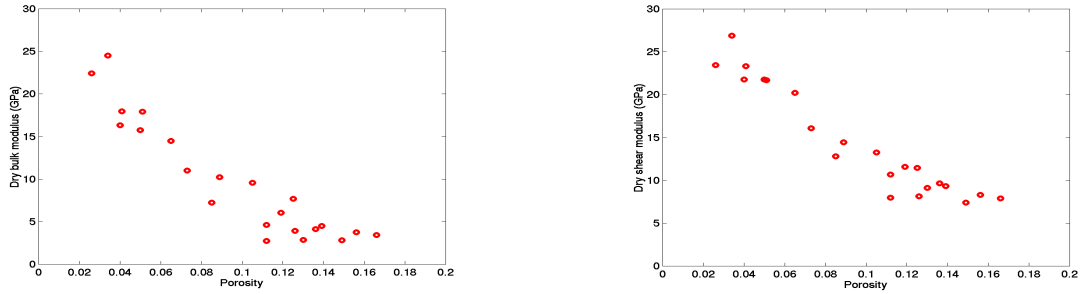


Figure 3.17 Plot of porosity versus the dry bulk modulus and shear modulus.

The second case is at high effective pressure, at which thin cracks have closed. The drastic variation in the crack concentration is reduced and round pores play a more important role in elastic moduli determination. Figure 3.18 indicates in comparison with Figure 3.12 that at 40 MPa the crack concentration decreases and becomes less variable while the round pore concentration almost stays the same. As a result, a more linearity can be seen in Figure 3.19 than in Figure 3.5.

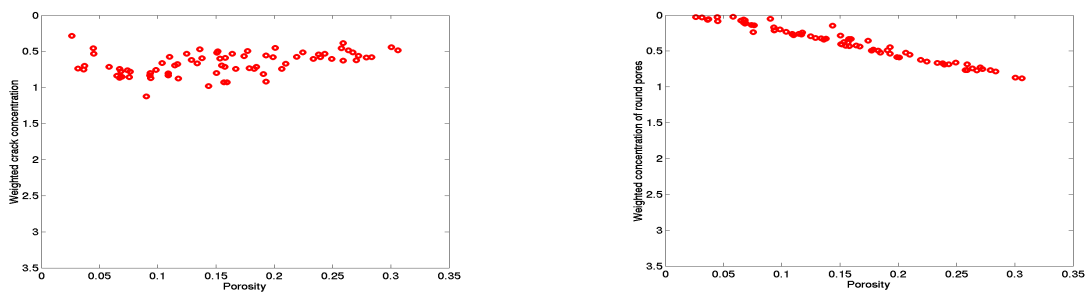


Figure 3.18 Plot of total porosity versus weighted concentration of spherical pores (right) and weighted crack concentration (left) at 40 MPa.

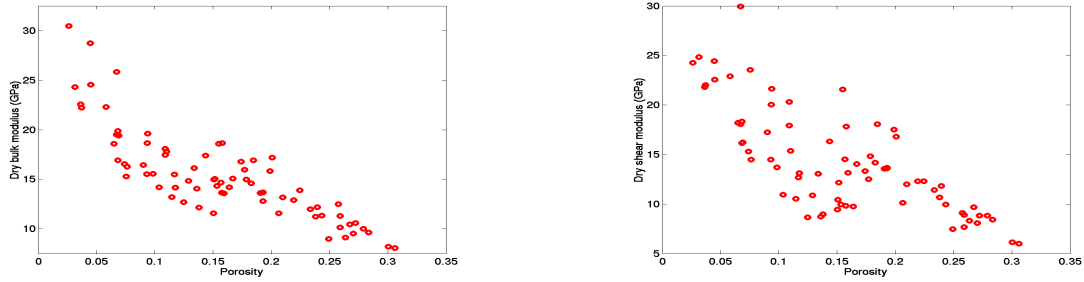


Figure 3.19 Plot of porosity versus dry bulk modulus and shear modulus at 40 MPa.

The third case is fluid saturation, at which the variation of the bulk modulus decreases according to the Gassmann's equation. The drastic change in Figure 3.5 (left) is expected to be reduced when sandstones are water-saturated. Figure 3.20 is the water-saturated bulk modulus calculated using the Gassmann's equation. It trends much more linearly than Figure 3.5 (left).

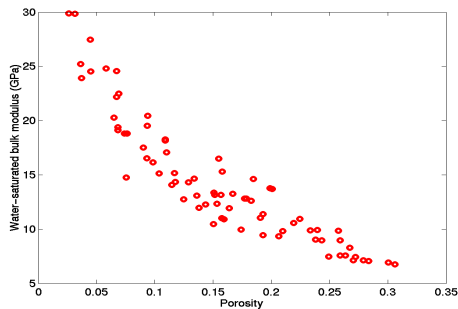


Figure 3.20 Plot of porosity versus water-saturated bulk modulus ($K_f=2.3$ GPa).

3.9 Pore geometry and change of the elastic moduli with effective pressure

The increase of the elastic moduli with increasing effective pressure depends on the amount of closed cracks. As seen in Figures 3.5 and 3.12, the elastic moduli at any given porosity vary mainly due to variation in the crack concentrations. As a result, when effective pressure increases, sandstones with

more cracks (including thin cracks) will increase more in the elastic moduli than those with less cracks. This variation accounts for the variability in the dependence of the elastic moduli on effective pressure at any given porosity as shown in Figure 3.21. The increase of the elastic moduli with effective pressure is also affected by round pores. Assuming the same crack concentration (including thin cracks), with increasing effective pressure sandstones of low porosity will increase more in the elastic moduli than those of high porosity because the increased effect of cracks on the elastic moduli (see section 3.7 for details). This result is illustrated in Figure 3.21 and is also observed by Dvorkin et al. (1996).

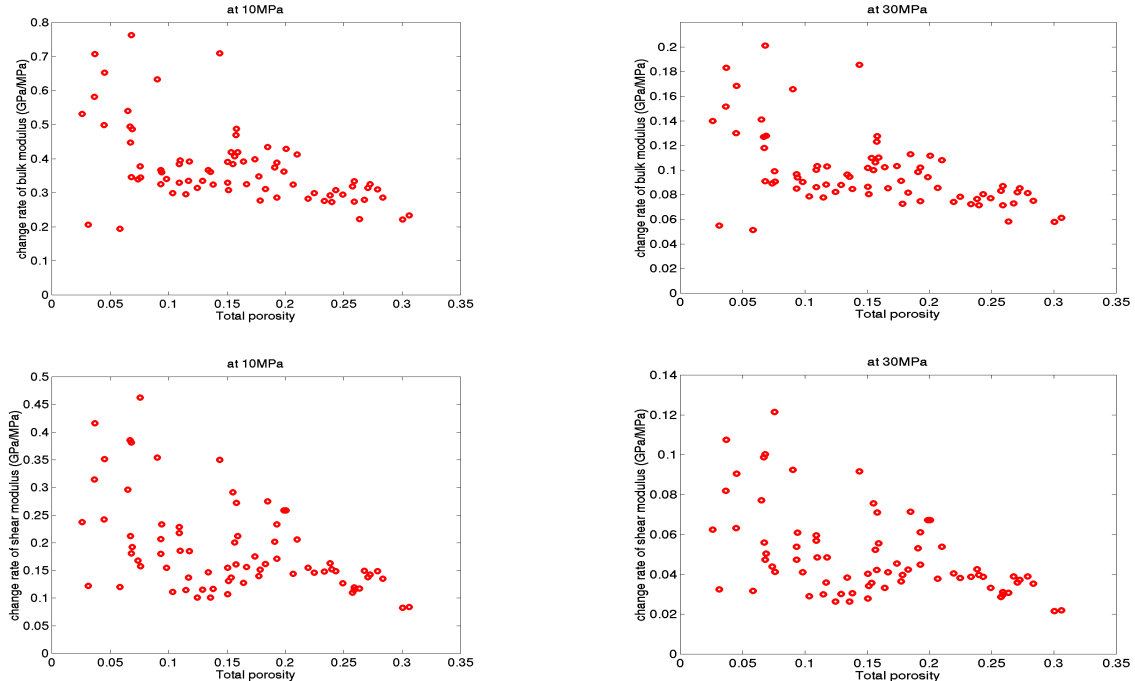


Figure 3.21 Plot of total porosity versus the rate of change of elastic moduli with respect to effective pressure at 10 and 30 effective pressure points for the first set of dry sandstones (see next chapter for detailed calculation).

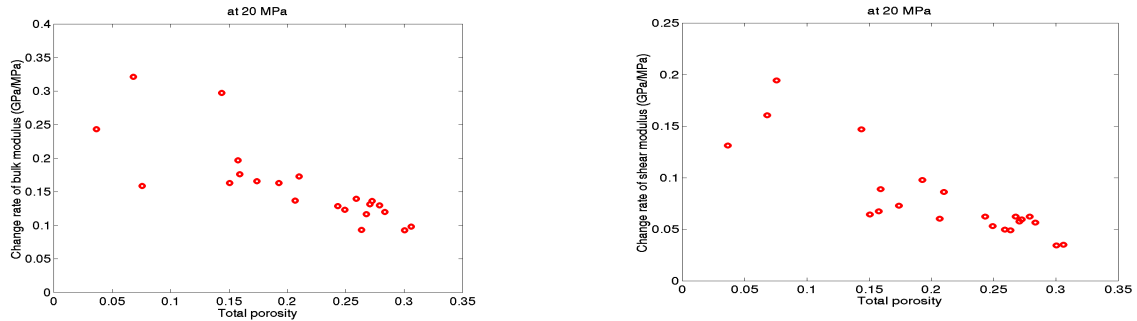


Figure 3.22 Plot of total porosity versus rate of change of the elastic moduli for the dry sandstones, which are lower than 3 GPa in bulk modulus at atmospheric pressure (see next chapter for detailed calculation).

3.10 Effect of clay content on pore geometry

The effect of clay on the pore geometry is poorly understood. Xu and White's model of clay-sand mixture (Xu and White, 1995) that sets the aspect ratio to be 0.15 for sand-related pores and 0.04 for clay-related pores seems that clay would shift pore space to low-aspect-ratio pores. Figure 3.23, however, indicates that for the first set of dry sandstones no relationship exists between clay content and the concentration of spherical pores and low-aspect-ratio cracks. Figure 3.24 further shows no correlation between clay content and pore aspect ratio for the second set of dry sandstones. Therefore, clay is not correlated to pore geometry. As stated previously, the effect of clay content on the elastic moduli is due to its effect on the elastic moduli of rock solid as shown in Figure 3. 1.

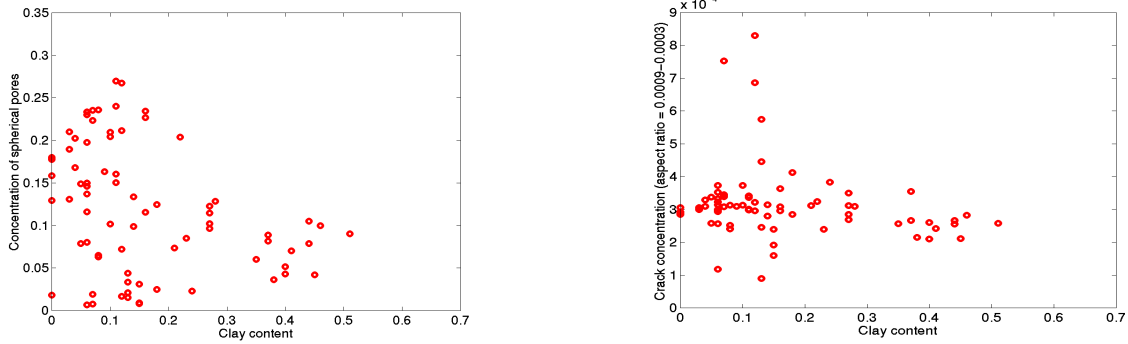


Figure 3.23 Plot of clay content versus concentration of spherical pores and low-aspect-ratio cracks, respectively, for the first set.

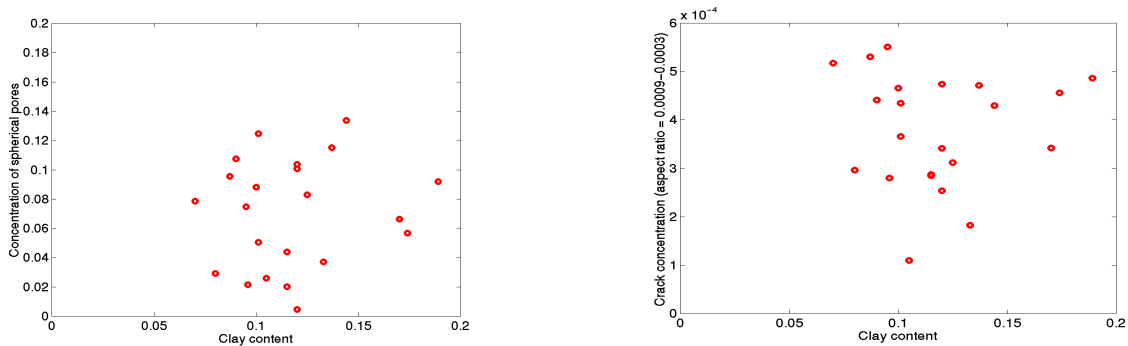


Figure 3.24 Plot of clay content versus concentration of spherical pores and low-aspect-ratio cracks, respectively, for the second set.

3.11 Discussion

An application of exploration seismology is to delineate porosity zones using seismic amplitude or velocity measurements. With the linear equations developed by some authors (Castagna et al., 1985; Han et al., 1986; Kowallis et al., 1984; Tosaya and Nur, 1982), geophysicists tend to linearly correlate velocity and porosity. Otherwise, this problem is intractable. According to this research,

linearity between porosity and the elastic moduli is possible in some cases. Despite no clear evidence, the crack concentration and porosity for reservoir rocks under similar geological settings may trend regularly with porosity. Reservoir rocks are always under certain effective pressure as to close cracks. Reservoir rocks are always saturated with fluids to decrease the difference of the elastic moduli. These situations are favorable for linearity for in-situ reservoir rocks.

Weak linearity between porosity and the elastic moduli also poses a problem for deriving porosity from sonic well logging. As shown in Figure 3.5, at the same porosity, the elastic moduli may vary significantly, especially at low porosity. The porosity obtained from the Wyllie equation will be overestimated for rocks with more cracks and underestimated for rocks with few cracks. The reason for this discrepancy is that the Wyllie equation is based on ray theory, but the propagation of borehole sonic wave is according to effective medium theory.

In seismic monitoring of production or injection, the change in effective pressure in response to the change in pore fluid pressure may cause enough changes in the elastic moduli and velocities to be detected seismically. The evaluation of these changes is thus of great significance to time-lapse seismic surveys. The change in the elastic moduli with effective pressure depends on the amount of cracks, which open or close in response to effective pressure, and the distribution of other pores. At high effective pressure, most cracks have closed and no much change with effective pressure can happen. This favours shallow or strongly-overpressured reservoirs. At high porosity, the decreased effect of cracks on the elastic moduli results in the small change of the elastic moduli with effective pressure. This favours sandstones of small or medium porosity.

The role of clay is disputable in determining elastic moduli. This research indicates that it has no effect on pore aspect ratio spectra and consequently on the change of the elastic moduli with effective pressure. Taking a close look at clay, clay in aggregates forms round pores (microporosity) in addition to flat pores between fine grains no matter where it is located, and it has no preference to any specific type of pores. In grain-supported sandstones with relatively small amounts of clay, the change in clay content may affect the amount of clay located in grain contacts, which in turn affects the elastic moduli of rock solid, but the number of grain contacts, a key factor to influence the quantity of flat pores, is controlled by porosity and grain size not clay content. So the amount of clay does not exert any influence on pore aspect ratio spectra. If clay content increases to the limit, where sandstones are clay-supported, porosity consists largely of micropores and may be more stable than grain-supported, but, as stated previously, no quantitative relations between clay content and pore aspect ratio spectra can be expected. The exception is shale, in which clay minerals are aligned along the bedding plane, and flat pores dominate pore space.

3.12 Conclusions

We have presented a method of obtaining pore aspect ratio spectra by inverting the laboratory measurements of ultrasonic compressional- and shear-wave velocities as a function of effective pressure. It is found that the concentration of spherical pores is in direct proportion to porosity, while that of cracks, despite being small, vary among individual samples with no connection to clay content. The linearity between porosity and the elastic moduli depends on how the crack concentration varies with porosity. Linearity is possible when cracks change regularly with porosity or when most cracks close at high effective pressure or when pore space is saturated with fluids. We have also discovered

that the effect of cracks on the elastic moduli decreases with increasing porosity. Consequently the variation of the elastic moduli with changing effective pressure will generally become small at high porosity. In addition, clay has no effect on pore aspect ratio spectra and consequently on the change of elastic moduli with effective pressure.

CHAPTER 4

A QUANTITATIVE MODEL FOR THE RATE OF CHANGE OF THE ELASTIC MODULI OF DRY SANDSTONES WITH EFFECTIVE PRESSURE

4.1 Calculation of the rate of change of the dry elastic moduli with effective pressure

Based on Tables 3.1 and 3.2 and equations 3.1-3.7, the dry elastic moduli for the two sets of samples were calculated at the effective pressures, at which velocities were measured in laboratory. The relationship of velocity versus effective pressure for some samples is shown in Figures 3.3 and 3.4. Figures 4.1 and 4.2 are the corresponding relationship between the dry elastic moduli and effective pressure. The circles are the theoretical calculations of the dry elastic moduli.

There are many functions, which can fit the theoretical values in Figures 4.1 and 4.2. However, the fitting model should satisfy the observations that with increasing effective pressure the elastic moduli increase rapidly in the beginning and then followed by levelling off almost to a constant at high effective pressure. The exponential function $dM/dP = a \cdot \exp(-bP)$ is a good candidate to model the rate of change of elastic moduli with effective pressure. By integration, $M = A - B \cdot \exp(-bP)$. In fact, several authors have employed similar functions to do regression analysis. Eberhart-Phillips et al. (1989) proposed the formula $V = A + K \cdot P_e - B \cdot \exp(-D \cdot P_e)$ to fit the velocity-pressure relationship. Khaksar et al. (1999) found that despite good fit of data using this formula both positive and negative K is unrealistic and inconsistent with the pressure dependence of wave velocities when extrapolating to high pressures. They developed $dV/dP = a \cdot \exp(-b \cdot P)$, i.e., $V = A - B \cdot \exp(-D \cdot P)$. Similarly, Zhang and Bentley (2000) obtained the

exponential relationship to describe the rate of change of the dry elastic moduli with effective pressure: $dM/dP = a \cdot \exp(-b \cdot P)$. However, the data show that the error percentage for the exponential model is considerable. The reason is that the logarithmic of dM/dP {obtained from another fitting model, $y = [a_1 + b_1 \cdot \ln(x)] + [a_2 + b_2/x]$ } is not a straight line but a polynomial in most cases. The numerical experiments demonstrate that the cubic polynomial is the best function to model the index of $dM/dP = \exp[f(P)]$. In Figures 4.1 and 4.2, the solid and dashed lines are regression lines {fitted with the function, $y = [a_1 + b_1 \cdot \ln(x)] + [a_2 + b_2/x]$, which give a reliable estimate of the relationship between the dry elastic moduli and effective pressure. The good fits of Khaksar et al.'s data with the exponential function are due to the effective pressure-velocity curves being flatter than the effective pressure-elastic moduli curves.

Due to great variability in the magnitude of the elastic moduli between samples, a direct empirical formula would require more parameters as mentioned above. For simplicity, it is better to deal with the rate of change of the elastic moduli with effective pressure, which vary less between individual samples.

The regression lines for the relationship between the elastic moduli and effective pressure were used to calculate the derivative with respect to effective pressure (rate of change). We plotted the derivative against total porosity to examine the effect of porosity. Figure 3.21 for the first set of sample.

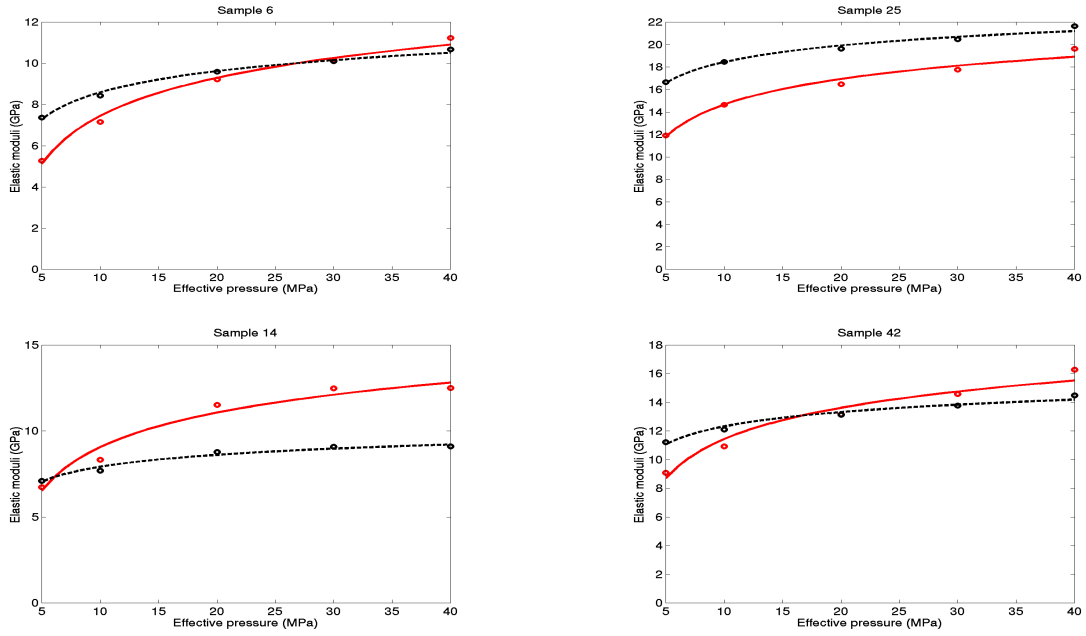


Figure 4.1 Plot of elastic moduli versus effective pressure for the first set of dry sandstones. The red and black circles are the theoretical calculations of bulk and shear moduli respectively. The red solid and black dashed lines are the corresponding regression lines.

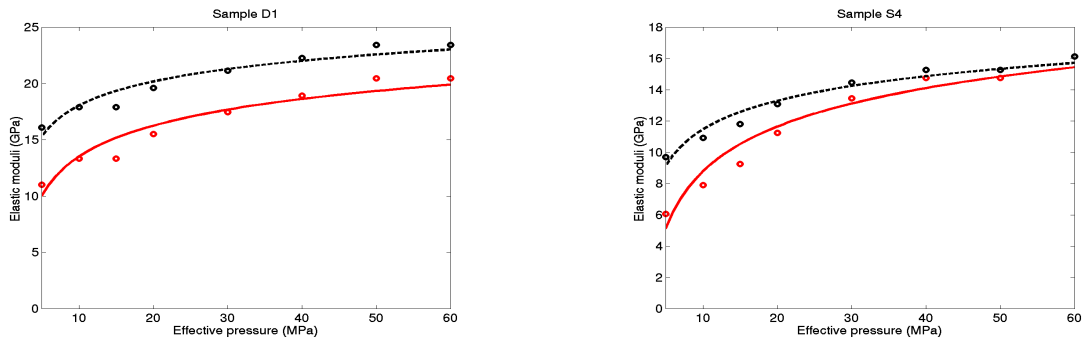


Figure 4.2 Plot of elastic moduli versus effective pressure for the second set of dry sandstones. The red and black circles are the theoretical calculations of bulk and shear moduli respectively. The red solid and black dashed lines are the corresponding regression lines.

4.2 A quantitative model for the rate of change of the dry elastic moduli with effective pressure

The goal of this section is to develop an empirical expression to predict the rate of change of the dry elastic moduli with respect to changing effective pressure. The expression can then be used to estimate, in the absence of laboratory data, the change in the dry elastic moduli due to changes in reservoir pressure. As stated previously, the best model to fit the rate of change of dry elastic moduli with effective pressure is:

$$dM/dP = \exp(a + bP + cP^2 + dP^3) \quad 4.1$$

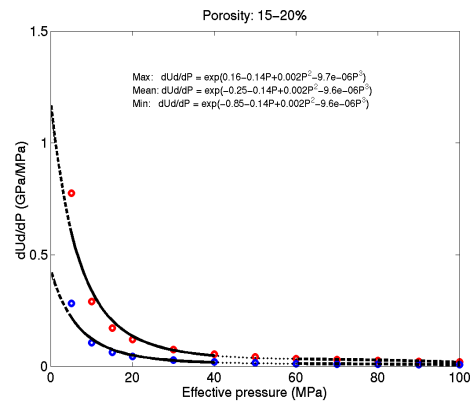
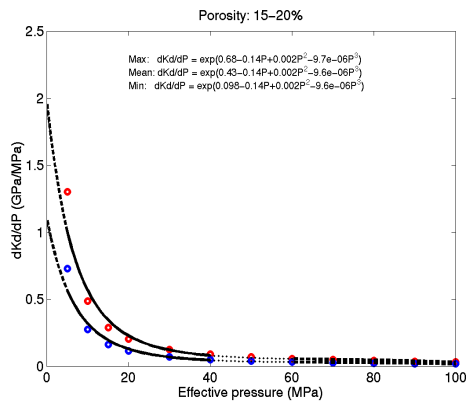
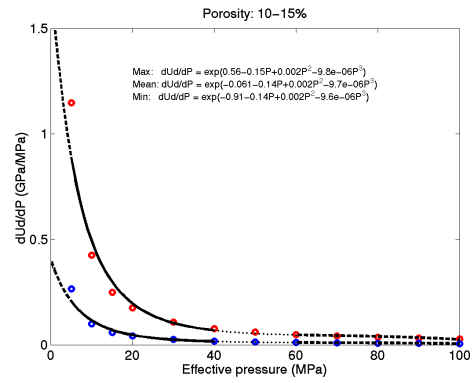
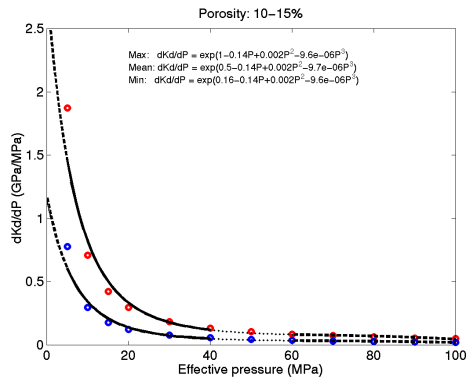
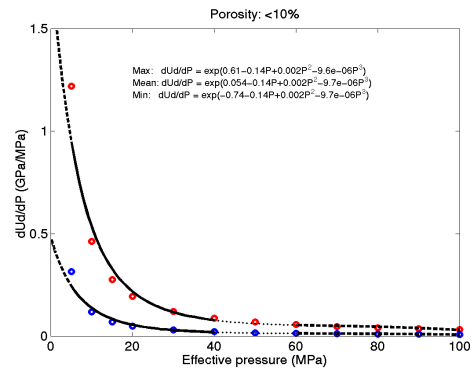
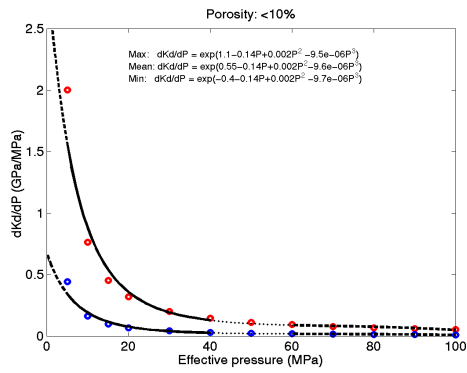
where M is the dry elastic modulus, P is the effective pressure and a , b , c , d are scalar coefficients. In most cases, b , c and d are approximately -0.14 , 0.002 and -9.6×10^{-6} , respectively, and the only difference is the coefficient a . This simplifies greatly regression analysis.

As shown in Figure 3.21, the rate of change of elastic moduli with effective pressure may be roughly divided into 5 sections in terms of the variability with porosity. The greatest variability occurs with porosity lower than 10%. The section ranging between 10% and 15% is also very variable. Appreciable decrease in variability is in 15% to 20%. The range from 20% to 25% varies less. The smallest variability is in the section of large porosity greater than 25%. For each porosity section, the upper and lower bounds and the average values were calculated at the effective pressures, at which velocities were measured, according to the regression equations. Figure 4.3 is the results, in which the upper and lower bounds and the average values are also fitted respectively with equation 4.1. Figure 4.3 indicates that two major factors affect the rate of change of the dry elastic moduli with effective pressure. The higher the porosity, the

lower the rate of change and the less variability; the higher the effective pressure, the lower the rate of change and the less variability. It is also noted that the rate of change of the bulk modulus with effective pressure is larger and more variable than that of the shear modulus.

The validity of these models can be tested by applying them to other sandstones. D. Freund (1992) measured the velocities of 88 dry samples taken from the well SALZWEDEL 2/64 at depths of 3340 to 3670 m, Germany. These clastic rocks are strongly consolidated with porosity from 0.5-15%. The effective pressure, in which measurements were made, ranges between 8 to 300 MPa. Yet the values we used to calculate the rate of increase of elastic moduli with effective pressure are those under 80 MPa because grain crushing will happen at high effective pressure (Zhang et al., 1990). About 70% of the samples for the rate of change of the bulk modulus and 57% for the rate of change of the shear modulus fall in the range delineated by the maximum and minimum lines. Some points out of the range are twice as large as the maximum line and others tend to be zero, implying that there is more variability in crack concentration in these samples than is shown in Figures 3.11 and 3.12. M. S. King (1966) measured the velocities of several dry sandstones under elevated effective pressures. The increase of elastic moduli with effective pressure for Banda, Berea and Torpedo sandstones can be predicted from the equations in Figure 4.3, but the models in Figure 4.3 slightly underestimate St. Peter sandstone and overestimate Boise sandstone. Navajo sandstone (Cheng and Toksoz, 1979) fits very well in the range.

In summary, the empirical equations to model the rate of change of dry elastic moduli with effective pressure were derived and their dependence on porosity was also included. The rate of change of the dry elastic moduli for a large portion of sandstones fall in the range defined by these empirical equations.



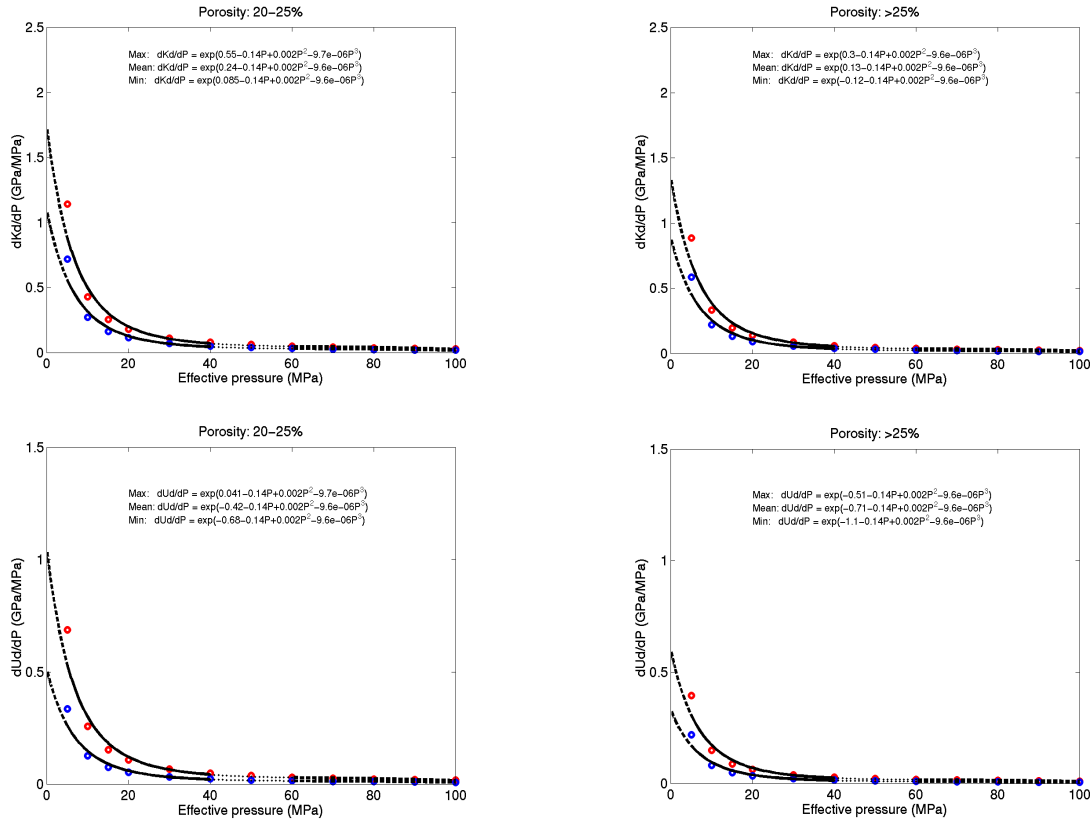


Figure 4.3 Rate of change of dry elastic moduli with effective pressure. The range with data from both sets of samples is represented by the solid lines; the dotted lines are only with the data from the second set; the dashed lines are extrapolation.

4.3 Conclusions

The rate of change of elastic moduli with effective pressure for all sandstones can be fitted well with the quasi-exponential function, i.e., $dM/dP = \exp[f(P)]$, $f(P)$ is a cubic polynomial. Its upper and lower bounds for each porosity sections are also found and modelled in this quasi-exponential function. Data from other sources indicate that the empirical bounds work well for a large portion of sandstones.

CHAPTER 5

EFFECT OF TEMPERATURE ON ELASTIC MODULI OF DRY SANDSTONES

Temperature affects the elastic moduli of a dry rock by changing the elastic moduli of the rock solid (e.g. quartz and clay) and its pore aspect ratio spectrum. The former is negligibly small, as discussed in Chapter 2, and will not be considered. The latter plays a significant role. When temperature increases, pore volume increases (even if the magnitude is small) and differential thermal expansion of the constitute minerals may cause new cracks to open (Hellwege, 1982), especially at grain boundaries. The opening of cracks occurs whenever temperature increases at a rate higher than $100^{\circ}\text{C} / 100\text{MPa}$ at high temperature (Kern, 1978). Below 200°C , however, the experimental data (Wang and Nur, 1988; Carmichael, 1989) do not observe the opening of cracks, a non-linear event. Therefore, with the exception of extreme thermal event such as those associated with steam flooding, the change of elastic moduli with temperature is attributable to the pore volume change, a linear event.

In order to find the slope of the straight line, velocity measurements and their change with temperature are collected. Carmichael's (1989) data for dry sandstone are plotted in Figures 5.1 and 5.2, which show a linear trend for the bulk and shear moduli. The slope can be approximated as:

$$dK_d/dT = -0.0155 \quad 5.1$$

$$d\mu_d/dT = -0.0065 \quad 5.2$$

The above equations are used to calculate elastic moduli in order to assess whether or not the deviation from the measurements is reasonable. Wang and Nur (1988) measured a series of velocities at different temperatures. Table 5.1 shows the measured versus calculated values for Massillon sandstone. The densities in Table 5.1 were calculated based on the formulae, $\rho_{\text{dry}} = (1-\phi) * \rho_s,$

where ρ_{dry} and ρ_s are the densities of dry sandstone and rock solid respectively, and ϕ is porosity. Since the change of density with temperature is small and roughly on the order of a few percent over 1000 °C (Carmichael, 1989), the change of ρ_{dry} over the range of 100 °C is negligible.

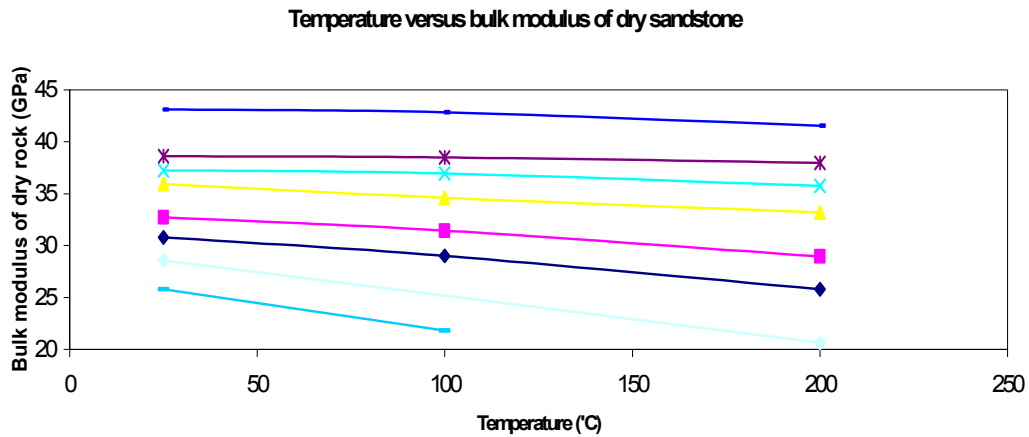


Figure 5.1 Bulk moduli versus temperature for sandstone (after Carmichael, 1989)

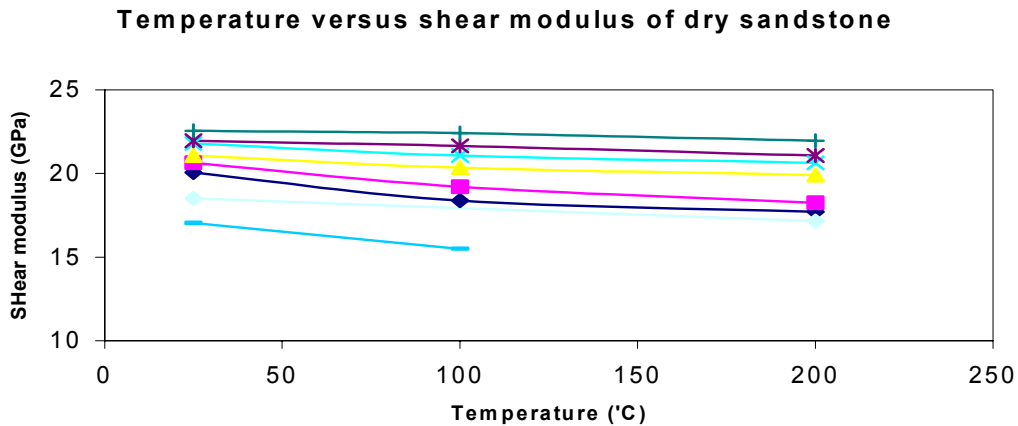


Figure 5.2 Shear moduli versus temperature for sandstone (after Carmichael, 1989)

Table 5.1 Dry velocities and elastic moduli for Massillon sandstone

T (°C)	Density	Vp	Vs	K	μ	calculated	calculated
--------	---------	----	----	---	-------	------------	------------

	(kg/cm ³)	(km/s)	(km/s)	(GPa)	(GPa)	K (GPa)	μ (GPa)
20	2100	3.08	2.16	6.87	9.79	6.87	9.79
30	2100	3.06	2.14	6.84	9.62	6.72	9.72
40	2100	3.04	2.12	6.82	9.44	6.57	9.66
50	2100	3.00	2.11	6.43	9.35	6.42	9.59
60	2100	2.99	2.10	6.42	9.26	6.27	9.53
80	2100	2.98	2.09	6.42	9.17	5.97	9.40
100	2100	2.95	2.08	6.17	9.08	5.67	9.20
120	2100	2.94	2.05	6.39	8.82	5.37	9.14

The experimental and calculated values show the same trend and the order of magnitude of the variation is small. The change in bulk and shear moduli with temperature is also small. In the case of Massillon sandstone, 7% and 10% changes for bulk and shear moduli respectively occur for 100°C change in temperature.

CHAPTER 6

FEASIBILITY OF SEISMIC MONITORING OF SANDSTONE RESERVOIRS

6.1 Introduction

Recent examples of time-lapse seismic surveys (Jack, 1998; Sonneland et al., 1997) have demonstrated potential for inferring reservoir conditions from seismic data. It appears that the seismic detectability of changes in reservoir conditions due to production or injection is most pronounced in poorly cemented and poorly consolidated sandstone reservoirs. These zones are easily observed at shallow depths or in geopressured zones, which are a result of undercompaction in rapidly deposited sedimentary basins and can be located at great depths. In this paper we examine the effect of the major recovery processes on seismic velocities and acoustic impedance for sandstones of varying porosity and effective pressure, and then find the factors most sensitive to changes in reservoir conditions. The depth effect on seismic monitoring of sandstone reservoirs is also discussed. The method presented here can be also used as a tool to analyze feasibility of seismic monitoring of sandstone reservoirs.

6.2 Quantitative rock physics models

6.2.1 Relationship between porosity and dry elastic moduli. All physical properties (such as mechanical, acoustic, electrical, thermal, magnetic etc.) of rocks are influenced by pore structure (after Gueguen and Palciauskas, 1994), one of the most common descriptions of which is porosity. So in prediction of elastic behaviour, porosity is an important parameter. Nur et al. (1991 and 1995)

found a linear trend of elastic moduli between the mineral values at zero porosity and the suspension values at the critical porosity. The critical porosity separates the mechanical and acoustic behaviour into two distinct domains, i.e., the load-bearing domain and the suspension domain. This leads to the convenient mathematic expressions for calculation of dry elastic moduli at high effective pressure in the load-bearing domain (Mavko et al., 1998):

$$K_d = K_s (1 - \phi / \phi_c) \quad 6.1$$

$$\mu_d = \mu_s (1 - \phi / \phi_c) \quad 6.2$$

where K_d and μ_d are dry bulk and shear moduli, K_s and μ_s are bulk and shear moduli of rock solid or grain, ϕ_c is critical porosity (40% for sandstone, Mavko et al., 1998), ϕ is porosity. Obviously $K_d = \mu_d = 0$ at $\phi = \phi_c$. High effective pressure refers to pressures at which rocks are almost linearly elastic and the change of elastic moduli and velocities with effective pressure tend to be zero. For most sandstones, 100 MPa may be considered high enough to flatten the curve. K_s and μ_s are influenced by clay content, but the exact formula to describe their relationship is unavailable in literature. Based on the linear relationship of velocities to porosity and clay content (Castagna et al., 1985; Han et al., 1986; Tosaya and Nur, 1982), we may extrapolate velocities to those at zero porosity and predict the change of the elastic moduli of rock solid with clay content.

The increase of dry elastic moduli with effective pressure can be explained in terms of closing of cracks, which are very small in volume. The study in Chapters 3 and 4 calculated dry elastic moduli of sandstone samples at a variety of effective pressures and found the quasi-exponential relationship between the rate of increase of dry elastic moduli and effective pressure as follows:

$$dK_d/dP = \exp(A1+B1P+C1P^2+D1P^3) \quad 6.3$$

$$d\mu_d/dP = \exp(A2+B2P+C2P^2+D2P^3) \quad 6.4$$

where K_d and μ_d are in GPa, P is effective pressure in MPa, $A1, B1, C1, D1, A2, B2, C2, D2$ are constants, which vary among individual sandstones because porosity and crack concentration differ. The study in Chapters 3 and 4 also found that the rate of change of elastic moduli with effective pressure generally becomes low with increasing porosity and derived these constants for the average case at different porosities. These constants were used in this Chapter.

We employed Han's empirical linear relationship of velocities to porosity and clay content (Han et al., 1986) to predict the change of the elastic moduli of rock solid with clay content. This was achieved by extrapolating velocities to those at zero porosity based on this linear relationship. Then according to equations 6.1–6.4, dry elastic moduli were expressed as a function of porosity and effective pressure at a given clay content. Supposing 10% of clay content, the contour of dry elastic moduli was drawn on the plane of porosity and effective pressure (such as Figure 6.1).

6.2.2 Elastic moduli of fluid-saturated sandstones Gassmann's model connects the elastic moduli of the fluid-saturated rock to the corresponding dry elastic moduli through the following equations:

$$K_u = K_d + \frac{(1 - \frac{K_d}{K_s})^2}{\frac{\phi}{K_f} + \frac{1 - \phi}{K_s} - \frac{K_d}{K_s^2}} \quad 6.5$$

$$\mu_u = \mu_d \quad 6.6$$

where K_u and μ_u are the bulk and shear moduli of the fluid-saturated rocks, K_f is the fluid bulk modulus, ϕ is porosity. When the rock is saturated with more than one fluid, the bulk modulus of the effective fluid is used. If fluids equilibrate in

pressure in one period when seismic wave propagates, they are considered to be homogeneously distributed and the bulk modulus of the effective fluid is a harmonic averaging of the bulk moduli of all fluids (Reuss model); if fluids differ in pressure between different phases of fluids on a coarse scale, the bulk modulus of the effective fluid can be approximated as an arithmetic averaging (Mavko et al., 1998). Obviously, whether harmonic or arithmetic averaging is used depends on seismic frequency. Mavko et al. (1998) uses L_c to identify these two cases. If the scale of saturation inhomogeneity is small relative to seismic wavelength and at the same time larger than L_c , the arithmetic averaging are used. Otherwise, pressure is assumed to be equal among fluids. $L_c = (\kappa K_f / f \eta)^{1/2}$, where f is the seismic frequency, κ is the permeability, and η and K_f are the viscosity and bulk modulus of the most viscous fluid phase (Mavko et al., 1998). In practice, the size of regions containing different fluid phases is unknown. Considering a hydrocarbon pool, the water resides with the pore space next to the grain walls and in cracks while the oil or gas stays in the center of the pores. This situation happens in most water-wet sandstone reservoirs before production. Despite saturation inhomogeneity on the grain scale, simple calculations indicate that pressure equilibrium occurs in seismic frequency. It is thus safe to assume fluids before production are homogeneously mixed. After production or injection, the situation becomes much more complicated. When water or other fluids flood oil or gas, fluid fingering or patchy saturation on coarse scale may happen. Mavko et al. (1998) simulated patchy saturation with data from a West Texas reservoir. Laboratory results also seem to support patchy saturation. The drainage curve discordant with the imbibition curve (Knight et al., 1990), in which fluids are considered homogeneously mixed, is evident for the existence of patchy saturation. Water flooding gas experiments (Wang et al., 1991) show the compressional velocity increases by more than 5%, implying a possible patchy saturation. In these two cases, if fluids are assumed to be homogeneously distributed, velocity increase with increasing water saturation

cannot take place according to Domenico's effect (Domenico, 1976). Most importantly, Sonneland et al. (1997) observed that sonic velocities increased where water had displaced oil in the Gullfaks Field, Norwegian North Sea. It is therefore reasonable to assume patchy saturation after fluid drive or flood.

6.2.3 Velocities and acoustic impedance of fluid-saturated sandstones The bulk density of fluid-saturated sandstones is simply the weighted-by-volume average of the constituent densities given by the equation:

$$\rho_b = \phi S_o \rho_o + \phi S_g \rho_g + \phi S_w \rho_w + (1-\phi)\rho_s \quad 6.7$$

where ρ_o , ρ_g , ρ_w and ρ_s are densities of oil, gas, water and rock solid respectively.

The P-, S-wave velocities and acoustic impedance of fluid-saturated sandstone reservoirs are calculated as:

$$V_p = \sqrt{\frac{K_u + \frac{4}{3}\mu_u}{\rho_b}} \quad 6.8 \quad V_s = \sqrt{\frac{\mu_u}{\rho_b}} \quad 6.9 \quad AI = \rho_b V_p \quad 6.10$$

Based on 6.1 - 6.10, we can calculate the velocities and acoustic impedance before and after a certain recovery process at varying porosity and effective pressure and then identify the most important factors, which cause the velocity and acoustic impedance changes. If the regional compaction curve and the fluid gradient are given, the velocity and acoustic impedance changes due to the recovery can be predicted in terms of effective pressure and depths. The method can be used to study feasibility of seismic monitoring of reservoirs.

6.3 Quantitative evaluation of production or injection processes in terms of velocities and acoustic impedance

Before application of the rock physics model to feasibility study in the real geological setting, we should evaluate the validity of the dry elastic moduli at varying porosity and effective pressure calculated based on our theoretical model and see if they can approximate those in situ with the same porosity and effective pressure. According to our study, the volume concentration of round pores at some porosity is in direct proportion to the magnitude of that porosity, but the crack volume concentration is variable, depending on effective pressure and other lithological factors. Despite being very small in volume, cracks can contribute a lot to decreasing elastic moduli. This leads to the uncertainty in elastic moduli for a given porosity and effective pressure. However, porosity and elastic moduli become linearly related when cracks close at high effective pressure, as indicated by the KT model (Kuster and Toksoz, 1974) and the linear relationship proposed by Nur et al. (1991 and 1995). Equations 6.3 and 6.4 are derived from the average case of crack concentrations for 97 sandstone samples. So the dry elastic moduli in our theoretical model are the average values, around which those in situ may vary. It is also noted that the variability around the average case becomes less when porosity increases due to decreasing effect of cracks on elastic moduli, which implies that for high-porosity sandstones the theoretical values may be accurate.

6.3.1 Water drive Many of the most important reservoirs in the world are producing by water drive, in which the goal of seismic monitoring is to identify bypassed oil pockets for infill drilling. The most important characteristic in water drive is that pressure remains high at low rates of production. Clark (1969) pointed out that pressure still maintained 70% of the initial even after 60% of the oil had been produced from reservoirs. The water drive may be therefore

reasonably considered as a process of water substitution for oil with a small pressure drop. Temperature can also be assumed constant because replacing water is located close to replaced oil. These assumptions imply that the changes in fluid properties such as bulk moduli and densities are minimal during water drive.

To enable the calculation of velocities and acoustic impedance of rocks at certain porosity and effective pressure, a group of parameters have to be assigned, including fluid bulk moduli and densities, irreducible water saturation before production and residual oil saturation after water drive. We chose to use the data of fluid properties from Domenico (1974) and the average case of irreducible water saturation and residual oil saturation for sandstone reservoirs from Smith et al. (1992). Figure 6.1 shows the contours of the absolute change and the percentage change in fluid-saturated bulk modulus due to fluid substitution by water drive, with the dotted lines as the contour of the dry bulk modulus. The absolute change in fluid-saturated bulk modulus is affected by both dry bulk modulus and porosity as shown in the Gassmann equation (equation 6.5) and the left part of Figure 6.1. For a given porosity, the lower the dry bulk modulus, the more the change. For a given dry bulk modulus, the lower the porosity, the more the change. However, in most cases, the decrease in dry bulk modulus is accompanied by the increase in porosity. What happens to this complex situation? According to the left of Figure 6.1, the absolute change always increases along the opposite direction of K_d gradient regardless of porosity and it also increases in most other cases. So the dry bulk modulus may play a major role. Since the fluid-saturated bulk modulus decreases with decreasing the dry bulk modulus in most cases shown in Figure 6.2, the percentage change is generally predominantly controlled by the dry bulk modulus. The effect of porosity is limited to the range of low porosity and low effective pressure. This is shown in the right of Figure 6.1. Figure 6.3 shows the

Vp and AI percentage changes. The shape of the Vp and AI percentage change contours to those of dry bulk modulus further indicates that dry bulk modulus is the most important factor. The smaller the dry elastic modulus, the greater the percentage changes. If the minimum changes are set in order for these changes to be observable on seismic sections (Jack, 1998; Lumley et al., 1997), the largest values of dry bulk modulus to create these changes may be found from Figure 6.3. These values would be larger at low porosity due to the porosity effect.

The contrast between the bulk modulus of the original and the substituted fluid is another factor because the fluid bulk modulus affects fluid-saturated bulk modulus through the Gassmann equation. Figure 6.4 shows a considerable increase in the percentage changes due to an increase in water bulk modulus (to 3.1 GPa). The percentage increase is large for small dry bulk modulus. Similarly, a large decrease in the percentage changes takes place in Figure 6.5 due to a decrease in water bulk modulus (to 1.4 GPa).

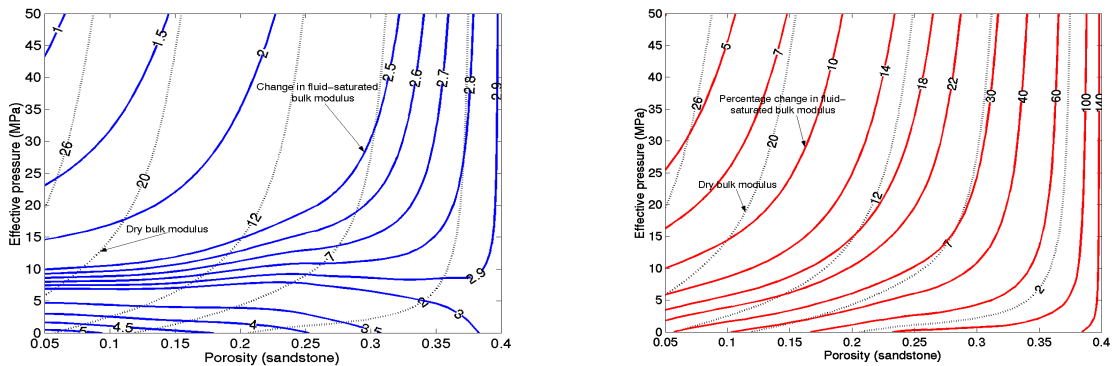


Figure 6.1 Contours of the absolute change and the percentage change in fluid-saturated bulk modulus. The dotted lines are dry bulk modulus. The absolute change of the fluid-saturated bulk modulus is defined as $\Delta K = K_{\text{after}} - K_{\text{before}}$, where K_{after} and K_{before} are the fluid-saturated bulk modulus after and before water drive, respectively. The percentage change is $\Delta K / K_{\text{before}} * 100\%$. Fluid properties are assumed: before production, $D_o = 0.749 \text{ (g/cm}^3\text{)}$, $K_o = 0.67 \text{ (GPa)}$, $S_o = 75\%$, $D_w = 1.089 \text{ (g/cm}^3\text{)}$, $K_w = 2.38 \text{ (GPa)}$, $S_w = 25\%$; after water drive, $D_o = 0.749 \text{ (g/cm}^3\text{)}$, $K_o = 0.67 \text{ (GPa)}$, $S_o = 15\%$, $D_w = 1.089 \text{ (g/cm}^3\text{)}$, $K_w = 2.38 \text{ (GPa)}$, $S_w = 85\%$.

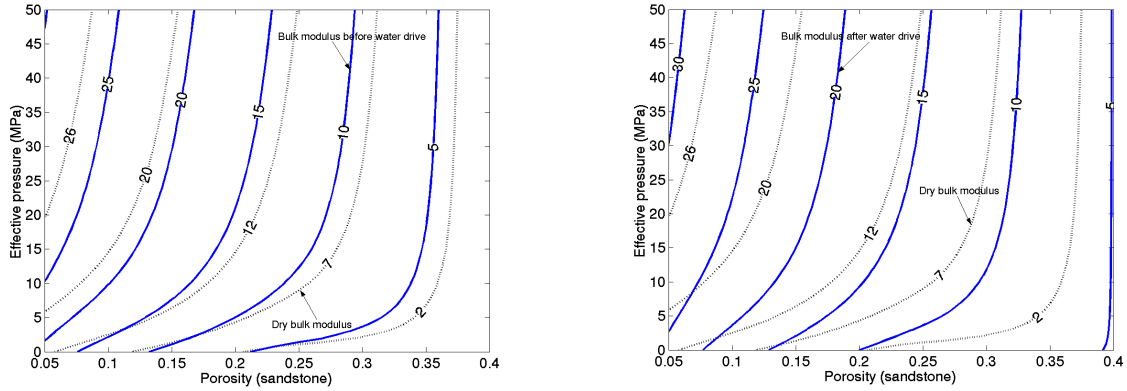


Figure 6.2 Contours of the fluid-saturated bulk modulus before and after water drive. The fluid properties are the same as those in Figure 6.1.

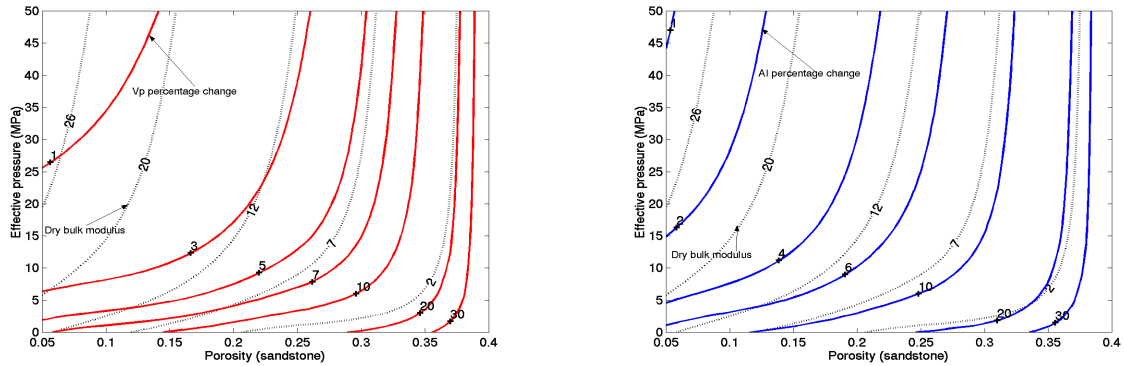


Figure 6.3 Contours of V_p and AI percentage changes. Fluid properties are the same as those in Figure 6.1. The V_p percentage change is defined as $\Delta V_p / V_{p\text{-before}} * 100\% = (V_{p\text{-after}} - V_{p\text{-before}}) / V_{p\text{-before}} * 100\%$, where $V_{p\text{-after}}$ and $V_{p\text{-before}}$ are the primary wave velocity after and before water drive, respectively (the same below). The AI percentage change is defined as $\Delta AI / AI_{\text{before}} * 100\% = (AI_{\text{after}} - AI_{\text{before}}) / AI_{\text{before}} * 100\%$, where AI_{after} and AI_{before} are the acoustic impedance after and before water drive, respectively (the same below).

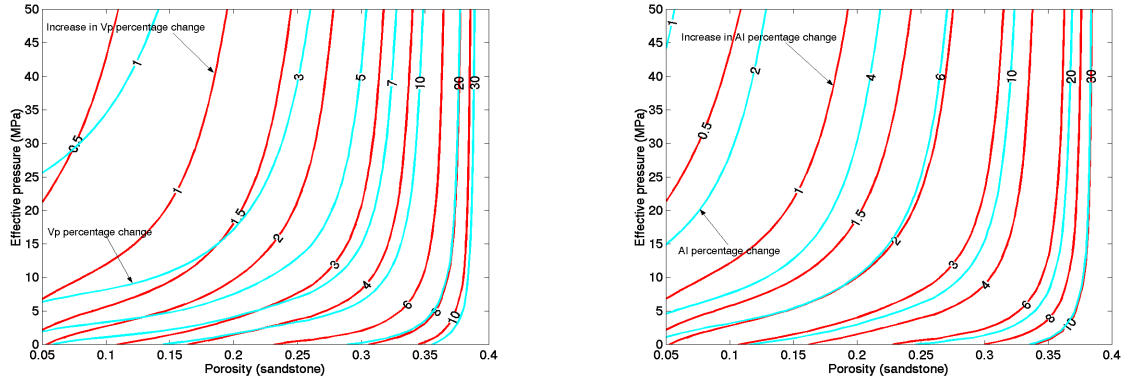


Figure 6.4 Contours of increase in the V_p (left) and AI (right) percentage changes due to an increase in water bulk modulus (to 3.1 GPa). The contour lines of the percentage changes are computed based on the same fluid properties as those in Figure 6.1. The increase in V_p percentage change is defined as $(\Delta V_p/V_{p\text{-before}} * 100\%)_{\text{adjusted water bulk modulus}} - (\Delta V_p/V_{p\text{-before}} * 100\%)_{\text{original case}}$. The increase in AI percentage change is defined as $(\Delta AI/AI_{\text{before}} * 100\%)_{\text{adjusted water bulk modulus}} - (\Delta AI/AI_{\text{before}} * 100\%)_{\text{original case}}$.

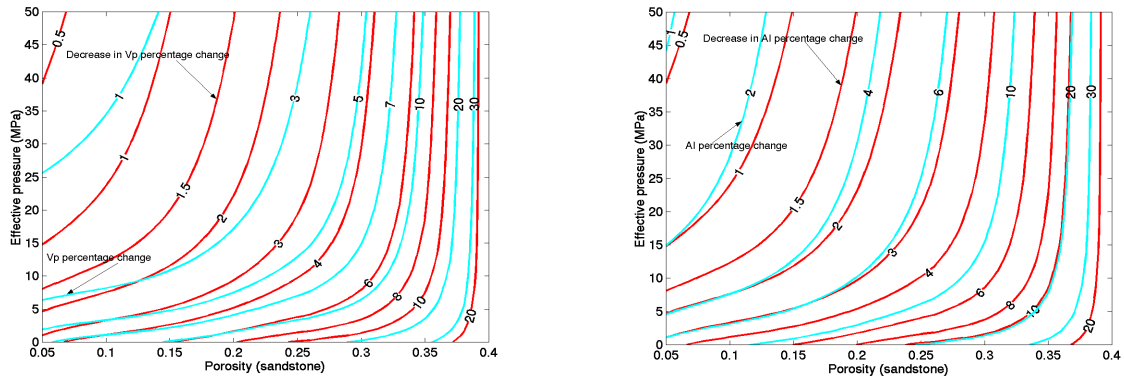


Figure 6.5 Contours of decrease in the V_p (left) and AI (right) percentage changes due to a decrease in water bulk modulus (to 1.4 GPa). The contour lines of the percentage changes are computed based on the same fluid properties as those in Figure 1. The decrease in V_p percentage change is defined as $(\Delta V_p/V_{p\text{-before}} * 100\%)_{\text{original case}} - (\Delta V_p/V_{p\text{-before}} * 100\%)_{\text{adjusted water bulk modulus}}$. The decrease in AI percentage change is defined as $(\Delta AI/AI_{\text{before}} * 100\%)_{\text{original case}} - (\Delta AI/AI_{\text{before}} * 100\%)_{\text{adjusted water bulk modulus}}$.

Fluid density may play a significant role in the percentage changes. By increasing density contrast between oil and water, V_p percentage change will decrease and the AI percentage change will increase. The maximum effect of

fluid density on the percentage changes can be obtained by comparing the percentage changes with large density contrast (0.7 for oil and 1.14 for water, Gretener, 1993) with those with small or no density contrast (1.0 for both oil and water, Gretener, 1993). Irreducible water saturation and residual oil saturation are also set to be small. In Figure 6.6, the amount of decrease or increase in the percentage changes depends on porosity. The higher the porosity, the more the decrease or increase. Yet the value is relatively small, having no substantial impact on the percentage changes especially at high porosity. In the real case of water drive, the density effect will be smaller because the density contrast will not be so large and irreducible water saturation and residual oil saturation may not be so small. Thus, the fluid density contrast is not as important as the fluid bulk modulus contrast in water drive.

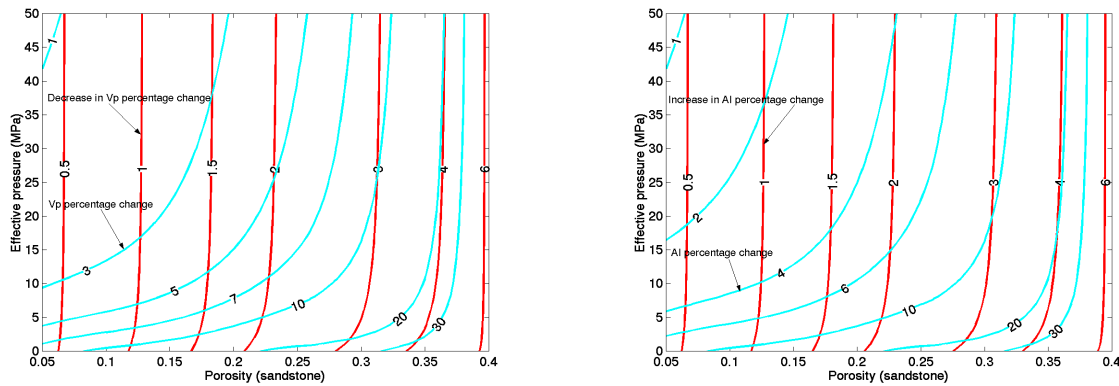


Figure 6.6 Contours of decrease in V_p percentage change (left) and increase in AI percentage change (right) due to an increase in the density contrast (0.7 for oil, 1.14 for water). The decrease in V_p percentage change is defined as $(\Delta V_p / V_{p\text{-before}} * 100\%)_{\text{small density contrast}} - (\Delta V_p / V_{p\text{-before}} * 100\%)_{\text{large density contrast}}$. The increase in AI percentage change is defined as $(\Delta AI / AI_{\text{before}} * 100\%)_{\text{large density contrast}} - (\Delta AI / AI_{\text{before}} * 100\%)_{\text{small density contrast}}$. The percentage changes are based on the following data: before production, $D_o=1.00(\text{g}/\text{cm}^3)$, $K_o=0.67$ (GPa), $S_o=90\%$, $D_w=1.00(\text{g}/\text{cm}^3)$, $K_w=2.38$ (GPa), $S_w=10\%$; after water drive, $D_o=1.00(\text{g}/\text{cm}^3)$, $K_o=0.67$ (GPa), $S_o=5\%$, $D_w=1.089(\text{g}/\text{cm}^3)$, $K_w=2.38$ (GPa), $S_w=95\%$.

The saturation affects the percentage changes because it affects the fluid density and bulk modulus. Suppose two cases: small changes in oil and water saturations before and after water drive, and large ones. As demonstrated in Figure 6.7, the contours of the increase in the percentage changes due to increasing saturation contrast are almost parallel to the percentage changes (for the small saturation contrast), just as those observed due to the change in water bulk modulus in Figures 6.4 and 6.5. The increase is different than that indicated in Figure 6.6. This implies that the saturation effect on the fluid bulk modulus is much more important than on the fluid density. So the saturation effect on the percentage changes is due to its effect on the fluid bulk modulus.

If fluid pressure drops after water drive, the dry elastic moduli will increase in response to an increase in effective pressure, and simultaneously the densities and bulk moduli of oil and water will decrease in response to a decrease in fluid pressure. The increase in the dry elastic moduli is affected by porosity and effective pressure, as indicated by equations 6.3 and 6.4. The decrease in the densities and bulk moduli of oil and water can be influenced by both fluid temperature and pressure. As shown in Figure 6.8, the curves are almost linear and the density gradient with pressure for both water and brine is small in the range of 0.0002-0.0003 (g/cm³)/MPa, despite varying temperature and salinity. The change of oil densities with pressure is more complicated because R_{so} will evolve with pressure. Above the bubble-point pressure (or constant compositions), however, it becomes simply pressure and temperature dependent. Batzle and Wang (1992) proposed the formula (see equations 2.32 and 2.33) to compute the density of dead oil at any temperature and pressure. The gradient may be extended to that of live oil above the bubble-point pressure. As shown in Figure 6.9, the gradient at pressures less than 70 MPa is a little larger than that of water, between 0.0004-0.0008 (g/cm³)/MPa. Considering a

small drop of fluid pressure and the small effect of density in Figure 6.6, the effect of density change for oil and water is not of significance.

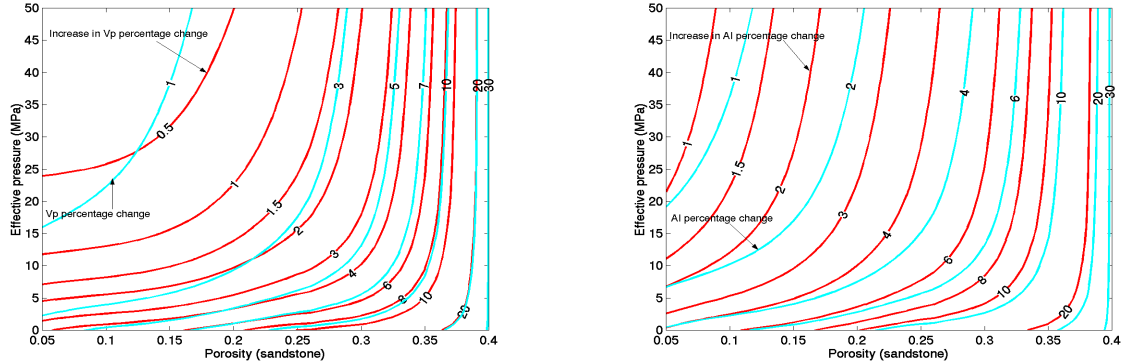


Figure 6.7 Contours of increase in V_p (left) and AI (right) percentage changes (left) due to increasing saturation contrast. The increase in V_p percentage change is defined as $(\Delta V_p / V_{p\text{-before}} * 100\%)_{\text{large saturation contrast}} - (\Delta V_p / V_{p\text{-before}} * 100\%)_{\text{small saturation contrast}}$. The increase in AI percentage change is defined as $(\Delta AI / AI_{\text{before}} * 100\%)_{\text{large saturation contrast}} - (\Delta AI / AI_{\text{before}} * 100\%)_{\text{small saturation contrast}}$. The small saturation change is assumed to be: before production, $D_o=0.749$ (g/cm³), $K_o=0.67$ (GPa), $S_o=50\%$, $D_w=1.089$ (g/cm³), $K_w=2.38$ (GPa), $S_w=50\%$; after water drive, $D_o=0.749$ (g/cm³), $K_o=0.67$ (GPa), $S_o=30\%$, $D_w=1.089$ (g/cm³), $K_w=2.38$ (GPa), $S_w=70\%$. The large saturation change is assumed to be: before production, $D_o=0.749$ (g/cm³), $K_o=0.67$ (GPa), $S_o=90\%$, $D_w=1.089$ (g/cm³), $K_w=2.38$ (GPa), $S_w=10\%$; after water drive, $D_o=0.749$ (g/cm³), $K_o=0.67$ (GPa), $S_o=5\%$, $D_w=1.089$ (g/cm³), $K_w=2.38$ (GPa), $S_w=95\%$. The percentage changes in this figure are based on the data of the small case.

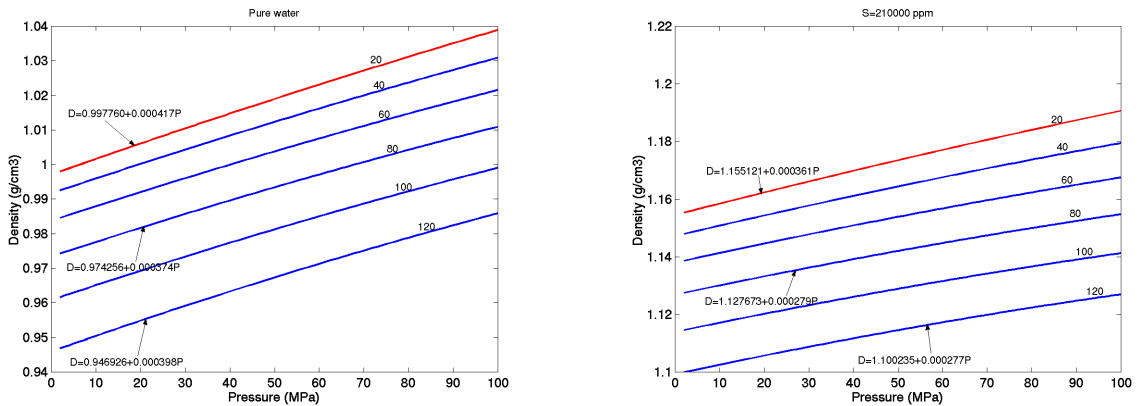


Figure 6.8 Change of water density with pressure. The calculation is based on equations 2.28 and 2.29.

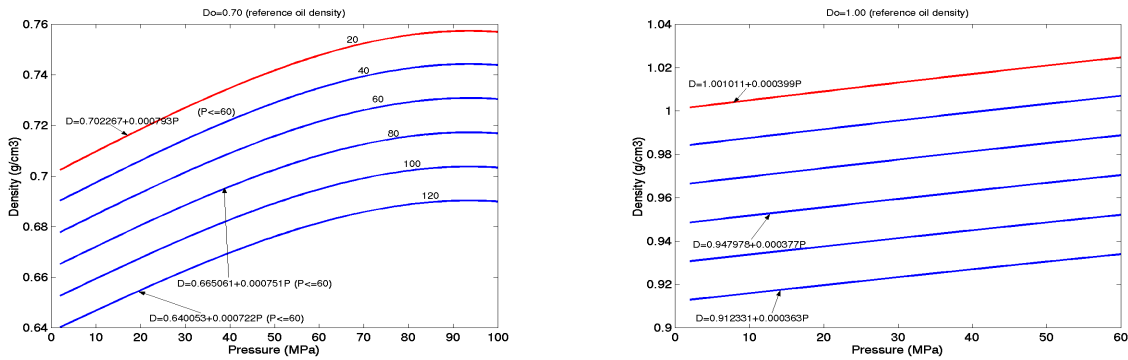


Figure 6.9 Change of oil density with pressure. The calculation is based on equations 2.32 and 2.33. The equations are applicable to the oil of constant compositions.

Figure 6.10 is the change of the bulk modulus of water with pressure, showing that the gradients of the bulk modulus of water with pressure are similar at the same salinity in spite of temperature variation. The gradient difference due to salinity changes is insignificant. Most importantly, the magnitude of the gradient is not large. Except for a drastic pressure drop, the substantial decrease of the bulk modulus of water will not take place. For example, 5 MPa pressure decline causes at most 0.05 GPa decrease, failing to produce appreciable modification to the results. For the change of oil bulk modulus with pressure, the equation (20b) of Batzle and Wang (1992) or equation 2.31 may be used to evaluate the gradient if it is assumed that the oil is above the bubble-point pressure. Figure 6.11 is the results based on the equation (20b) of Batzle and Wang (1992). Despite increase in the gradient, the magnitude of gradient is still small. If pressure does not drop by a large amount, the decrease in oil bulk modulus is not considerable.

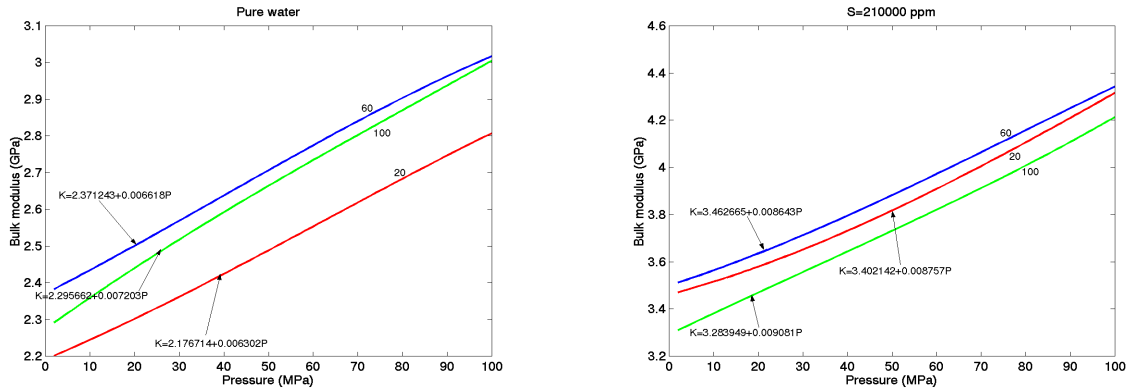


Figure 6.10 Change of water bulk modulus with pressure. The calculation is based on equations 2.25, 2.26, 2.27, 2.28 and 2.29.

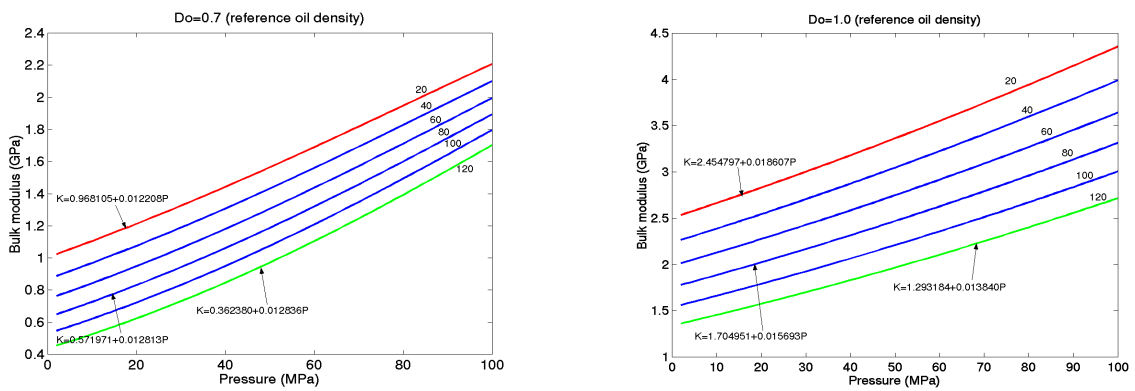


Figure 6.11 Change of oil bulk modulus with pressure. The calculation is based on equations 2.32 and 2.33 in chapter 2 and equation 20b in the paper by Batzle and Wang (Batzle and Wang, 1992).

Figure 6.12 is the contours of increase in the percentage changes due to an increment of 5MPa in effective pressure in addition to fluid substitution. It does not consider the decrease of the fluid bulk modulus and density due to pressure drop. As expected, the increase in the percentage changes becomes large and appreciable at low effective pressure and small at high effective pressure. So the percentage changes are sensitive to effective pressure chiefly at low effective

pressure. When a decrease in the bulk moduli of water and oil due to pressure drop after water drive is included, the percentage changes will be smaller than those without considering the change in fluid bulk modulus. As indicated in Figure 6.13, the difference is negligibly small. It is therefore concluded that fluid pressure drop in water drive causes the increase in the percentage changes chiefly through increasing dry elastic moduli at low effective pressure.

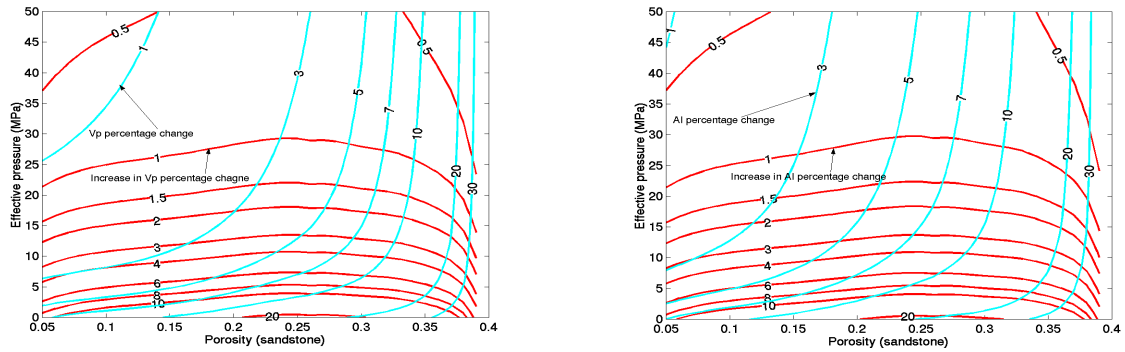


Figure 6.12 Contours of increase in V_p (left) and AI (right) percentage changes due to a decrease of 5MPa in fluid pressure in addition to fluid substitution. The increase in V_p percentage change is defined as $(\Delta V_p / V_{p\text{-before}} * 100\%)_{5\text{MPa fluid pressure drop plus fluid substitutions}} - (\Delta V_p / V_{p\text{-before}} * 100\%)_{\text{only fluid substitution}}$. The increase in AI percentage change is defined as $(\Delta AI / AI_{\text{before}} * 100\%)_{5\text{MPa fluid pressure drop plus fluid substitution}} - (\Delta AI / AI_{\text{before}} * 100\%)_{\text{only fluid substitution}}$. The contours of V_p and AI percentage changes due to fluid substitution are the same as those in Figure 6.1.

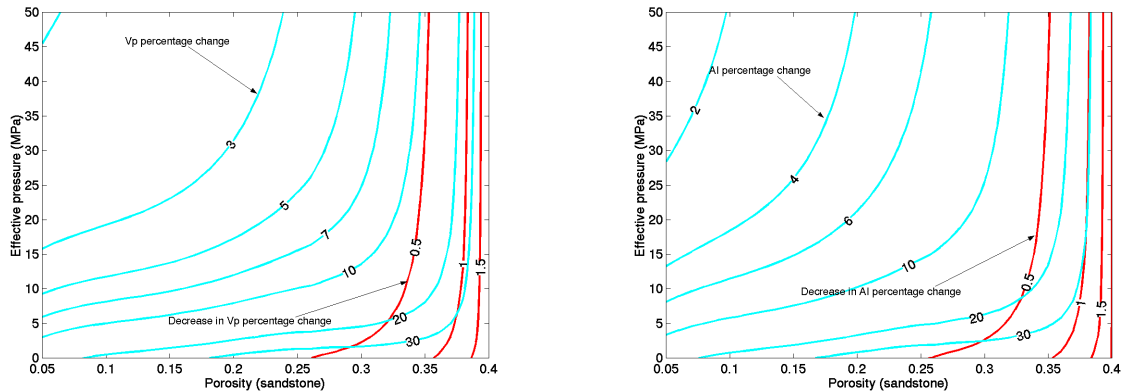


Figure 6.13 Contours of decrease in V_p (left) and AI (right) percentage changes due to a decrease of fluid bulk moduli (0.05 for water and 0.1 for oil, after water drive). The decrease in V_p

percentage change is defined as $(\Delta V_p/V_{p\text{-before}} * 100\%)_{\text{without fluid change}} - (\Delta V_p/V_{p\text{-before}} * 100\%)_{\text{with fluid change}}$. The decrease in AI percentage change is defined as $(\Delta AI/AI_{\text{before}} * 100\%)_{\text{without fluid change}} - (\Delta AI/AI_{\text{before}} * 100\%)_{\text{with fluid change}}$. The contours of the percentage changes are caused by a combination of fluid substitution and a decrease of 5MPa in fluid pressure with the same fluid properties as those in Figure 6.1.

It is also found that fluid pressure drop (by 5 MPa) causes the increase of V_s , which is in sharp contrast to the decrease due to fluid substitution. This behavior may be used to distinguish purely fluid substitution from a combination of fluid substitution and fluid pressure drops. In purely fluid substitution, V_p increases (the left of Figure 6.1) while V_s decreases (the left of Figure 6.14); in the case of a combination of fluid substitution and fluid pressure drop in water drive, both V_p and V_s increase (the left of Figure 6.13 and the right of Figure 6.14). However, caution must be taken because fluid pressure drop may be small and may not offset the decrease of V_s due to fluid substitution.

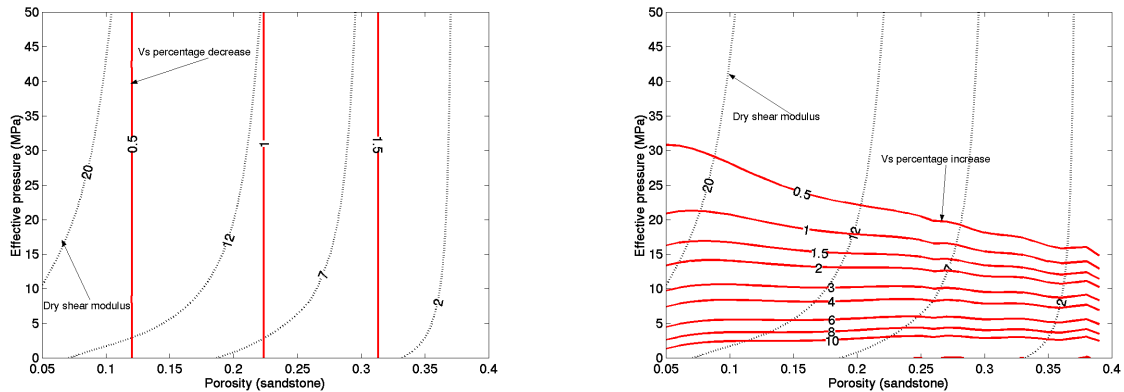


Figure 6.14 Contours of the V_s percentage change. V_s percentage decrease is defined as $-\Delta V_s/V_{s\text{-before}} * 100\%$. V_s percentage increase is defined as $\Delta V_s/V_{s\text{-before}} * 100\%$. The left is the V_s percentage decrease due to purely fluid substitution, and the right is the V_s percentage increase due to a combination of fluid substitution and a decrease of 5MPa in fluid pressure. The fluid properties are assumed the same as those in Figure 6.1.

For gas reservoirs, water drive will cause the greater percentage changes because of the greater contrast in the bulk modulus between gas and water even if gas residual saturation in the water-drive zone is normally in the range of 30-50% (Smith et al., 1992). Figure 6.15 is the contour of the computed percentage changes based on the fluid properties from Domenico (1974). Obviously, V_p and AI percentage changes are larger than those for water-drive oil reservoirs as shown in Figure 6.3.

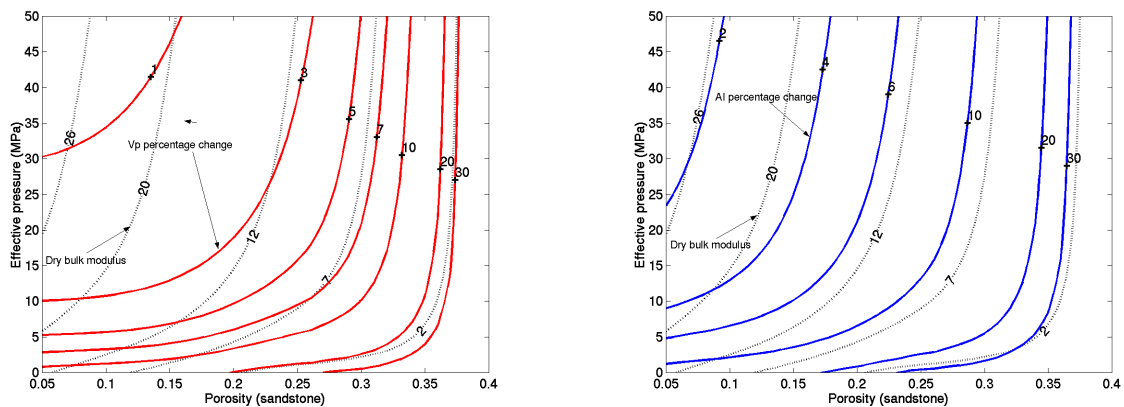


Figure 6.15 Contours of V_p and AI percentage changes. V_p percentage change is defined as $\Delta V_p / V_{p\text{-before}} * 100\%$. AI percentage change is defined as $\Delta AI / AI_{\text{before}} * 100\%$. Fluid properties are assumed: before production, $D_g=0.103(\text{g}/\text{cm}^3)$, $K_g=0.021$ (GPa), $S_g=75\%$, $D_w=1.089(\text{g}/\text{cm}^3)$, $K_w=2.38$ (GPa), $S_w=25\%$; after water drive, $D_g=0.103(\text{g}/\text{cm}^3)$, $K_g=0.021$ (GPa), $S_g=40\%$, $D_w=1.089(\text{g}/\text{cm}^3)$, $K_w=2.38$ (GPa), $S_w=60\%$.

6.3.2 Water flood For weak water drive resulting from low permeability or insufficient size of aquifers, pressure maintenance by water injection, before reservoir pressure drops appreciably, will generally lead to greater oil recovery. Water flood is thus the dominant fluid injection recovery technique in oil industry. In water flood, cold water is injected into reservoirs at high pressure to displace oil. It changes the reservoir conditions. Lowering the temperature increases the elastic moduli of rock framework (dry rock), but the amount of

increase is negligible if there is no drastic temperature change (Zhang and Bentley, 1999). The densities and bulk moduli of oil and water are also affected by temperature. According to Figures 6.8 and 6.9, the density gradient with temperature is roughly $-0.05285 \text{ (g/cm}^3\text{)}/100^\circ\text{C}$ for water and $-0.07545 \text{ (g/cm}^3\text{)}/100^\circ\text{C}$ for oil. However, as explained in Figure 6.6, the percentage changes resulting from a small density modification are not appreciable. In Figure 6.10, the bulk modulus of water does not change monotonically with temperature. It peaks around 60°C and decreases away from that point. So the range of temperature change needs to be specified in order to compute the change of bulk modulus. In Figure 6.11, the gradient of oil bulk modulus with temperature is approximately $-0.67779 \text{ (GPa) }/100^\circ\text{C}$. Moreover, high injection pressure decreases the elastic moduli of rock framework (dry rock) and increases the densities and bulk moduli of fluids. Yet the pressure effect on the fluid bulk modulus and density is believed to be insignificant if pressure change is not drastic as indicated in Figures 6.8 to 6.11. Another important parameter is the salinity of injected water. Generally speaking, brine is preferred economically and technically to fresh water because a shortage of surface fresh water exists in many potential water flood areas and fresh water causes clay expansion, which decreases permeability.

Suppose that an injected fluid with the same properties as that in Figure 6.1 causes an increase of 5MPa fluid pressure and a decrease of 50°C temperature. As a matter of fact, injection pressure cannot be so high that it generates fractures and reduces sweep efficiencies, and injection temperature cannot be so low that it precipitates wax in pore space. In the Bradford oilfield (USA), water flood reduced temperature only by a maximum of 6.1°C (Sayre et al., 1952). Figure 6.16 shows the results based on these assumptions (no drastic change in pressure and temperature).

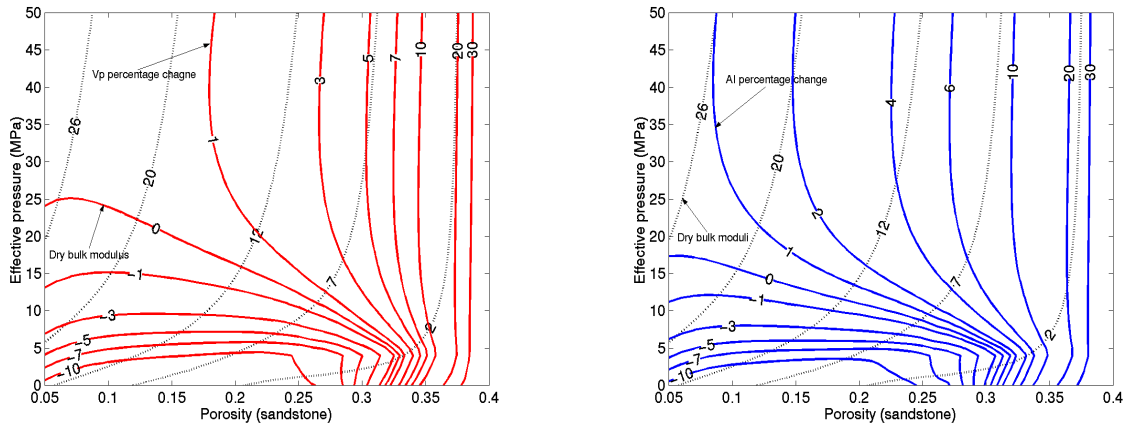


Figure 6.16 Contours of V_p and AI percentage changes. V_p percentage change is defined as $\Delta V_p / V_{p\text{-before}} * 100\%$. AI percentage change is defined as $\Delta AI / AI_{\text{before}} * 100\%$. Fluid properties are assumed: before production, $D_o=0.749(\text{g}/\text{cm}^3)$, $K_o=0.67$ (GPa), $S_o=75\%$, $D_w=1.089(\text{g}/\text{cm}^3)$, $K_w=2.38$ (GPa), $S_w=25\%$; after water injection, $D_o=0.787(\text{g}/\text{cm}^3)$, $K_o=1.01$ (GPa), $S_o=15\%$, $D_w\text{-inj}=1.089(\text{g}/\text{cm}^3)$, $K_w\text{-inj}=2.38$ (GPa), $S_w\text{-inj}=60\%$, $D_w\text{-irr}=1.115(\text{g}/\text{cm}^3)$, $K_w\text{-irr}=2.60$ (GPa), $S_w\text{-irr}=25\%$.

The added injection pressure alters the percentage changes for the zones of low effective pressure so much that they become negative at relatively low porosity. The reason is that the effect of decreased dry bulk modulus due to increased fluid pressure on the percentage changes exceeds that of increased fluid bulk modulus due to fluid substitution. With increasing porosity, the effect of the fluid bulk modulus on fluid-saturated bulk modulus is increasing while that of the fluid pressure is decreasing. As a result, V_p and AI will increase. If porosity is very high, there are always the positive percentage changes in water injection. Figure 6.17 is the case that the bulk modulus of injected fluid increases to 3.1 (GPa). As expected, the negative area decreases and the positive percentage changes expand.

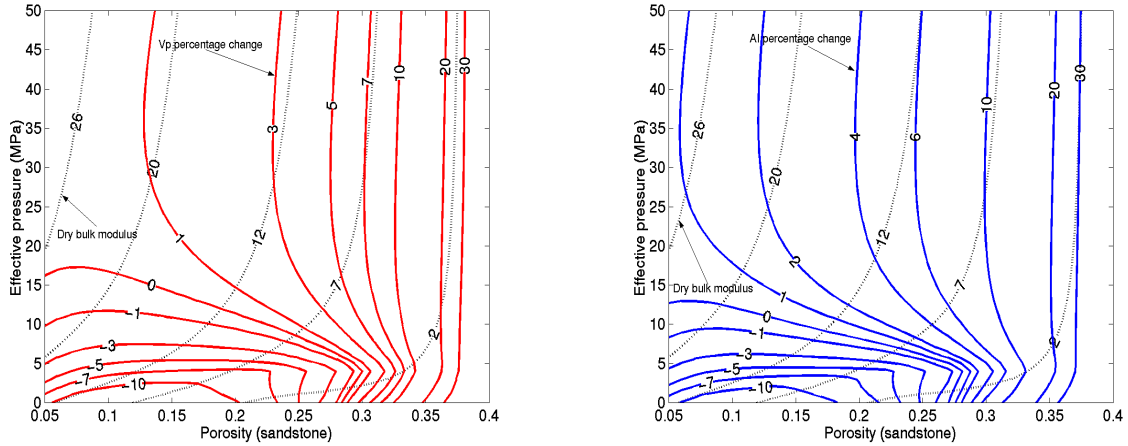


Figure 6.17 Contours of Vp and AI percentage changes. Fluid properties are assumed: before production, $D_o=0.749(\text{g}/\text{cm}^3)$, $K_o=0.67$ (GPa), $S_o=75\%$, $D_w=1.089(\text{g}/\text{cm}^3)$, $K_w=2.38$ (GPa), $S_w=25\%$; after water injection, $D_o=0.787(\text{g}/\text{cm}^3)$, $K_o=1.01$ (GPa), $S_o=15\%$, $D_w\text{-inj}=1.089(\text{g}/\text{cm}^3)$, $K_w\text{-inj}=3.10$ (GPa), $S_w\text{-inj}=60\%$, $D_w\text{-irr}=1.115(\text{g}/\text{cm}^3)$, $K_w\text{-irr}=2.60$ (GPa), $S_w\text{-irr}=25\%$.

Vs percentage change is always negative in water injection as shown in Figure 6.18 because of the combined effect of increased density and decreased dry shear modulus. This may be a criterion to distinguish it from water drive, in which Vs percentage change may be positive due to increased effective pressure.

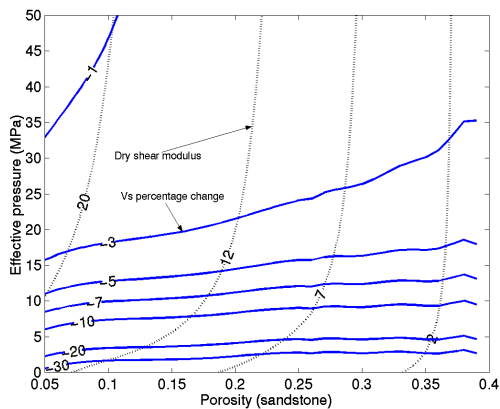


Figure 6.18 Contours of Vs percentage changes. Fluid properties are assumed: before production, $D_o=0.749(\text{g}/\text{cm}^3)$, $K_o=0.67$ (GPa), $S_o=75\%$, $D_w=1.089(\text{g}/\text{cm}^3)$, $K_w=2.38$ (GPa), $S_w=25\%$; after water injection, $D_o=0.787(\text{g}/\text{cm}^3)$, $K_o=1.01$ (GPa), $S_o=15\%$, $D_w\text{-inj}=1.089(\text{g}/\text{cm}^3)$, $K_w\text{-inj}=3.10$ (GPa), $S_w\text{-inj}=60\%$, $D_w\text{-irr}=1.115(\text{g}/\text{cm}^3)$, $K_w\text{-irr}=2.60$ (GPa), $S_w\text{-irr}=25\%$.

6.3.3 Gas cap drive On many occasions, gas and oil coexist in separate phases in reservoirs. Gas bubbled up to the top and formed a gas cap and oil is located on the bottom. When oil production proceeds, oil level falls and the gas expands down into the section of the reservoir originally containing oil. Pressure maintenance and recovery rates depend on the size of the gas cap. The larger the volume of the gas cap, the less the pressure will drop and the higher percentage of oil will be produced from beneath the cap. In gas cap drive, pressure decline will be an important control on Vp and AI percentage changes by increasing the elastic moduli of rock framework (dry rock). As mentioned in the previous section, the effect of pressure on the fluid density and bulk modulus is not significant and will be neglected in calculation. Figure 6.19 depicts the percentage changes for a pressure drop of 5 MPa. The large increase in Vp and AI takes place at low effective pressure. As opposed to water injection, there are positive percentage changes at relatively low porosity and the negative percentage changes at high porosity. The positive is due to the increase in dry elastic moduli and the negative is due to the decrease in the fluid bulk modulus due to gas substitution.

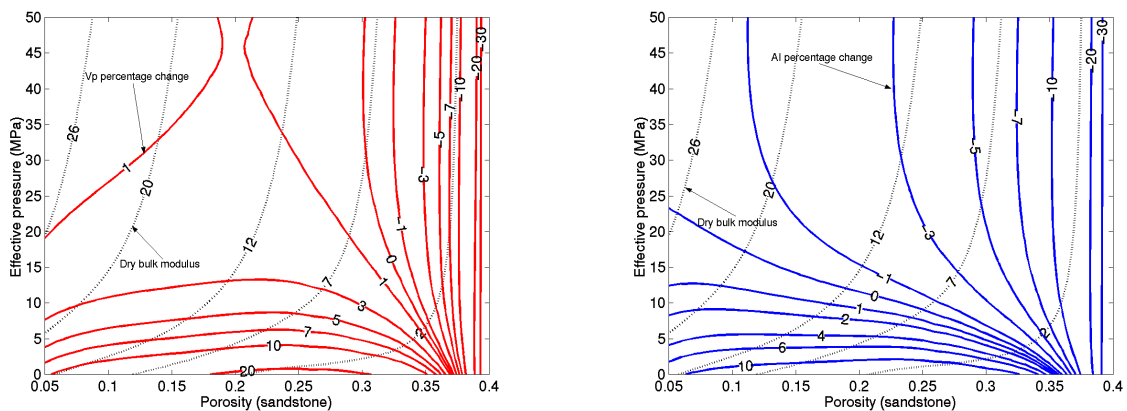


Figure 6.19 Contours of Vp and AI percentage changes. Fluid properties are assumed: before production, $D_o=0.749(\text{g}/\text{cm}^3)$, $K_o=0.67$ (GPa), $S_o=75\%$, $D_w=1.089(\text{g}/\text{cm}^3)$, $K_w=2.38$ (GPa), $S_w=25\%$; after gas cap drive, $D_o=0.749(\text{g}/\text{cm}^3)$, $K_o=0.67$ (GPa), $S_o=15\%$, $D_g=0.103(\text{g}/\text{cm}^3)$, $K_g=0.021$ (GPa), $S_g=60\%$, $D_w=1.089(\text{g}/\text{cm}^3)$, $K_w=2.38$ (GPa), $S_w=25\%$.

6.3.4 Gas injection To augment inadequate gas cap drive by gas injection is a conventional recovery operation. Similar to water injection, fluid pressure buildup will decrease the V_p , V_s and AI. Displacement of oil by gas further decreases V_p and AI, but increases V_s due to the density decrease. Figure 6.20 is the V_p and AI percentage changes due to an increase of 5MPa in fluid pressure. At low effective pressure, the V_p and AI decrease a lot, but at high effective pressure the decrease becomes small. At high porosity, the decrease is large and seems independent of effective pressure. This reflects the major effect of the decreased fluid bulk modulus due to the gas displacement of oil. In Figure 6.21, V_s decreases at low effective pressure but increases at high effective and at high porosity due to the decreased density.

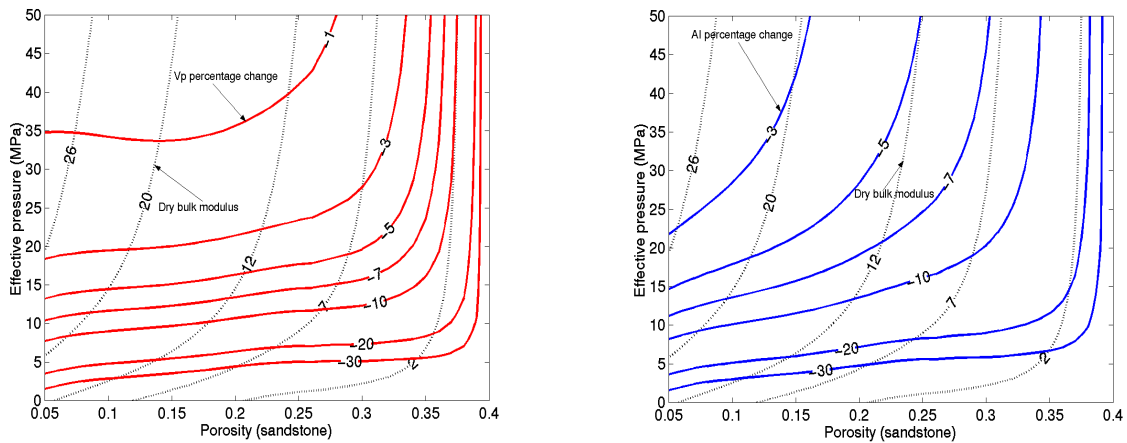


Figure 6.20 Contours of V_p and AI percentage changes. Fluid properties are assumed: before production, $D_o=0.749(\text{g}/\text{cm}^3)$, $K_o=0.67$ (GPa), $S_o=75\%$, $D_w=1.089(\text{g}/\text{cm}^3)$, $K_w=2.38$ (GPa), $S_w=25\%$; after gas injection, $D_o=0.749(\text{g}/\text{cm}^3)$, $K_o=0.67$ (GPa), $S_o=15\%$, $D_g=0.103(\text{g}/\text{cm}^3)$, $K_g=0.021$ (GPa), $S_g=60\%$, $D_w=1.089(\text{g}/\text{cm}^3)$, $K_w=2.38$ (GPa), $S_w=25\%$.

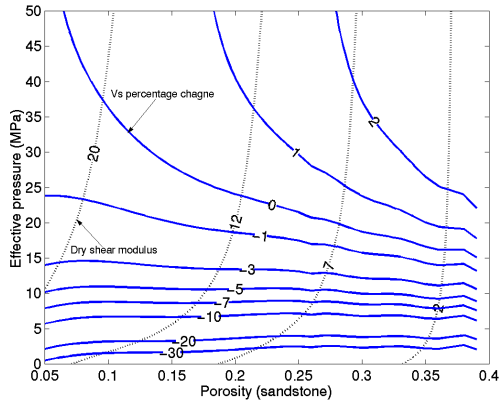


Figure 6.21 Contours of V_s percentage changes. Fluid properties are assumed: before production, $D_o=0.749(\text{g}/\text{cm}^3)$, $K_o=0.67$ (GPa), $S_o=75\%$, $D_w=1.089(\text{g}/\text{cm}^3)$, $K_w=2.38$ (GPa), $S_w=25\%$; after gas injection, $D_o=0.749(\text{g}/\text{cm}^3)$, $K_o=0.67$ (GPa), $S_o=15\%$, $D_g=0.103(\text{g}/\text{cm}^3)$, $K_g=0.021$ (GPa), $S_g=60\%$, $D_w=1.089(\text{g}/\text{cm}^3)$, $K_w=2.38$ (GPa), $S_w=25\%$.

6.3.5 Solution gas drive Many oil reservoirs are volumetric, with the porous area completely surrounded by impermeable rocks. A reservoir of this physical nature inevitably becomes a solution gas drive type of reservoir when produced. Below the bubble-point pressure, the production is a result of expansion of the gas released from solution. With the oil withdrawal, pressure declines and more gas evolves from solution. When the gas saturation reaches the critical value, gas begins to flow and pressure drops faster. At the final stage, the pressure is so low that both oil and gas flow ceases with large quantities of oil remaining in the reservoir rocks. So solution gas drive is the most inefficient type of primary recover drive. The significant changes in reservoir conditions are substantial pressure drop and the occurrence of gas on grain scale. The increase in effective pressure leads to the increase in V_p , AI and V_s , but the existence of gas may decrease V_p and AI, but increase V_s . Figure 6.22 is the V_p and AI percentage changes due to a fluid pressure drop of 10 MPa. The large V_p and AI increase take place at low effective pressure. At high porosity, the V_p and AI decrease due to the decrease in the fluid bulk modulus and the decreased effect of the fluid pressure. Figure 6.23 is the V_s percentage increase. The situation is very similar to what happens in gas cap drive.

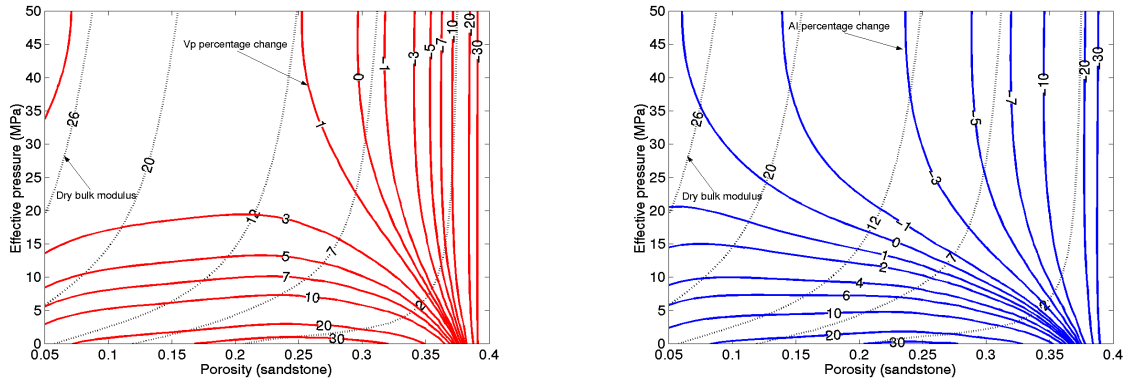


Figure 6.22 Contours of Vp and AI percentage changes. Fluid properties are assumed: before production, $D_o=0.749(\text{g}/\text{cm}^3)$, $K_o=0.67$ (GPa), $S_o=75\%$, $D_w=1.089(\text{g}/\text{cm}^3)$, $K_w=2.38$ (GPa), $S_w=25\%$; after solution gas drive, $D_o=0.749(\text{g}/\text{cm}^3)$, $K_o=0.67$ (GPa), $S_o=15\%$, $D_g=0.103(\text{g}/\text{cm}^3)$, $K_g=0.021$ (GPa), $S_g=60\%$, $D_w=1.089(\text{g}/\text{cm}^3)$, $K_w=2.38$ (GPa), $S_w=25\%$.

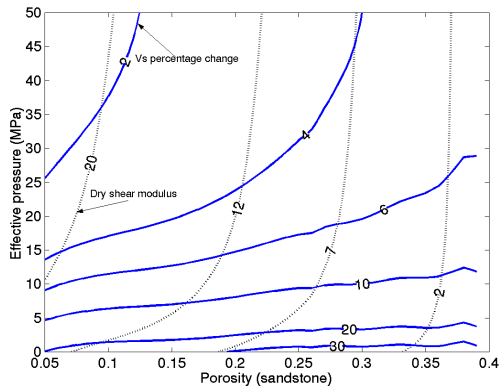


Figure 6.23 Contours of Vs percentage changes. Fluid properties are assumed: before production, $D_o=0.749(\text{g}/\text{cm}^3)$, $K_o=0.67$ (GPa), $S_o=75\%$, $D_w=1.089(\text{g}/\text{cm}^3)$, $K_w=2.38$ (GPa), $S_w=25\%$; after solution gas drive, $D_o=0.749(\text{g}/\text{cm}^3)$, $K_o=0.67$ (GPa), $S_o=15\%$, $D_g=0.103(\text{g}/\text{cm}^3)$, $K_g=0.021$ (GPa), $S_g=60\%$, $D_w=1.089(\text{g}/\text{cm}^3)$, $K_w=2.38$ (GPa), $S_w=25\%$.

6.3.6 Steam injection Steam injection increases the reservoir temperature and displaces oil, which was originally very thick and viscous and as a result did not migrate readily to producing wells. There exist three zones away from the injection well: steam-swept, hot water drive (due to steam condensing) and cold oil bank. Temperature increase lowers the elastic moduli of both pore fluids and dry rock. The former can be calculated according to Figures 6.10 and 6.11. The latter is approximated with linear equations (Zhang and Bentley, 1999; also see equations 5.1 and 5.2) as follows:

$$dK_d/dT = -0.0155 \quad 6.11 \quad d\mu_d/dT = -0.0065 \quad 6.12$$

where K_d and μ_d are the dry bulk and shear modulus (GPa) and T is temperature ($^{\circ}\text{C}$). When temperature increases, differential thermal expansion of constituent minerals may generate new cracks, especially at grain boundary, leading to the large decrease in dry elastic moduli. If this case happens, these formulae are no longer valid. Below 200°C , however, the opening of new cracks was not observed in experiments (Wang and Nur, 1988; Carmichael, 1989). Considering high injection pressure, equations 6.11 and 6.12 may hold for steam injection. Simultaneously, high injection pressure further decreases the dry elastic moduli. Suppose an increase of temperature by 120°C and of fluid pressure by 10 MPa. Figure 6.24 is the Vp and AI percentage changes due to steam drive. The Vp and AI percentage decreases extend to high effective pressure and relatively low porosity because of the large decrease of both the fluid bulk modulus and the dry elastic moduli caused by steam substitution, high temperature and high fluid pressure.

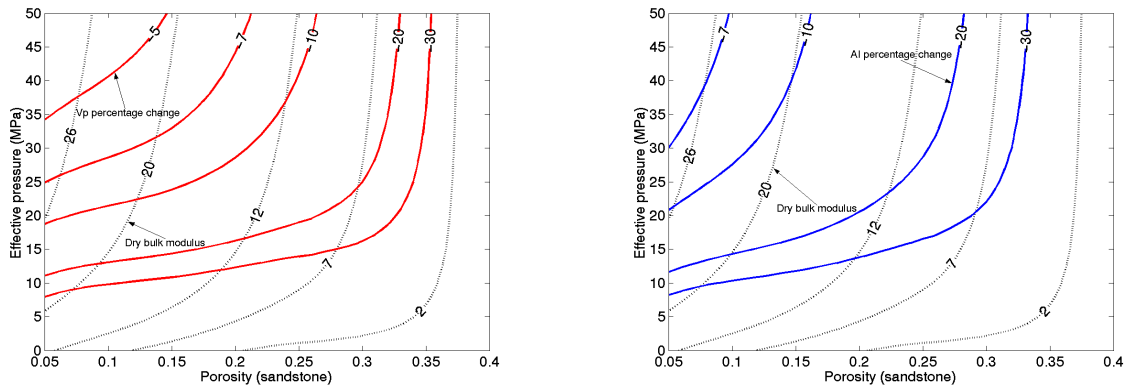


Figure 6.24 Contours of Vp and AI percentage changes. Fluid properties are assumed: before production, $D_o=0.99(\text{g}/\text{cm}^3)$, $K_o=2.50$ (GPa), $S_o=90\%$, $D_w=1.089(\text{g}/\text{cm}^3)$, $K_w=2.38$ (GPa), $S_w=10\%$; after steam injection (with steam substitution), $D_o=0.899(\text{g}/\text{cm}^3)$, $K_o=1.687$ (GPa), $S_o=10\%$, $D_g=0.103(\text{g}/\text{cm}^3)$, $K_g=0.021$ (GPa), $S_g=80\%$, $D_w=1.026$ (g/cm³), $K_w=2.10$ (GPa), $S_w=10\%$.

6.4 Depth effect on seismic monitoring of sandstone reservoirs

Porosity reduction with depth or, more accurately, with effective pressure is a complex result of mechanical compaction and chemical diagenesis. With burial, the number of grain contacts will increase, contact types will change (Taylor, 1950), and grain fracturing may take place, leading to porosity reduction. Simultaneously, chemical processes such as dissolution, replacement and cementation further influence porosity. These mechanical and chemical actions depend on many geological factors such as grain size and compositions, amount of unstable minerals, pore fluid composition, temperature, geological time etc.. It is therefore frequently not possible to successfully obtain a simple and universal compaction curve. However, regional compaction curves, which may be caused by some dominant geological factors, do exist, as found by many authors (Atwater and Miller, 1965; Chilingarian, 1983; Somosna, 1989; so on). For normally consolidated sediments, Mailart (1989) proposed the following expression:

$$\phi = \phi_r + (\phi_0 - \phi_r)e^{-\beta z} \quad 6.13$$

where ϕ is porosity at depth z , ϕ_r is residual porosity at great depth, ϕ_0 is porosity at surface (taken to be 40% for sandstone), and β is an empirical parameter that may include the effects of chemical diagenesis. If effective overburden pressure is a linear function of depth z , equation 6.13 can be converted to the porosity-effective pressure relationship as follows:

$$\phi = \phi_r + (\phi_0 - \phi_r)e^{-\gamma P} \quad 6.14$$

where $\gamma = \beta / (\rho_b - \rho_w)g$, P is effective pressure. From equation 6.14, a plot of porosity versus effective pressure can be created for specific areas by assigning the parameters obtained from regression analysis of sandstone porosities. Figure 6.25 is the compaction curve of sandstone plotted on Figure 6.3 (Vp and AI percentage changes from water drive), where $\beta = 0.0005 / \text{m}$ (Einsele, 1992), $\rho_b = 2.3 \cdot 10^3 \text{kg/m}^3$, $\rho_w = 1.04 \cdot 10^3 \text{kg/m}^3$, $g = 9.8 \text{m/s}^2$ and $\phi_r = 5\%$ are assumed. Along the compaction curve to high effective pressure, porosity decreases and consequently Vp and AI percentage changes become small. Thus a relationship can be established between effective pressure and the percentage changes. It enables us to predict the percentage changes at varying effective pressures for reservoirs that may be located at different depths. As shown in Figure 6.25, if we set a minimum of the percentage changes required to seismically monitor recovery processes, the maximum effective pressure can be estimated, above which time-lapse seismic surveys cannot differentiate the changes in reservoir conditions.

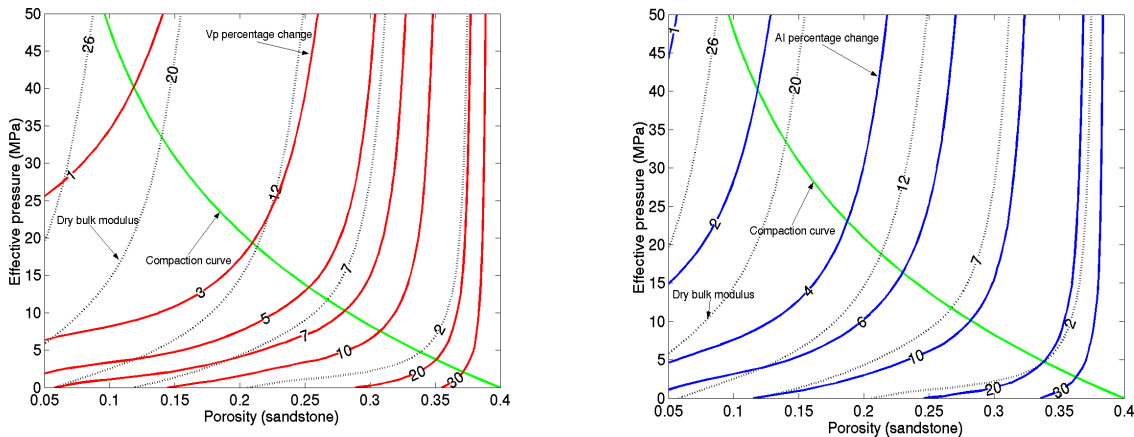


Figure 6.25 Compaction curve of sandstones. The Vp and AI percentage changes are the same as those in Figure 5.1

Effective pressure is not equivalent to depth if formation pressure is not hydrostatic or sediments are not normally compacted. Their relationship can be expressed as follows:

$$D = P_{\text{eff}} / (S_{\text{grd}} - P_{\text{f-grd}}) \quad 6.15$$

where D is the depth, P_{eff} is the effective pressure, S_{grd} is the overburden pressure gradient and $P_{\text{f-grd}}$ is the formation pressure gradient. In most cases, the overburden pressure gradient can be roughly estimated. So the relationship depends chiefly on the formation pressure gradient. If the formation pressure gradient is constant (say, hydrostatic or normal compaction), the depth and effective pressure are linearly correlated. In the section with overpressured zones, however, the formation pressure gradient varies and the depth is no longer uniquely related to effective pressure. Instead their correlation depends on formation pressure gradient. Figure 6.26 is the graphical representation of the change of the depth with the formation pressure gradient at a given effective pressure. The larger the formation pressure gradient is, the deeper the depth at which reservoir conditions can be monitored seismically.

Now that effective pressure does not correspond to depth in many situations, the parameter 'depth' should be used with caution. The deep-situated reservoirs are not necessarily infeasible for time-lapse seismic surveys because effective pressure may be small due to the high formation pressure gradient. In the oilfields of the North Sea, the widespread abnormally high fluid pressure leads to low effective pressure and high porosity at great depths. At 2000 m, porosity is as high as 34%. Above 3000 m, porosity still maintains 24%. In the Gulf of Mexico, some sands buried at 6000m deep bear almost the same porosity as when they were deposited (Domenico, 1974). These reservoirs are good candidates for time-lapse seismic surveys despite deep depths.

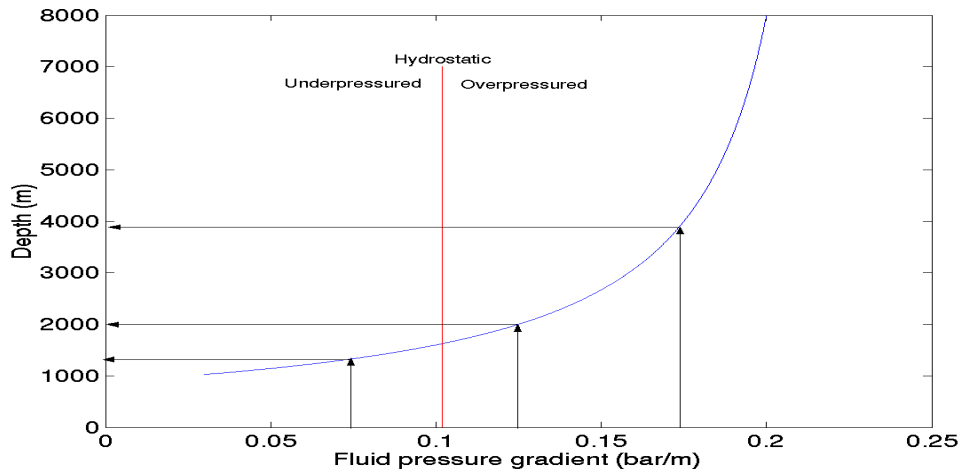


Figure 6.26 Change of the depth with the fluid pressure gradient at a given effective pressure (20 MPa). Assume $S_{\text{grd}} = 0.225 \text{ bar/m}$ ($2.3 \cdot 10^3 \text{ kg/m}^3 \cdot 9.8 \text{ m/s}^2 / 10^5$).

6.5 Discussion

In terms of rock physics the most important changes due to hydrocarbon recovery are the pore aspect ratio spectrum (a description of pore shape and volume concentration) and the bulk modulus of the effective fluid. The variation of elastic moduli of rock solid is negligibly small. The change in pore aspect ratio spectrum is caused by the changes in pressure and temperature. The change in the bulk modulus of the effective fluid is due to the changes in saturation and pressure and temperature.

Effective pressure can change the pore aspect ratio spectrum either elastically or irreversibly. When the amount of change is not drastic, the opening or closing of existent cracks occurs, leading to a change in dry elastic moduli. At high effective pressure, most cracks are closed and little change is expected in

response to effective pressure change. In addition, at high porosity, effective pressure may not play as significant a role due to the decreasing effect of cracks on elastic moduli. Therefore, the change in effective pressure strongly influences the dry elastic moduli only for reservoir rocks of low high porosity at low effective pressure. When the amount of change in effective pressure is substantial, the decrease may generate hydraulic fractures, greatly decreasing dry elastic moduli, and the increase may crush grains, decreasing porosity and consequently increasing dry elastic moduli considerably. This case is difficult to model.

Temperature change can decrease or increase pore volume, which in turn modifies dry elastic moduli by a small amount. This is the situation most encountered in hydrocarbon recovery. But the large temperature increase such as steam injection may create cracks due to differential thermal expansion, tremendously decreasing dry elastic moduli.

The bulk modulus of the effective fluid is affected by pressure, temperature and saturation. Pressure and temperature can cause phase changes and consequently changes in the fluid bulk modulus. Pressure and temperature also influence directly the fluid bulk modulus as shown in Figures 6.8, 6.9, 6.10 and 6.11. Fluid drive or flood can change saturations, which may be heterogeneously distributed on coarse scale (patchy saturation). It is noted that whether or not the change in the bulk modulus of the effective fluid has a significant effect on the fluid-saturated elastic moduli and velocities depend chiefly on the magnitude of dry elastic moduli as shown in Figure 6.3. The smaller the dry elastic moduli, the larger the change in velocity and acoustic impedance that will take place.

When the effect of fluid substitution on V_p and AI is opposite to that of change in effective pressure, V_p and AI can increase or decrease. In the range of low porosity and low effective pressure, V_p and AI depend on the effect of effective pressure. At high porosity, V_p and AI are generally determined by the impact of fluid substitution.

6.6 Conclusions

The feasibility of seismic monitoring of sandstone reservoirs depends chiefly on the magnitude of dry elastic moduli, the contrast in the fluid bulk modulus, and the changes in pressure and temperature. The fluid density does not have a significant effect. The contrast in the fluid bulk modulus includes the effect of saturation, pressure and temperature. The good candidates for time-lapse seismic surveys are the reservoir rocks of low dry elastic moduli with a large fluid bulk modulus contrast, the reservoir rocks that undergo a large pressure change at low effective pressure, and those subject to a large temperature change. The sandstones of high porosity at low effective pressure are most suitable for seismic monitoring. They may be located at shallow or great depths depending on the fluid pressure gradient. In the absence of laboratory data, the method in the paper can be used to predict the change of V_p and AI with effective pressure and depth.

CHAPTER 7

FEASIBILITY OF SEISMIC MONITORING OF THE BLACKFOOT RESERVOIRS

7.1 Introduction

The Blackfoot reservoir is located southeast of Calgary. In the following, we investigate the potential for using time-lapse seismic surveys to infer changes in the pressure and fluid distribution within the reservoir due to production and injection. The goal of time-lapse surveys is to provide information useful to reservoir engineers in their production decisions. Since the Blackfoot reservoir is a representative of the glauconitic incised-valley system, the study also provides useful information as to the value of conducting time-lapse surveys over an important class of Alberta hydrocarbon reservoirs.

The Blackfoot reservoir is an incised channel filled with porous cemented sand. In the area of interest (Figure 7.1), the reservoir consists of three cross cutting channels at an approximate depth of 1550 m below ground level (Dufour, et al., 1999). From top to bottom they are the upper channel, the lithic channel and the lower channel (Figure 7.2). The lithic channel is more cemented and pressure data indicate that it is a hydraulic barrier between the upper and lower channels. At the location of well 09-08, the thickness of the layers are approximately 25 m, 5 m and 12 m for the upper, lithic and lower channels, respectively. The average porosity of the producing pools is approximately 0.20. The area of interest appears to be isolated from other reservoirs in the channel system by shale plugs to the north and south.

7.2 Exploration and production history

The first three-D seismic survey was conducted over the area in 1993. Subsequently, the discovery well 09-08 was drilled and it was first tested on August 31, 1994. The original pressure and temperature in the reservoir were 11,770 KPa and 45.9 °C respectively. The interpretation is that the upper channel contained an oil leg of approximately 9 m underlying a gas cap of 16 m. The lower channel was interpreted as oil filled. Subsequently wells 08-08, 00/09-08, 02/09-08 01-08, 16-05 and 09-05 were put on production. In December, 1994 the gas oil ratio (GOR) began to rise rapidly, indicating that the bubble point had been reached. Consequently, water injection was started in 08-08 in August, 1995 with 00/09-08, 02/09-08 and 01-08 continuing as production wells. In November of 1995, a 3D-3C seismic survey was completed over the area (Yang et al., 1996). At this time the pressure in the upper pool was 11474 KPa, but the lower pool pressure had been reduced to 8722.1 KPa. As production and injection continued, the upper pool maintained its pressure and the lower pool continued to decline in pressure. Water breakthrough was not observed at the producing wells. Finally, a two-D seismic line was shot through the location of 09-08 in 1997 (Stewart, et al., 1997). By September 28, 1998, the pressure in the lower pool had declined to 6,046 KPa while the upper pool maintained a pressure of approximately 11,200 KPa.

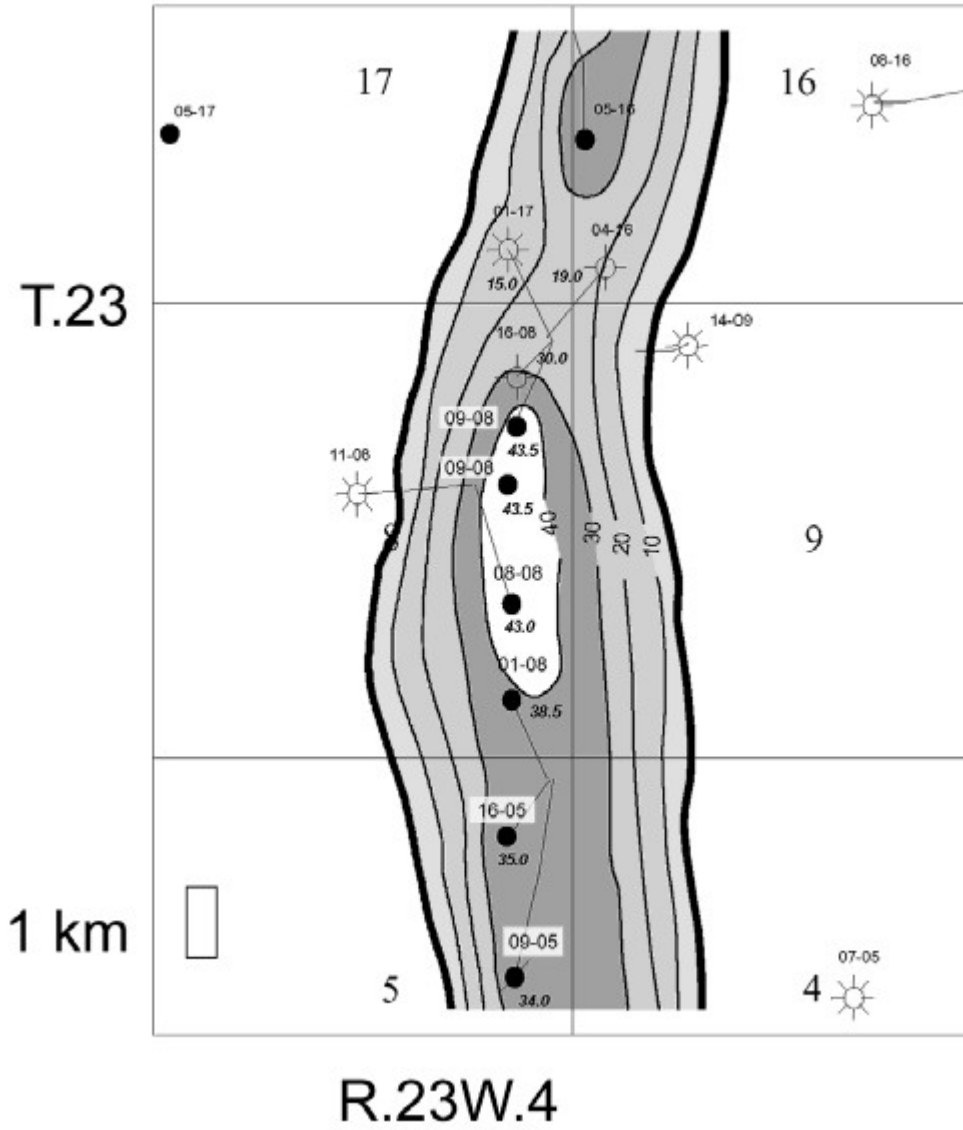


Figure 7.1. Blackfoot Reservoir Isopach (Courtesy of J. Dufour, PanCanadian Petroleum).

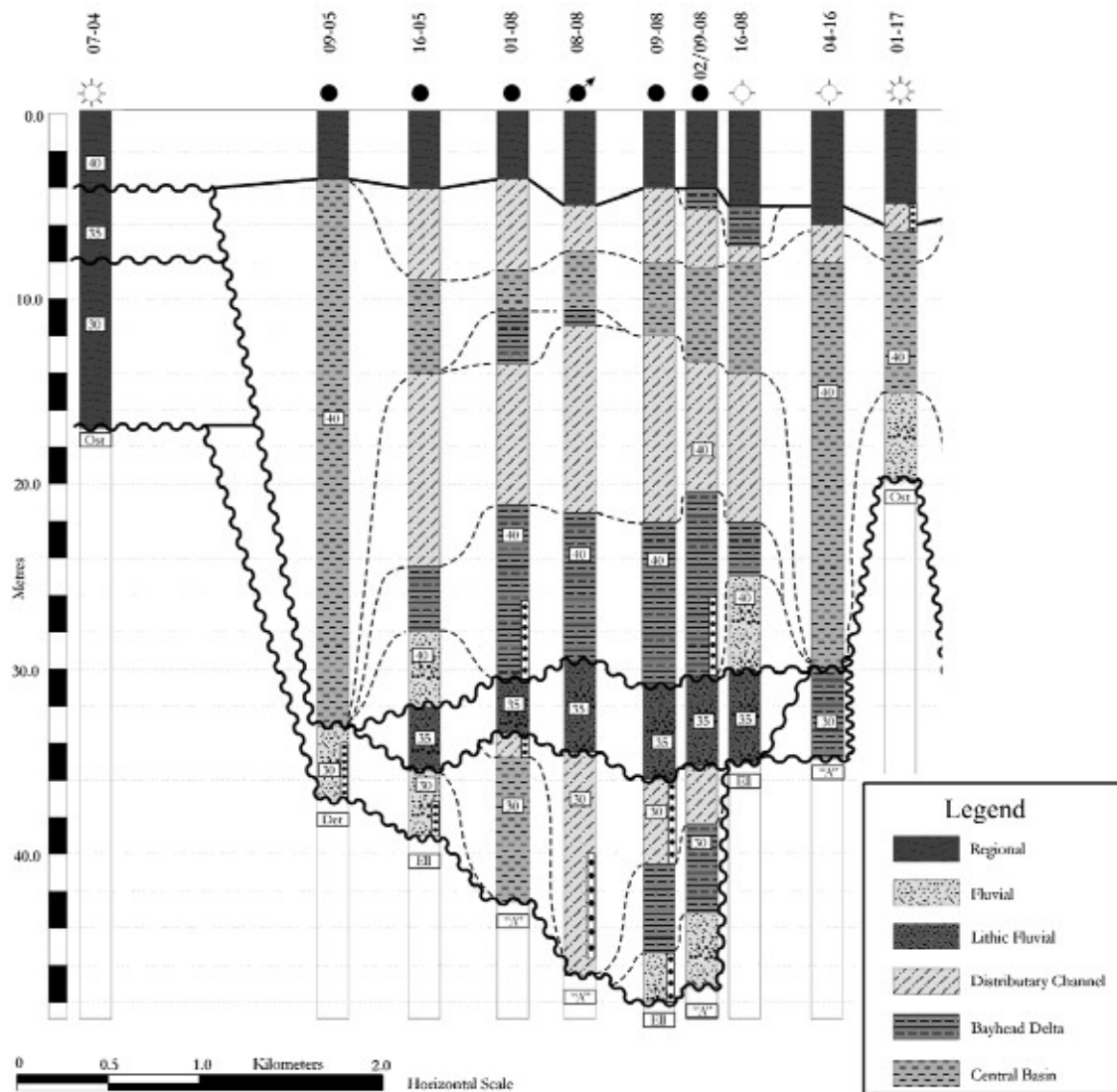


Figure 7.2. North-south cross section of Blackfoot reservoir showing lower channel (30), lithic channel (35) and upper channel (40) (courtesy of J. Dufour, PanCanadian Petroleum).

7.3 Data acquisition

In the previous chapter we discussed the feasibility of sandstones in a general sense with the dry elastic moduli obtained from the theoretical model and the fluid properties assumed from literature. In order to conduct feasibility study in an actual hydrocarbon reservoir, however, we need the accurate data of the dry elastic moduli and fluid properties from wherever they are available. In the following, we will deal with the acquisition of these data.

7.3.1 Gas Measured values of the Blackfoot specific gravity of gas at standard conditions were not available, so the specific gravity of the Rockyford upper Manville formation gas (0.786) was used as a surrogate (Galas, et al., 1995). The specific gravity of gas needs to be corrected for separator pressure and temperature. An assumed separator pressure of 689.5 KPa and an assumed temperature of 15.6°C were used with equation (1) from Vasquez and Beggs (1980) to obtain a corrected specific gravity of 0.772. The bulk modulus (K_G) and density (ρ_G) of the gas at specified reservoir pressures and reservoir temperature of 45.9 °C were estimated using equations 2.39-2.45 (in Chapter 2).

7.3.2 Oil Three measurements of the Blackfoot oil yielded an average 37.0 ° API (839.8 kg/m³ at standard conditions). The oil formation volume factor (B_o) and solution gas oil ratio (R_s) at selected reservoir pressures and temperature were provided by PanCanadian Petroleum (Table 6.2, Jacques Millette, pers. com.). Equation 2.31 for an undersaturated oil is used to compute the compressibility and bulk modulus (K_o). The density of the oil at reservoir conditions (ρ_o) is derived from mass balance:

$$\rho_o = \frac{\rho_o^{\text{std}} + R_{so}^{\text{std}} \rho_G^{\text{std}}}{B_o} \quad 7.1$$

where ρ_G^{std} and ρ_o^{std} are the densities of gas and oil at standard conditions (also see equation 2.34). Results are found in Table 7.1.

7.3.3 Water The connate water salinity is approximately 25,000 ppm (Galas, 1995). Water density (ρ_w) was approximated using equations 2.28 and 2.29. The water bulk modulus (K_w) was approximated using equations 2.25-2.27 and Table 2.2. Results are found in Table 7.1.

Table 7.1 Fluid properties

Pressure (KPa)	K_G (GPa)	ρ_G (Kg/m ³)	K_O (GPa)	ρ_o (Kg/m ³)	K_w (GPa)	ρ_w (Kg/m ³)
11830	0.0213	143	0.565	764	2.53	1011
11200	0.0196	134	0.562	768	2.53	1011
6046	0.0089	64.8	0.0606	798	2.49	1009

Table 7.2 PVT values

Pressure (KPa)	B_o (Rm ³ /Sm ³)	R_s (Rm ³ /Sm ³)
11830	1.1876	71.2
11200	11786	67.6
6046	10917	32.16

7.3.4 Fluid Mixture Properties In general, gas, oil and water will exist in the pore spaces with saturations S_G , S_O and S_W , respectively. The mixture of fluids can be viewed as an effective fluid in terms of their collective effect on the elastic properties of the fluid-saturated rock. The density of the effective fluid was calculated as the volume-weighted average using the in situ density of gas, oil and water. The bulk modulus of the effective fluid depends on the details of the fluid distribution. Before production, it is calculated with the isostress model or the harmonic averaging of the fluid bulk moduli. After fluid drive or flooding, it is calculated with the isostrain model, or the arithmetic averaging.

7.3.5 Porosity Porosity was estimated using core and well log data from 08-08. A full waveform sonic log and a density log were run on October 1, 1996 (check date). The average density of the solid grains as determined from core data is 2.65 gm/cm^3 . The assumed fluid saturations are $S_G=0.75$ and $S_W=0.25$ in the gas zone of the upper channel, $S_O=0.75$ and $S_W=0.25$ in the oil zone of the upper channel and $S_O=0.75$ and $S_W=0.25$ in the lower channel. The porosity at each point of the density log was calculated as follows:

$$\phi = \frac{\rho_s - \rho_u}{\rho_s - \rho_f} \quad 7.2$$

where ρ_s is the solid grain density derived from core measurements, ρ_f is the density of the effective fluid and ρ_u is the density from the well log.

7.3.6 Dry elastic moduli The undrained elastic moduli were obtained from the full wave form compressional and shear wave velocities and the bulk density derived from 08-08 density logs. The solid bulk modulus (K_s) is assumed to be 40 GPa, a typical value for quartz. Given the known values, the dry bulk modulus was estimated by solving the Gassmann equation as follow:

$$K_d = \frac{\phi K_s^2 K_u + (1-\phi) K_s K_u K_f - K_s^2 K_f}{\phi K_s^2 + (1-\phi) K_s K_f + K_u K_f - 2K_s K_f} \quad 7.3$$

where K_d is the dry bulk modulus, K_u is the undrained bulk modulus, ϕ is porosity, K_s is the bulk modulus of rock solid, K_f is the bulk modulus of the effective fluid. The dry shear modulus is considered to be equal to the undrained shear modulus because the fluid effect can be neglected.

7.3.7 Change of dry elastic moduli with effective pressure The dry elastic moduli increase with increasing effective pressure. Zhang and Bentley (1999), based on the seventy-five sandstone samples from Han et al. (1986), developed the exponential function to express the relationship between the rate of change of dry elastic moduli and effective pressure. The average case for these samples could be modelled as:

$$dK_d/dP = 0.746\exp(-0.0773P) \quad 7.4$$

$$d\mu_d/dP = 0.372\exp(-0.0791P) \quad 7.5$$

where K_d and μ_d are the dry bulk and shear moduli respectively in GPa and P is effective pressure in MPa.

7.4 Scenarios for computation of seismic responses

Three scenarios will be compared (Figure 7.3). The first scenario represents the original conditions in the reservoir. The upper channel has a gas zone and an oil zone. The lower channel has an oil zone. Scenario 2 represents condition in November, 1995 away from the water flood zone. The lower channel

has reached bubble point, and now contains all three fluid phases, gas, water and oil. Gas and oil saturations were computed from production data and mass balance given estimated reservoir volume. Water is at residual saturation. The upper channel is assumed to have no change in saturation or gas-oil contact location, but the density and bulk modulus have been corrected for change in pressure. The dry moduli have been corrected for effective pressure changes. Scenario 3 represents conditions in November, 1995 in the water flood zone. Since pressure has not been maintained in the lower channel, we assume that no water is in this zone. The zone is assumed to have the same conditions as in the area away from the water flood, that is a mixture of gas, oil and water. Within the upper channel in the water flood zone, we assume that water has displaced gas and oil to residual saturations of $S_G=0.3$ and $S_O=0.25$, respectively. Densities and dry moduli have been corrected for changes in fluid pressure and effective pressure.

SCENARIOS

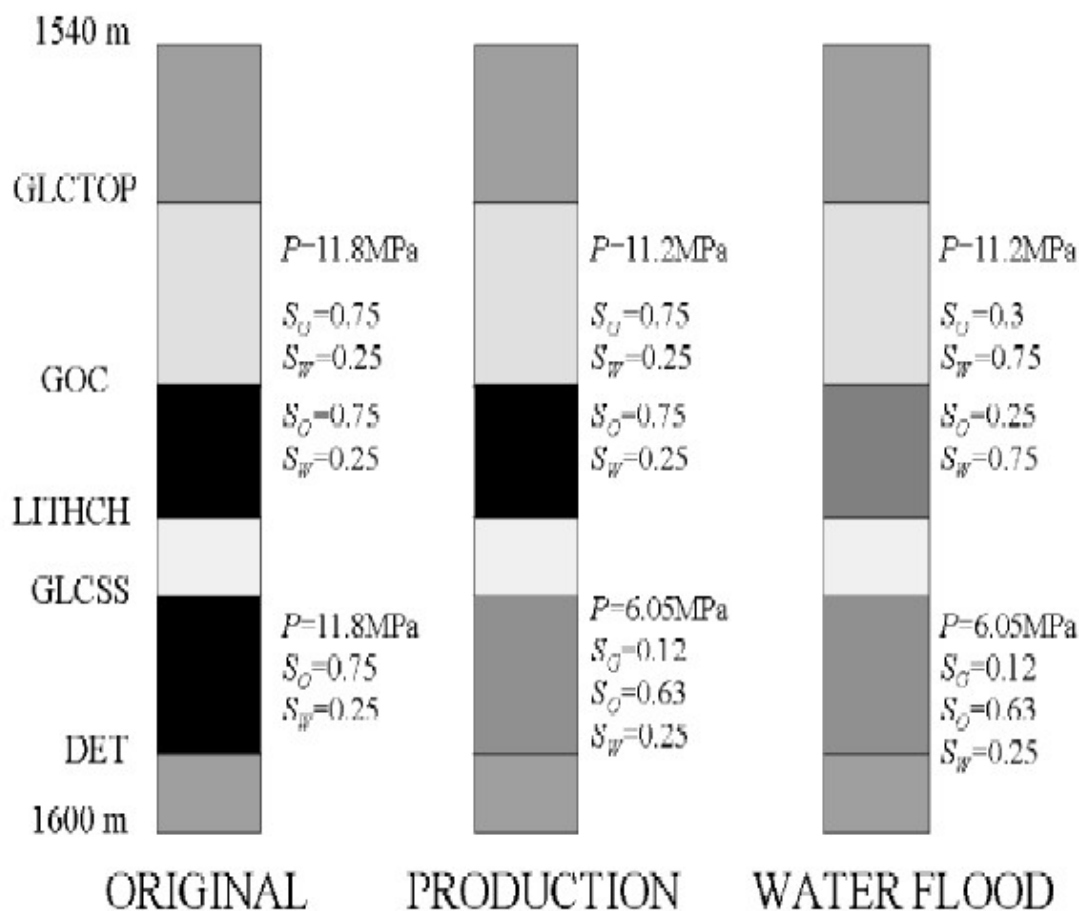


Figure 7.3 Reservoir condition scenarios used in computation of seismic responses

7.5 Synthetic seismograms

The velocities and acoustic impedance of three scenarios were computed for synthetic seismograms. Figure 7.4 shows the comparison of synthetic seismograms calculated for the original conditions versus scenario 3, in the water flood zone. NMO corrected shot gathers for the original conditions, water flood conditions and their differences are displayed. In addition, trace one of the

original condition shot gather is plotted against trace one of the difference plot. In this case, a large percentage change in the trace amplitude is created by the change in conditions. In addition, there is a noticeable difference in the AVO response between original and water flood responses.

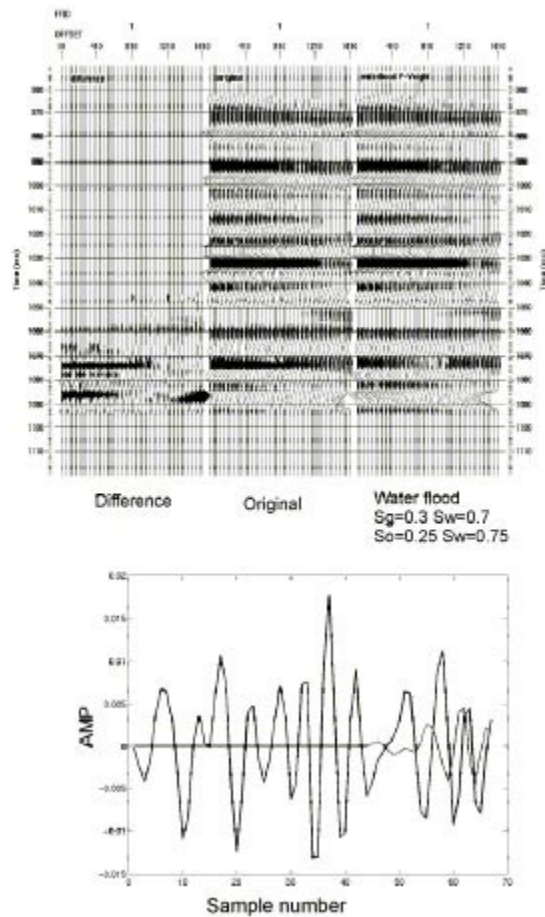


Figure 7.4. Comparison of a NMO corrected synthetic shot gather seismogram of the original reservoir conditions with that of post-production inside of the water flood area. In the lower portion of the figure, trace one of the original response is plotted with trace one of the difference.

Figure 7.5 shows the difference between original conditions and the post-production conditions outside of the water flood area. The change in response is

not as great as within the water flood area. Also, the character of the AVO response change is different. Although reduced, the proportional change in the response of trace one is significant.

Figures 7.6 show the difference in response for areas within and outside the water flood zone. The results indicate that a reasonably strong difference should exist between the two areas.

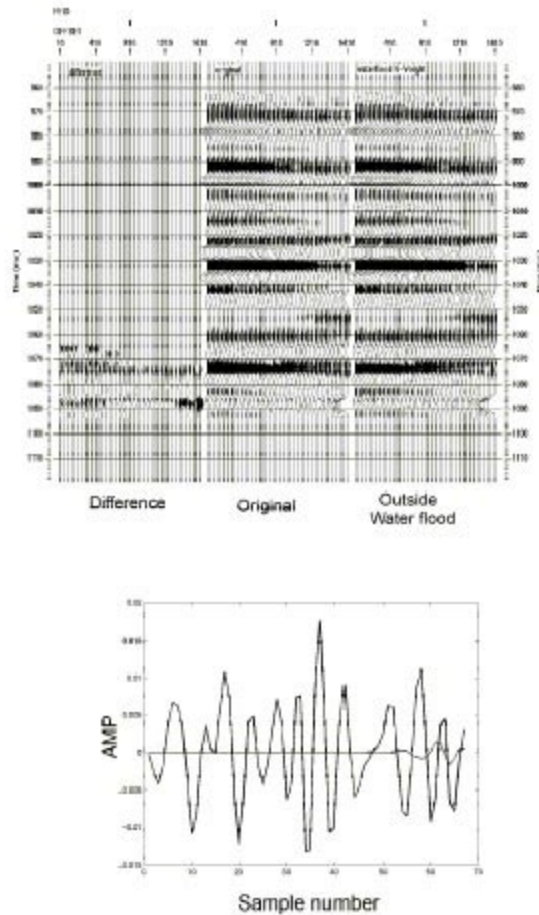


Figure 7.5 Comparison of synthetic seismogram of the original reservoir conditions with post-production conditions outside of the water flood zone. In the lower portion of the figure, trace one of the original response is plotted with trace one of the difference.

7.6 Difference Between 1995 and 1997 Surveys

The 1997, 2D-3C high-resolution line was shot across the location of well 00/09-08. A line was extracted from the 1995 3D-3C data volume that was contiguous with the location of the 1997 2D-3C high-resolution line. A match filter was applied to the 2D-3C data. The match-filtered output was subtracted from the extracted line from the 1995 3D-3C data volume and the results are shown in Figure 7.7. Several anomalies of the same magnitude exist, but the largest anomaly on the section is in the Blackfoot reservoir zone. The cause of the difference in seismic response is unclear. Water has not been produced from 00/09-08, indicating that the water flood front had not arrived at the well location. By the time of the 1995 survey, the lower reservoir had already reached the bubble point, so gas would be present in the lower reservoir during the acquisition of both surveys. Pressure was maintained in the upper reservoir during the interval between the surveys. One difference between the surveys is that the pressure in the lower reservoir had declined between 1995 and 1997. An explanation for the differences between the surveys and an analysis on whether or not the seismic response differences are significant remain issues for future work. However, the fact that an apparently observable change in seismic response is located in a region where the reservoir conditions had not changed dramatically is encouraging.

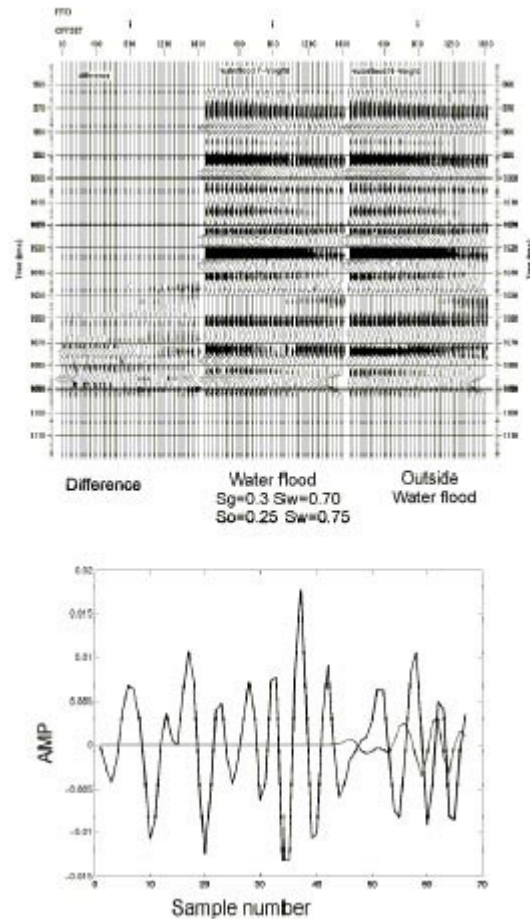


Figure 7.6 Comparison of synthetic seismogram of outside the water flood with inside the water flood zone.

7.7 Conclusions

Three scenarios of fluid and pressure distribution within the Blackfoot reservoir have been tested for differences in seismic response. Synthetic shot gathers were generated for each scenario and were compared. The predicted changes in seismic response were significant. The actual change in seismic response may be equally significant. The seismic response of the 1997 2D-3C was compared with a contiguous line extracted from the 1995 3D-3C seismic data

volume. Only moderate changes in the reservoir pressure were expected. Nevertheless, the largest change in the difference section is found at the location of the Blackfoot reservoir zone. The change is only slightly larger than some other changes in the difference section, but the results are encouraging, given the moderate change in the reservoir conditions. The results indicate that small to moderate changes in the seismic response would be observed in time-lapse seismic monitoring of the Blackfoot reservoir. The results also indicate that the water flood zone would be seismically distinct from the non-water flood areas.

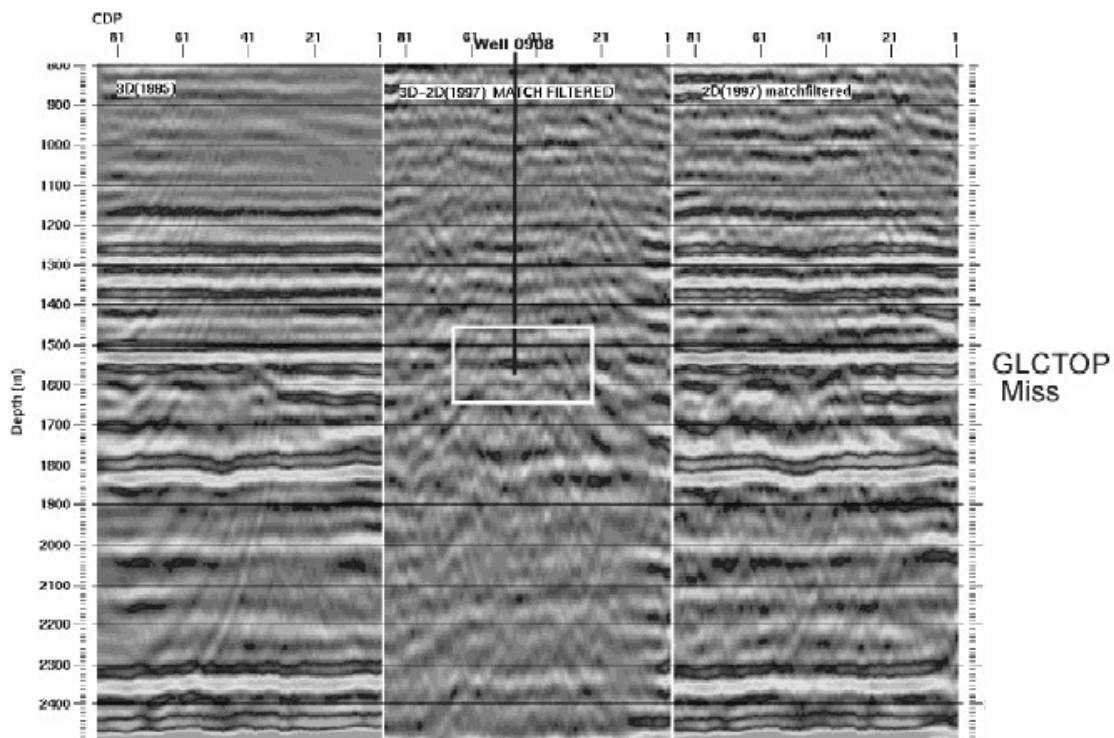


Figure 7.7 Difference Section. The left section was extracted from the 1995 3D-3C seismic data volume across the same location of the 1997 2D-3C seismic survey. The 1997 match filter profile is shown to the right. The difference between the two sections is shown in the center. The highest amplitude anomaly is located in the Blackfoot reservoir zone.

CHAPTER 8

CONCLUSIONS

Pore geometry is the major factor to influence the elastic moduli of rocks. The compressibility of cracks is enormously larger than that of spherical pores. Consequently, cracks may decrease the elastic moduli substantially in spite of being small in volume. Another factor is the elastic moduli of rock solid. The effect depends chiefly on the amount of minerals of low elastic moduli such as clay. Note that the elastic moduli of rock solid are less affected by pressure and temperature. The bulk modulus of the pore fluid can increase the elastic moduli of the fluid-saturated rock considerably, especially at high frequencies.

It is found from the pore aspect ratio spectra obtained from the inverse KT modelling of ninety-seven sandstone samples that the concentration of round pores is in direct proportion to porosity while that of cracks, despite being very small, vary among individual samples. The uncertainty in the elastic moduli for a given porosity can be attributed chiefly to that in the crack concentration. It is also discovered that the decreasing effect of cracks on the elastic moduli with increasing porosity.

In terms of rock physics the most important changes due to hydrocarbon recovery are the pore geometry and the fluid bulk modulus. The change in pore geometry is caused by the changes in pressure and temperature. The change in the fluid bulk modulus is due to the changes in saturation and pressure and temperature.

Effective pressure can close or open cracks and affect the elastic moduli. At high effective pressure, most cracks are closed and no much change in the

elastic moduli occurs. At high porosity, the opening or closing of cracks does not affect the elastic moduli appreciably because of the decreased effect of cracks on the elastic moduli.

Temperature change can decrease or increase pore volume, which in turn modifies the elastic moduli by a small amount. This is the situation most encountered in hydrocarbon recovery. But the large temperature increase such as steam injection may create cracks due to differential thermal expansion, tremendously decreasing the elastic moduli.

The fluid bulk modulus is affected by pressure, temperature and saturation. Pressure and temperature can cause phase changes, and can also influence the fluid bulk modulus directly. Fluid drive or flood can change saturations, which may be heterogeneously distributed on coarse scale. However, the effect of the pore fluid on the elastic moduli of the fluid-saturated rocks is generally limited to the rocks of low dry elastic moduli. This implies it is significant for rocks of high porosity at low effective pressure.

The good candidates for time-lapse seismic surveys are the reservoir rocks of low dry elastic moduli with a large fluid bulk modulus contrast, the reservoir rocks that undergo a large pressure change at low effective pressure, and those subject to a large temperature change. The sandstones of high porosity at low effective pressure, which may be located at shallow or great depths depending on the fluid pressure gradient, are most suitable for seismic monitoring. The Blackfoot oilfield, due to high effective pressure and not high porosity, is marginally feasible for seismic monitoring.

REFERENCES

Akbar, Nabi, Gary Mavko, Amos Nur and Jack Dvorkin, 1994, Seismic signature of reservoir transport properties and pore fluid distribution, *Geophysics*, 59(8), 1222-1236.

Atwater, G. I. And E. E. Miller, 1965, The effect of decrease in porosity with depth on future development of oil and gas reserves in south Louisiana, *AAPG*, 49(3), 334.

Batzle, Michael and Zhijing Wang, 1992, Seismic properties of pore fluids, *Geophysics*, 57(11), 1396-1408.

Bentley, L. R., J. J. Zhang and Han-xing Lu, 1999, Four-D seismic monitoring feasibility, the CREWES report, p. 777-786.

Biot, M. A., 1956 a, Theory of propagation of elastic waves in a fluid saturated porous solid, I: Low frequency range, *J. Acoust. Soc. Am.*, 28, 168-178.

Biot, M. A., 1956 b, Theory of propagation of elastic waves in a fluid saturated porous solid, II: High frequency range, *J. Acoust. Soc. Am.*, 28, 179-191.

Biot, M. A., 1962, Generalized theory of acoustic propagation in porous dissipative media, *J. Acoust. Soc. Am.*, 54, 1254-1264.

Birch, F., 1938, The effect of pressure upon the elastic parameters of isotropic solids, according to Murnaghan's theory of finite strain, *J. Appl. Phys.*, 9, 279-288.

Birch, F. and Bancroft, D., 1938, The effect of pressure on the rigidity of rocks, *J. Geol.*, 46, 59-87 and 131-134.

Brace, W. F., E. Silver, K. Hadley and C. Goetze, 1972, Cracks and pores: A closer look, *Science*, 168, 162-163.

Brown, R. J. S and Korringa, J., 1975, On the dependence of the elastic properties of a porous rock on the compressibility of the pore fluid, *Geophysics*, 40(4), 608-616.

Carmichael, Robert S., 1989, *Practical Handbook of Physical Properties of Rocks and Minerals*, Florida: CRC Press.

Castagna, J. P., Batzle, M. L., and R. L. Eastwood, 1985, Relationships between compressional-wave and shear-wave velocities in clastic silicate rocks, *Geophysics*, 50, 571-581.

Cheng, Chuen Hon and M. Nafi Toksoz, 1979, Inversion of seismic velocities for the pore aspect ratio spectrum of a rock, *Journal of Geophysical Research*, 84(B13), 7533-7543.

Chilingarian, GV, 1983, Compactional diagenesis, In: Parker A, Sellwood BW (eds) *Sediment diagenesis*. NATO ASI series C 115, Reidel, Dordrecht, 57-168.

Clark, Norman J., 1969, *Elements of petroleum reservoirs*, Dallas: AIMMPE.

Clark, S. P. Jr. (Editor), 1966, *Handbook of physical constants*, Geological Society of America, *Memoir 97*, 587 pp.

Craft, B.C. and M. F. Hawkins, 1991, *Applied petroleum reservoir engineering*, NJ: Prentice Hall PTR.

Domenico, S. N., 1974, Effect of water saturation on seismic reflectivity of sand reservoirs encased in shale, *Geophysics*, 39(6), 759-769.

Domenico, S. N., 1976, Effect of brine-gas mixture on velocity in an unconsolidated sand reservoirs, *Geophysics*, 41(5), 882-894.

Dufour, J., Squires, J., Goodway, W., Edmunds, A. and Shook, I., 1999, "Integrated geological and geophysical interpretation, and lame rock parameter extractions using AVO analysis on the Blackfoot 3C-3D data, southern Alberta," *Geophysics*, (in review).

Dvorkin, Jack and Amos Nur, 1993, Dynamic poroelasticity: A unified model with the squirt and the Biot mechanism, *Geophysics*, 58(4), 524-533.

Dvorkin, Jack, Amos Nur and Caren Chaika, 1996, Stress sensitivity of sandstones, *Geophysics*, 61(2), 444-455.

Dvorkin, Jack, Richard Nolen-Hoeksema and Amos Nur, 1994, The squirt-flow mechanism: Macroscopic description, *Geophysics*, 59(3), 428-438.

Eberhart-Phillips, D., Han, D-H., and Zoback M. D., 1989, Empirical relationships among seismic velocity, effective pressure, porosity, and clay content in sandstones, *Geophysics*, 54, 82-89.

Einsele, Gerhard, 1992, *Sedimentary basins*, Berlin: Springer-Verlag Berlin Heidelberg.

Endres, Anthony L. and Rosemary Knight, 1989, The effect of microscopic fluid distribution on elastic wave velocities, *The Log Analyst*, 30, 437-445.

Eshelby, J. D., 1957, The determination of the elastic field of an ellipsoidal inclusion, and related problems, *Proc. Roy. Soc. London, Ser. A*, 241, 376-396.

Freund, D., 1992, Ultrasonic compressional and shear velocities in dry rocks as a function of porosity, clay content, and confining pressure, *Geophysical Journal International*, 108, 125-135.

Galas, C., 1995, "Reservoir simulation study water flood feasibility, Blackfoot Glauconitic Channel TWP 23 RGE 23 W4M," PanCanadian internal report.

Gassmann, F., 1951, Über die elastizität poroser medien: *Vierteljahrreschr. Naturforsch. Ges. Zurich*, 96, 1-21.

Geertsma, J., 1957, The effect of fluid pressure decline on volumetric changes of porous rocks, *Transactions of the AIME*, 210, 331-340.

Gretener, P. E., 1993, *Course Notes*, University of Calgary.

Gueguen, Yves and Victor Palciauskas, 1994, *Introduction to the Physics of Rocks*, NY: Princeton Univ. Press.

Hadley, K., 1976, Comparison of calculated and observed crack densities and seismic velocities in Western granite, *Journal of Geophysical Research*, 81, 3484-3494.

Han, De-hua, A. Nur and Dale Morgan, 1986, Effects of porosity and clay content on wave velocities in sandstones, *Geophysics*, 51, 2093-2107.

Hashin, Z., 1983, Analysis of composite materials, *Journal of Applied Mechanics*, 50, 481-498.

Hashin, Z., and Shtrikman, S., 1963, A variational approach to the theory of elastic behaviour of multiphase materials: *J. Mech. Phys. Solids*, 11, 127-140.

Hellwege, K-H, 1982, *Physical properties of rocks*, volume 1, Berlin: Springer-Verlag Berlin-Heiddberg.

Hill, R., 1952, The elastic behaviour of a crystalline aggregate: Proc. Phys. Soc. London ser. A., 65, 349-354.

Hill, R., 1963, Elastic properties of reinforced solid: some theoretical principles, J. Mech. Phys. Solids, 11, 357-372.

Jack, Ian, 1998, Time-lapse seismic in reservoir management, SEG course notes.

Johnston, David H., 1989, Recent advances in exploration geophysics, The Leading Edge, 8(2), 22-28.

Jones, S. M., 1995, Velocities and quality factors of sedimentary rocks at low and high effective pressures, Geophysical Journal International, 123, 774-780.

Kern, H., 1978, The effect of high temperature and high confining pressure on compressional wave velocities in quartz-bearing and quartz-free igneous and metamorphic rocks, Tectonophysics, 44, 185-203.

Khaksar, A., C. M. Griffiths and C. McCann, 1999, Compressional- and shear-wave velocities as a function of confining stress in dry sandstones, Geophysical Prospecting, 47, 487-508.

King, M. S., 1966, Wave velocities in rocks as a function of changes in overburden pressure and pore fluid saturants, Geophysics, 31, 50-73.

Knight, Rosemary and Richard Nolen-Hoeksema, 1990, A laboratory study of the dependence of elastic wave velocities on pore scale fluid distribution, Geophysical Research Letters, 17(10), 1529-1532.

Kowallis, B. J., L. E. A. Jones and H. F. Wang, 1984, Velocity-porosity-clay content systematics of porosity consolidated sandstones, Journal of Geophysical Research, 89(B12), 10355-10364.

Kuster, Guy T. and M. Nafi Toksoz, 1974, Velocity and attenuation of seismic waves in two-phase media: part 1. Theoretical formulations, Geophysics, 39, 587-606.

Landau, L., and E. Lifchitz, 1967, Theory of elasticity, Moscow: Editions Mir.

Love, A. E., 1944, A treatise on the mathematical theory of elasticity: Dover, New York.

Lumley, D.E., Behrens, R.A. and Wang, Z., 1997, Assessing the technical risk of a 4-D seismic project, *The Leading Edge*, 16(9), 1287-1291.

MacKenzie, J. K., 1949, The elastic constants of a solid containing spherical holes, *Proceedings of the Physical Society of London*, 63(B), 2-11.

Maillart, J., 1989, *Differentiation entre tectonique syn sedimentaire et compaction differentielle*. These 1'Ecole Nationale Superieure des Mines, Paris, 193p.

Mavko, M., 2000, *Rock physics for geophysical reservoir characterization and recovery monitoring*, SEG course notes.

Mavko, G. and Amos Nur, 1979, Wave attenuation in partially saturated rocks, *Geophysics*, 44, 161-178.

Mavko, G. M. and Amos Nur, 1978, The effect of nonelliptical cracks on the compressibility of rocks, *Journal of Geophysical Research*, 83, B9, 4459-4468.

Mavko, Gary and Diane Jizba, 1991, Estimating grain-scale fluid effects on velocity dispersion in rocks, *Geophysics*, 56(12), 1940-1949.

Mavko, G., Mukerji, T. and J. Dvorkin, 1998, *The rock physics handbook*, Cambridge: Cambridge University Press.

Mavko, Gary and Tapan Mukerji, 1998, Bounds on low-frequency seismic velocities in partially saturated rocks, *Geophysics*, 63(3), 918-924.

McCain, William D., Jr., 1990, *The Properties of Petroleum Fluids*, Tulsa: PennWell Publishing Company.

Mindlin, R. D., 1949, Compliance of elastic bodies in contact, *Journal of Applied Mechanics*, 16, 259-268.

Murnaghan, F. D., 1937, Finite deformations of an elastic solid, *Am. J. Math.*, 59, 235-260.

Murphy, W. F., 1982, Effect of partial water saturation on attenuation in Massillon sandstone and Vycor porous glass, *J. Acoust. Soc. Am.*, 71, 1458-1468.

Murphy, W. F., 1984a, Acoustic measures of partial gas saturation in tight sandstone, *Journal of Geophysical Research*, 89, 11549-11559.

Murphy, W. F., 1984b, Seismic to ultrasonic velocity drift: intrinsic absorption and dispersion in crystalline rock, *Geophysical Research Letters*, 11, 1239-1242.

Murphy III, William, Kenneth W. Winkler and Robert L. Kleinberg, 1986, Acoustic relaxation in sedimentary rocks: Dependence on grain contacts and fluid saturation, *Geophysics*, 51(3), 757-766.

Nur, A., Marion, D. and Yin, H., 1991, Wave velocities in sediments, in *Shear Waves in Marine Sediments*, J. M. Hovem, M. D. Richardson, and R. D. Stoll, eds. Kluwer Academic Publishers, Dordrecht, The Netherlands, 131-140.

Nur, A., Mavko, G., Dvorkin, J., and Gal, D., 1995, Critical porosity: the key to relating physical properties to porosity in rocks, in *Proc., 65th Ann. Int. Meeting, Society of Exploration Geophysicists*, 878.

Nur, Amos, 1989, Four-dimensional seismology and (true) direct detection of hydrocarbons: The petrophysical basis, *The Leading Edge*, 8(2), 30-36.

O'Connell, R. J. and Budiansky, B., 1974, Seismic velocities in dry and saturated cracked solids, *Journal of Geophysical Research*, 79, 5412-5426.

Pros, Z., Vanek, J., and Klima, K., 1962, The velocity of elastic waves in diabase and graywacke under pressures up to 4 kilobars, *Studia Geoph. et Geod.*, 6, 347-367.

Reuss, A., 1929, Berechnung der fließgrenze von mischkristallen auf grund der plastizitatbedingung fur einkristalle: *Zeitschrift fur Angewandte Mathematik aus Mechanik*, 9, 49-58.

Sack, R. A., 1946, Extension of Griffith's theory of rupture to three dimensions, *Proc. Phys. Soc. London, A*, 58, 729-736.

Sayre, Allyn T., Jr. and Wm T. Wertman, 1952, Effects of water flooding on reservoir temperatures and wax precipitation in the Bradford, Pennsylvania, oil field, Bureau of Mines, US Department of the Interior.

Scholz, Christopher H. and Stephen H. Hickman, 1983, Hysteresis in the closure of a nominally flat crack, *Journal of Geophysical Research*, 88, 6501-6504.

Sheriff, Robert E., 1984, *Encyclopedic dictionary of exploration geophysics*, SEG.

Sheriff, Robert E., 1984, *Encyclopedic dictionary of exploration geophysics*, SEG.

Sheriff, Robert E., and Lord P. Geldart, 1995, *Exploration Seismology*, Cambridge: Univ of Cambridge Press.

Smith, Charles R., Tracy, G. W. and R. Lance Farrar, 1992, *Applied reservoir engineering*, volume 1, Tulsa: OGC Publications.

Sokolnikoff, I. S., 1956, *Mathematical theory of elasticity*, New York: McGraw-Hill.

Sonneland, L., Veire, H.H., Raymond, B., Signer, C., Pedersen, L., Ryan, S. and Sayers, C., 1997, Seismic reservoir monitoring on Gullfaks, *The Leading Edge*, 16(9), 1247-1252.

Smosna R., 1989, Compaction law for Cretaceous sandstones of Alaska north slope, *J Sediment Petrol*, 59, 572-584.

Spiesberger, J. L. and Metzger, K., 1991, New estimate of sound speed in water, *Journal of Acoustical Society of America*, 89, 1697-1700.

Sprunt, Eve S. and W. F. Brace, 1974, Direct observation of microcavities in crystalline rocks, *Int. J. Rock Mech. Min. Sci. Geomech., Abstr.*, 11, 139-150.

Stewart, R.S., Hoffe, B., Bland, H.C., Margrave, G., Gallant, E. E. and Bertram, M. B., 1997, "The Blackfoot high-resolution 3-C seismic survey: design and initial results," *CREWES Research Report*, ch. 5, 1-26.

Taylor, Jane M., 1950, Pore-space reduction in sandstones, *AAPG*, 34(4), 701-716.

Thomas, L. K., Hankinson, R. W. and Phillips, K. A., 1970, Determination of acoustic velocities for natural gas, *Journal of Petroleum Technology*, 22, 889-892.

Timur, A., W. B. Hemphins and R. M. Weinbrandt, 1971, Scanning electron microscopic study of pore systems in rocks, *Journal of Geophysical Research*, 76(20), 4932-4948.

Tittmann, B. R., Bulau, J. R., and Abel-Gawad, M., 1984, Dissipation of elastic waves in fluid saturated rocks, in Johnson, D. L., and Sen, P. N., Eds., *Physics and chemistry of porous media*, Am. Inst. of Physics.

Toksoz, M. N., C. H. Cheng and A. Timur, 1976, Velocities of seismic waves in porous rocks, *Geophysics*, 41, 621-645.

Toksoz, M. N. and D. H. Johnston, 1981, Seismic wave attenuation, Society of Exploration Geophysists.

Tosaya, Carol and Amos Nur, 1982, Effects of diagenesis and clays on compressional velocities in rocks, *Geophysical Research Letters*, 9(1), 5-8.

Touloukian, Y. S., W. R. Judd and R. F. Yoy, 1981, *Physical Properties of Rocks and Minerals*, Purdue Research Foundation.

Vazquez, M. and Beggs, H. D., 1980, Correlations for fluid physical property prediction, *Journal of Petroleum Technology*, 32, 968-970.

Voigt, W., 1928, *Lehrbuch der Kristallphysik*: Teubner, Leipzig.

Walsh, J. B., 1966, Seismic wave attenuation in rock due to friction, *Journal of Geophysical Research*, 71, 2591-2599.

Walsh, J. B., 1965, The effect of cracks on the compressibility of rock, *Journal of Geophysical Research*, 70, 381-389.

Wang, C. Y., N. H. Mao and F. T. Wu, 1980, Mechanical properties of clays at high pressure, *Journal of Geophysical Research*, 85(B3), 1462-1468.

Wang, Z. and A. M. Nur, 1991, *Seismic and Acoustic Velocities in Reservoir Rocks. Volume 2 Theoretical and Model Studies*, Society of Exploration Geophysists.

Wang, Z. and A. M. Nur, 1990, Dispersion analysis of acoustic velocities in rocks, *J. of Acoust. Soc. Am*, 87, 2384-2395.

Wang, Z. and A. M. Nur, 1988, Effect of temperature on wave velocities in sands and sandstones with heavy hydrocarbons, *SPE Reservoir Engineering*, 3(1), 158-164.

Wang, Z., Hirsche, W. K. and G. Sedgwick, 1991, Seismic monitoring of water floods? - A petrophysical study, *Geophysics*, 56(10), 1614-1623.

Winkler, Kenneth W. and Amos Nur, 1979, Pore fluids and seismic attenuation in rocks, *Geophysical Research Letters*, 6, 1-4.

Winkler, Kenneth W., 1985, Dispersion analysis of velocity and attenuation in Berea sandstone, *Journal of Geophysical Research*, 90(B8), 6793-6800.

Winkler, Kenneth W., 1986, Estimation of velocity dispersion between seismic and ultrasonic frequencies, *Geophysics*, 51(1), 183-189.

Woerber, A. F., Samuel Katz and T. T. Ahrens, 1963, Elasticity of selected rocks and minerals, *Geophysics*, 28(4), 658-663.

Wood, A. B., 1941, *A textbook of sound*, London: G. Bell and Sons.

Xu, Shiyu and Roy E. White, 1995, A new velocity model for clay-sand mixtures, *Geophysical Prospecting*, 43, 91-118.

Yang, G. Y. C., D. C. Lawton, R. R. Stewart, S. L. M. Miller, C. C. Potter and V. Simin, 1996, "Interpretation and analysis of the Blackfoot 3C-3D seismic survey," CREWES Research Report, 8, ch. 46, 1-41.

Zhang, J., T.-F. Wong and D. M. Davis, 1990, Micromechanics of pressure-induced grain crushing in porous rocks, *Journal of Geophysical Research*, 95(B1), 341-352.

Zhang, J. J. and L. R. Bentley, 1999, Change of elastic moduli of dry sandstone with effective pressure and temperature, *The CREWES report*, 11, 761-776.

Zimmerman, R. W., 1991, *Compressibility of sandstones*, Amsterdam: Elsevier Science Publishers B.V.

APPENDIX A

Compressibility of the rock with spherical pores and cracks

First we consider the simple case of dilute concentration of spherical pores. We assume numerous regions can be divided, each having one pore with the same porosity. Pressure at any point at the boundary between these regions equals the external pressure dP due to the great distance between pores. The tangential stress (σ_θ) and strain (ε_θ) at the boundary of a spherical pore is (Walsh, 1965):

$$\sigma_\theta = -(3dP/2)/(1-v_p/v) \quad \text{A.1}$$

$$\varepsilon_\theta = (1-\nu_s)(\sigma_\theta/E_s) \quad \text{A.2}$$

where ν_s and E_s are Poisson's ratio and Young's modulus of rock solid, v_p and v are the volume of the spherical pore and the volume of the region containing the pore. Since the perimeter of a circle is in direct proportion to the radius, ε_θ (ratio of the change of the perimeter to the perimeter) is equal to dr/r (r is the radius), which is $(dv_p/v_p)/3$. So $dv_p/v_p = 3\varepsilon_\theta$. Thus,

$$\begin{aligned} \frac{dv_p}{v_p} &= 3(1-\nu_s)\frac{\sigma_\theta}{E_s} \\ &= -\frac{9}{2}\frac{dP}{E_s}\frac{1-\nu_s}{1-v_p/v} \end{aligned} \quad \text{A.3}$$

Dividing two sides of equation A.3 by vdP/v_p gives

$$\frac{dv_p}{vdP} = -\frac{9}{2}\frac{1-\nu_s}{E_s}\frac{v_p/v}{1-v_p/v}$$

$$= -\frac{9}{2} \frac{1-v_s}{E_s} \frac{\phi}{1-\phi} \quad \text{A.4}$$

If dv_p is small, dv_p/v is equal to $d\phi$. So equation A4 is reformulated as:

$$\frac{d\phi}{dP} = -\frac{9}{2} \frac{1-v_s}{E_s} \frac{\phi}{1-\phi} \quad \text{A.5}$$

Since $C_s = 3(1-2v_s) / E_s$ (Sheriff, 1984), equation A.5 can be rewritten as:

$$\frac{d\phi}{dP} = -\frac{3}{2} C_s \frac{1-v_s}{1-2v_s} \frac{\phi}{1-\phi} \quad \text{A.6}$$

Substituting equation A.6 into equation 2.19 (in Chapter 2) results in:

$$C = C_s \left(1 + \frac{3}{2} \frac{1-v_s}{1-2v_s} \frac{\phi}{1-\phi} \right) \quad \text{A.7}$$

We invert equation A.7 to find the expression for the effective bulk modulus:

$$\begin{aligned} K &= K_s / \left(1 + \frac{3}{2} \frac{1-v_s}{1-2v_s} \frac{\phi}{1-\phi} \right) \\ &= 2K_s \frac{(1-2v_s)(1-\phi)}{2(1-2v_s)(1-\phi) + 3(1-v_s)\phi} \\ &= 2K_s \frac{(1-2v_s)(1-\phi)}{2(1-2v_s) + (1+v_s)\phi} \\ &= 2K_s \frac{(1-2v_s)/(1+v_s)}{2(1-2v_s)/(1+v_s) + \phi} (1-\phi) \end{aligned}$$

A.8

Since $v_s = (3K_s - 2\mu_s) / [2(3K_s + \mu_s)]$ (Sheriff, 1984), the equation A.8 is:

$$\begin{aligned}
 K &= 2K_s \frac{(1 - \frac{3K_s - 2\mu_s}{3K_s + \mu_s}) / (1 + \frac{3K_s - 2\mu_s}{2(3K_s + \mu_s)})}{2(1 - \frac{3K_s - 2\mu_s}{3K_s + \mu_s}) / (1 + \frac{3K_s - 2\mu_s}{2(3K_s + \mu_s)}) + \phi} (1 - \phi) \\
 &= \frac{4/3K_s\mu_s}{4/3\mu_s + K_s\phi} (1 - \phi) \\
 &= \frac{4/3K_s\mu_s + K_s^2\phi - K_s^2\phi - 4/3K_s\mu_s\phi}{4/3\mu_s + K_s\phi} \\
 &= K_s - K_s\phi \frac{4/3\mu_s + K_s}{4/3\mu_s + K_s\phi}
 \end{aligned}$$

A.9

In the case of dilute concentration of narrow cracks, we have the same assumption as that for spherical pores. Equation 2.18 (in Chapter 2) are rearranged as follows:

$$\begin{aligned}
 C &= C_s - 1/VdV_p/dP \\
 &= (C_sVPdP - PdV_p) / (VPdP)
 \end{aligned} \tag{A.10}$$

or, for a single region,

$$C = (C_s v P dP - P d v_p) / (v P dP) \tag{A.11}$$

The first term in the numerator on the right-hand side of equation A.11 is the strain energy associated with the region if there is no crack, and the second term is the increase in strain energy dw_p due to the cracks. Following the approach of Sack (1946), Walsh (1965) derived dw_p for the penny-shaped crack of half length c for a single region as:

$$dw_p = C_s \frac{16(1 - v_s^2)c^3}{9(1 - 2v_s)} PdP \tag{A.12}$$

The total strain energy dW_p due to all cracks is found by summing the values dw_p in equation A.12 over the total number of regions N :

$$\begin{aligned} dW_p &= C_s \sum \frac{16(1-v_s^2)c^3}{9(1-2v_s)} PdP \\ &= C_s \frac{16(1-v_s^2)}{9(1-2v_s)} PdP \sum c^3 \end{aligned}$$

A.13

Substituting A.13, which is $-dW_p$ due to dV_p being negative, into A.10 leads to:

$$C = C_s \left(1 + \frac{16}{9} \frac{1-v_s^2}{1-2v_s} \frac{\sum c^3}{V} \right) \quad \text{A.14}$$

If we define an average half crack length c_{ave} , where $Nc_{ave}^3 = \sum c^3$ and an average region volume v_{ave} , where $Nv_{ave} = V$, A.14 can be rewritten as:

$$C = C_s \left(1 + \frac{16}{9} \frac{1-v_s^2}{1-2v_s} \frac{c_{ave}^3}{v_{ave}} \right) \quad \text{A.15}$$

APPENDIX B

Isothermal compressibility of gas

The gas equation of state is:

$$PV = nZRT \quad \text{B.1}$$

where P , V , T are pressure, volume and absolute temperature respectively, R is the universal gas constant, n is the mole number, Z is the compressibility factor or gas deviation factor. Z is defined as the ratio of the volume actually occupied by a gas at given pressure and temperature to the volume the gas would occupy at the same pressure and temperature if it behaved like an ideal gas. The isothermal compressibility of gas is:

$$C_g = -\frac{1}{V} \left(\frac{\partial V}{\partial P} \right)_T \quad \text{B.2}$$

Differentiating equation B.1 with respect to pressure:

$$\begin{aligned} \left. \frac{\partial V}{\partial P} \right|_T &= -\frac{nZRT}{P^2} + \frac{nRT}{P} \frac{\partial Z}{\partial P} \\ &= -\frac{V}{P} + \frac{V}{Z} \left. \frac{\partial Z}{\partial P} \right|_T \end{aligned} \quad \text{B.3}$$

Substituting equation B.3 into B.2 gives:

$$C_g = \frac{1}{P} - \frac{1}{Z} \frac{\partial Z}{\partial P} \quad \text{B.4}$$

APPENDIX C

Derivation of the Gassmann's equation

Consider a representative volume element (V) subject to an external hydrostatic pressure (dP), which is supported by the fluid (dP_f) and the rock frame (dP_{eff}) on the solid framework. In the process of deformation, the fluid are assumed not to cross the element boundary. According to the definition of compressibility of the fluid-saturated rock, we can write

$$-dV/V = C dP \quad C.1$$

where C is the compressibility. The volume change ($-dV$) has three components, i.e., the volume change of fluid due to the fluid pressure [$C_f(\phi V)dP_f$], the volume change of the rock solid due to the fluid pressure [$C_s(1-\phi)V dP_f$] and the volume change of the rock solid due to the effective pressure ($C_s V dP_{eff}$). The first two components are understandable, and the third component is not direct but can be proved (see Appendix D for derivation). Thus,

$$\begin{aligned} -dV &= C_f (\phi V) dP_f + C_s [(1-\phi)V] dP_f + C_s V dP_{eff} \\ \text{i.e.} \quad -dV/V &= C_f \phi dP_f + C_s (1-\phi)dP_f + C_s dP_{eff} \end{aligned} \quad C.2$$

where C_f and C_s are the compressibilities of fluids and rock solid respectively.

Alternatively, the volume change ($-dV$) can be divided into two parts, the one due to the effective pressure ($C_d V dP_{eff}$) and the other due to the fluid pressure ($C_s V dP_f$). The first is the definition of dry bulk modulus. The latter is the change of the bulk volume when dP_f is applied on the volume element. The

application of hydrostatic pressure dP_f on the volume element results in the uniform hydrostatic pressure of magnitude dP_f throughout the rock solid (matrix). Consequently a uniform dilatation throughout the whole rock solid occurs (Geertsma, 1957). This state of stress and strain is exactly the same as that which would occur if the pores were hypothetically filled up with rock solid materials and the boundary conditions on the outer surface were left unchanged (Zimmerman, 1991). This leads to the bulk volume change equal to $C_s V dP_f$. Thus,

$$\begin{aligned} -dV &= C_d V dP_{\text{eff}} + C_s V dP_f \\ \text{i.e.,} \quad -dV/V &= C_d dP_{\text{eff}} + C_s dP_f \end{aligned} \quad \text{C.3}$$

where C_d is the compressibility of the solid framework. Solve dP_f and dP_{eff} from equations C.2 and C.3:

$$dP_f = \frac{(-dV/V)(C_s - C_d)}{\phi C_d (C_s - C_f) - C_d C_s + C_s^2} \quad \text{C.4}$$

$$dP_{\text{eff}} = \frac{(-dV/V)\phi(C_s - C_f)}{\phi C_d (C_s - C_f) - C_d C_s + C_s^2} \quad \text{C.5}$$

Note $dP = dP_f + dP_{\text{eff}}$. Substituting equations C.4 and C.5 into C.1 and reorganizing it result in:

$$\begin{aligned} \frac{1}{C} &= \frac{dP}{(-dV/V)} \\ &= \frac{dP_f + dP_{\text{eff}}}{(-dV/V)} \\ &= \frac{(C_s - C_d) + \phi(C_s - C_f)}{\phi C_d (C_s - C_f) - C_d C_s + C_s^2} \end{aligned} \quad \text{C.6}$$

Rewrite equation C.6 in terms of the bulk moduli (K_f , K_s , K_d) of the fluids the rock solid and the solid framework:

$$\begin{aligned}
K &= \frac{\left(\frac{1}{K_s} - \frac{1}{K_d}\right) + \phi\left(\frac{1}{K_s} - \frac{1}{K_f}\right)}{\phi \frac{1}{K_d} \left(\frac{1}{K_s} - \frac{1}{K_f}\right) - \frac{1}{K_d K_s} + \frac{1}{K_s^2}} \\
&= \frac{\left(\frac{K_d}{K_s} - 1\right) + \phi K_d \left(\frac{1}{K_s} - \frac{1}{K_f}\right)}{\phi \left(\frac{1}{K_s} - \frac{1}{K_f}\right) - \frac{1}{K_s} + \frac{K_d}{K_s^2}} \\
&= \frac{\phi K_d \left(\frac{1}{K_s} - \frac{1}{K_f}\right) - \frac{K_d}{K_s} + \frac{K_d^2}{K_s^2} + \frac{K_d}{K_s} - \frac{K_d^2}{K_s^2} + \left(\frac{K_d}{K_s} - 1\right)}{\phi \left(\frac{1}{K_s} - \frac{1}{K_f}\right) - \frac{1}{K_s} + \frac{K_d}{K_s^2}} \\
&= K_d + \frac{1 - 2\frac{K_d}{K_s} + \frac{K_d^2}{K_s^2}}{\frac{\phi}{K_f} + \frac{1-\phi}{K_s} - \frac{K_d}{K_s^2}} \\
&= K_d + \frac{\left(1 - \frac{K_d}{K_s}\right)^2}{\frac{\phi}{K_f} + \frac{1-\phi}{K_s} - \frac{K_d}{K_s^2}}
\end{aligned}$$

C.7

C 7 is the Gassmann's equation.

APPENDIX D

The effect of effective pressure on the volume change of rock solid

First, define the bulk and pore compressibilities as follows (Zimmerman, 1991):

$$C_{bs} = -\frac{1}{V} \left[\frac{\partial V}{\partial S} \right]_P \quad D.1$$

$$C_{bp} = \frac{1}{V} \left[\frac{\partial V}{\partial P} \right]_S \quad D.2$$

$$C_{ps} = -\frac{1}{V_p} \left[\frac{\partial V_p}{\partial S} \right]_P \quad D.3$$

where V and V_p are the bulk volume and the pore volume, respectively, P is the fluid pressure and S is the total stress.

According to the principle of superposition, an infinitesimal change in stress can be resolved into two components. Consequently, the strain is also the sum. When $\{dS, dP\}$ ($dS=dP$ assumed) is applied, the bulk volume change is:

$$dV\{dS, dP\} = -C_s V dS \quad D.4$$

where C_s is the compressibility of rock solid.

$\{dS, dP\}$ can be separated into $\{dS, 0\}$ and $\{0, dP\}$, which, according to equation D.1 and D.2, have the volume changes respectively:

$$dV\{dS, 0\} = -C_{bs} V dS \quad D.5$$

$$dV\{0, dP\} = C_{bp} V dP \quad D.6$$

Equating equation D.4 and equation D5 plus equation D.6 gives:

$$-C_s V dS = -C_{bs} V dS + C_{bp} V dP$$

i.e., $C_{bp} = C_{bs} - C_s$ D.7

The bulk compressibility (C_{bp}) can be related to the pore compressibility (C_{ps}) through use of the Betti reciprocal theorem of elasticity (Sokolnikoff, 1956; Zimmerman, 1991). This theorem states that if an elastic body is acted upon by two sets of forces, say F1 and F2, the work done by F1 acting through the displacement due to F2 will exactly equal the work done by F2 acting through the displacement due to F1. Applying the theorem to the two sets of forces $\{0, dP\}$ and $\{dS, 0\}$, the work done by the first set of force acting through the displacement due to F2 and the work done by the second set of force acting through the displacement due to F1 are:

$$W\{0, dP\} = dP (-C_{ps} V_p dS) = -C_{ps} V \phi dS dP \quad D.8$$

$$W\{dS, 0\} = dS (C_{bp} V dP) = C_{bp} V dS dP \quad D.9$$

Equating equation D.8 and equation D.9 gives:

$$C_{bp} = C_{ps} \phi \quad D.10$$

Substituting equation D.10 into equation D.7 results in:

$$C_{ps} \phi = C_{bs} - C_s \quad D.11$$

Equation D.11 can be reorganized as:

$$\left\{ -\frac{1}{V_p} \left[\frac{\partial V_p}{\partial S} \right]_P \right\} \phi = -\frac{1}{V} \left[\frac{\partial V}{\partial S} \right]_P - C_s$$

$$i.e. \quad \frac{1}{V} \left[\frac{\partial V}{\partial S} \right]_P - \frac{1}{V_p / \phi} \left[\frac{\partial V_p}{\partial S} \right]_P = -C_s$$

$$i.e. \quad \frac{1}{V} \left[\frac{\partial V_s}{\partial S} \right]_P = -C_s$$

D.12

Equation D.12 indicates the volume change of rock solid (dV_s) due to effective pressure is $C_s V dP_{\text{eff}}$ ($dS = dP_{\text{eff}}$).

APPENDIX E

Effective bulk modulus of the fluid mixture due to patchy saturation

Suppose that the fluids (oil, gas and water) are well separated in space with patch sizes significantly larger than the critical diffusion length L_c ($L_c = (\kappa K_f / f\eta)^{0.5}$, κ is the permeability, η and K_f are the viscosity and bulk modulus of the most viscous fluid phase, f is the seismic frequency) and their average saturations are S_o , S_g , S_w . In the case of the constant shear modulus over all patches, the P-wave modulus is a harmonic averaging of the P-wave moduli of these patches, written as (Hill, 1963; after Mavko and Mukerji, 1998):

$$\begin{aligned}
 \frac{1}{(K + 4/3\mu)} &= \frac{V_{\text{sat-gas}}}{(K_{\text{sat-gas}} + 4/3\mu)} + \frac{V_{\text{sat-oil}}}{(K_{\text{sat-oil}} + 4/3\mu)} + \frac{V_{\text{sat-water}}}{(K_{\text{sat-water}} + 4/3\mu)} \\
 &= \frac{(1 * \phi)S_g + (1 - \phi)S_g}{(K_{\text{sat-gas}} + 4/3\mu)} + \frac{(1 * \phi)S_o + (1 - \phi)S_o}{(K_{\text{sat-oil}} + 4/3\mu)} + \frac{(1 * \phi)S_w + (1 - \phi)S_w}{(K_{\text{sat-water}} + 4/3\mu)} \\
 &= \frac{S_g}{(K_{\text{sat-gas}} + 4/3\mu)} + \frac{S_o}{(K_{\text{sat-oil}} + 4/3\mu)} + \frac{S_w}{(K_{\text{sat-water}} + 4/3\mu)} \\
 &= \left\langle \frac{1}{(K_{\text{sat}} + 4/3\mu)} \right\rangle
 \end{aligned}$$

E.1

where the operator $\langle \rangle$ refers to a volume average.

The Gassmann's equation for a single patch with a single phase of fluid can be expressed as (after Mavko and Mukerji, 1998):

$$K_{\text{sat}} = K_d + \frac{\phi}{\phi_c} \left(\frac{1}{\frac{\phi_c}{K_f} + \frac{1-\phi_c}{K_s}} \right) \quad \text{E.2}$$

where $\phi_c = \phi / (1 - K_d / K_s)$. If $K_f \ll K_s$, E.2 can be approximated as:

$$K_{\text{sat}} = K_d + \frac{\phi}{\phi_c^2} K_f \quad \text{E.3}$$

Substituting equation E.3 into equation E.1 results in:

$$\frac{1}{(K + 4/3\mu)} = \left\langle \frac{1}{\left(K_d + \frac{\phi}{\phi_c^2} K_f + 4/3\mu \right)} \right\rangle \quad \text{E.4}$$

By inverting E.4, we obtain:

$$(K + 4/3\mu) = \left\langle \frac{1}{\left(K_d + \frac{\phi}{\phi_c^2} K_f + 4/3\mu \right)} \right\rangle^{-1} \quad \text{E.5}$$

If $K_g, K_o, K_w \ll (K_d + 4/3\mu)$, equation E.5 can be reorganized as:

$$\begin{aligned}
(K + 4/3\mu) &= \frac{1}{\left\langle \frac{1}{(K_d + 4/3\mu) + \frac{\phi}{\phi_c^2} K_f} \right\rangle} \\
&= \frac{1}{\left\langle \frac{1}{(K_d + 4/3\mu)(1 + \frac{\phi}{\phi_c^2} \frac{K_f}{K_d + 4/3\mu})} \right\rangle} \\
&= \frac{(K_d + 4/3\mu)}{\left\langle \frac{1}{(1 + \frac{\phi}{\phi_c^2} \frac{K_f}{K_d + 4/3\mu})} \right\rangle} \\
&\approx \frac{(K_d + 4/3\mu)}{\left\langle 1 - \frac{\phi}{\phi_c^2} \frac{K_f}{K_d + 4/3\mu} \right\rangle} \\
&= \frac{(K_d + 4/3\mu)}{1 - \frac{\phi}{\phi_c^2} \frac{\langle K_f \rangle}{K_d + 4/3\mu}} \\
&\approx (K_d + 4/3\mu) \left(1 + \frac{\phi}{\phi_c^2} \frac{\langle K_f \rangle}{K_d + 4/3\mu} \right) \\
&= K_d + \frac{\phi}{\phi_c^2} \langle K_f \rangle + 4/3\mu
\end{aligned}$$

i.e.,

$$K = K_d + \frac{\phi}{\phi_c^2} \langle K_f \rangle$$

E.6

where $\langle K_f \rangle$ is an arithmetic averaging of the bulk moduli of fluids. Equations E.3 and E.6 indicate that for completely separated fluid phases, the volume weighted arithmetic average of the fluid phases is the appropriate fluid bulk modulus for the Gassmann's equation.

APPENDIX F

The parameters for the KT equations

$$T_{ijj} = \frac{3F_1}{F_2}$$

$$T_{ijj} - \frac{1}{3}T_{ijj} = \frac{2}{F_3} + \frac{1}{F_4} + \frac{F_4F_5 + F_6F_7 - F_8F_9}{F_2F_4}$$

where

$$F_1 = 1 - [3/2(g+\theta) - R(3/2g + 5/2\theta - 4/3)]$$

$$F_2 = 1 - [1 + 3/2(g+\theta) - R/2(3g+5\theta)] + B(3-4R) - 1/2(3B-1)(3-4R)(g+\theta - R(g-\theta + 2\theta^2))$$

$$F_3 = 1 - 1/2(R(2-\theta) + (1+\alpha^2)/\alpha^2g(R-1))$$

$$F_4 = 1 - 1/4[3\theta + g - R(g-\theta)]$$

$$F_5 = B\theta(3-4R) - R(g+\theta - 4/3) + g$$

$$F_6 = B(1-\theta)(3-4R) - g + R(g+\theta)$$

$$F_7 = 2 - 1/4[9\theta + 3g - R(5\theta + 3g)] + B\theta(3-4R)$$

$$F_8 = B(1-\theta)(3-4R) - 1 + 2R - g/2(R-1) - \theta/2(5R-3)$$

$$F_9 = B\theta(3-4R) - g(R-1) + R\theta$$

$$B = 1/3 K_f/K_s$$

$$R = 3\mu_s / (3K_s + 4\mu_s)$$

$$\theta = \alpha / [(1 - \alpha^2)^{3/2}] (\alpha \cos(\alpha) - \alpha(1 - \alpha^2)^{0.5})$$

$$g = \alpha^2 / (1 - \alpha^2) (3\theta - 2)$$

$$E_1 = \frac{6\mu_{1A} I}{2\pi(3K_{1A} + 4\mu_{1A})}$$

$$E_2 = \frac{6\mu_{1A}}{4\pi(3K_{1A} + 4\mu_{1A})} (3I - 4\pi)$$

$$E_3 = \frac{\alpha^2 (3 - 9I/4\pi)(6K_{1A} + 2\mu_{1A})}{2(1 - \alpha^2)(3K_{1A} + 4\mu_{1A})} + \frac{6\mu_{1A} I}{8\pi(3K_{1A} + 4\mu_{1A})}$$

$$E_4 = \frac{1}{2} \left\{ \frac{(3 - 9I/4\pi)(6K_{1A} + 2\mu_{1A})}{2(1 - \alpha^2)(3K_{1A} + 4\mu_{1A})} - \frac{3\mu_{1A} (1 - I/\pi)}{(3K_{1A} + 4\mu_{1A})} \right\}$$

$$I = \frac{2\pi\alpha}{(1 - \alpha^2)^{3/2}} \{ \cos^{-1} \alpha - \alpha(1 - \alpha^2)^{1/2} \}$$